In-situ Spectroscopic and Kelvin Probe Studies of the Modification of Solid Surfaces in Low Temperature Plasmas

Dissertation

zur Erlangung des Grades eines
Doktors der Naturwissenschaften
der Fakultät für Naturwissenschaften der
Universität Paderborn

vorgelegt im Oktober 2008 von

Miroslaw Giza

Die vorliegende Arbeit wurde angefertigt am
Max-Planck-Institut für Eisenforschung GmbH
in Düsseldorf

Referent: Prof. Dr.-Ing. G. Grundmeier,
Institut für Technische und Makromolekulare Chemie
der Universität Paderborn

Coreferent: Prof. Dr. A. von Keudell,
Institut für Experimentalphysik II
der Ruhr-Universität Bochum

Danksagung – Aknowledgement

Die vorliegende Arbeit wurde am Max-Planck-Institut für Eisenforschung GmbH in Düsseldorf durchgeführt.

Meinem Doktorvater Herrn Prof. Dr.-Ing. G. Grundmeier danke ich sehr herzlich für die Vergabe des interessanten Themas, die intensive und konstruktive Betreuung dieser Arbeit, für die Ermöglichung der Vorstellung von Ergebnissen auf einer Vielzahl von interessanten Konferenzen sowie für den sportlichen Ausgleich zur wissenschaftlichen Arbeit in Form von spannenden Fussballspielen, wenn die Zeit es zuließ.

Herrn Prof. Dr. A. von Keudell danke ich für die freundliche Übernahme des Koreferats, die stete Diskussionsbereitschaft sowie sein Interesse am Fortgang der Arbeit.

Herrn Prof. Dr. M. Stratmann gilt mein Dank für die Möglichkeit der Durchführung aller experimetellen Arbeiten in der Abteilung für Grenzflächenchemie und Oberflächentechnik des MPIE. Allen Mitarbeitern der Abteilung danke ich für die angenehme Atmosphäre und die stete Hilfsbereitschaft sowie für die anregenden Diskussionen und unterhaltsamen Gespräche.

Dr. J. Raacke danke ich recht herzlich für die einleitenden Arbeiten zur Konstruktion des experimentellen Aufbaus sowie für seine Unterstützung und Hilfsbereitschaft insbesondere zu Beginn meiner Arbeit.

Ein grosser Dank gilt Fr. Dr. N. Fink, Dr. K. Wapner und M. Valtiner für die Durchführung einiger FE-REM, AFM und SKP Messungen. Bei R. Vlasak möchte ich mich für die Unterstützung bei der Präparation der Siliziumproben bedanken. Bei P. Thissen bedanke ich mich für die gute Zusammenarbeit bei der Durchführung der Adsorptionsexperimente auf Aluminium und der dazugehörigen QCM Messungen. I. Klüppel und T. Titz gilt

mein Dank für die anregenden Diskussionen zur Elektrochemie und Plasmaphysik.
Herrn Prof. C.-P. Klages und Herrn B. Michel vom Institut für Oberflächentechnik der TU Braunschweig danke ich für die sehr gute Zusammenarbeit und hilfreiche Diskussionen auf dem Gebiet der Plasmamodifikation von Siliziumoberflächen.

Mein besonderer Dank gilt meinen Eltern, die mich stets moralisch und finanziell unterstützt haben. Bei meiner lieben Frau Galina möchte ich mich für ihr Verständnis und ihre unermüdliche Geduld und Zuspruch sowie die fruchtbaren Diskussionen der SKP Ergebnisse bedanken.

Dem Bundesministerium für Bildung und Forschung danke ich für die Bereitstellung der Sach- und Personalmittel.

Contents

Introduction

Different technologies based on surface treatments by an ionized gas entered our everyday life many years ago. Two of many advantages of such plasma processes are the high efficiency by relatively low temperatures, in many cases down to the room temperature level, and the possibility of a continuous treatment of for example coil material.

Most industrial processes concerning the manufacturing of steel from rolling to surface conditioning are based on in-line coil processes. New innovative concepts for coil coating or further tailoring of the surface properties like adhesion promoting for later lacquer application or exchange of conventional corrosion protectors by a new thinnest top layer design based on the combination of ultra-thin films with special functions have to be compatible with current processes, due to the requirement of low invest costs for the implementation of the necessary equipment.

Since, the plasma processes could act mostly as pretreatment before further steps of surface refinement follow, in-situ characterization techniques are required to understand the mechanism of the obtained modifications.

A plasma cell for low and atmospheric pressure plasma treatment of polymer and metal substrates at room temperature is the main topic of the here presented work. It enables the in-situ investigation of the sample surface with FTIR spectroscopy at grazing incidence as well as the simultaneous

measurement of the Volta potential difference between the outmost surface layer and a reference electrode in vacuum or a defined atmosphere by means of a Kelvin probe. Details of this experimental setup will be given in chapter 2. To demonstrate the benefits of the device, the plasma modification of a model polymer and an oxide covered iron surface have been investigated and will be presented in chapter 3. It could be shown that even sub monolayer surface changes, e.g. the etching of the CH_3 and CH_2 groups and the generation of carbonyl functions on an octadecylmercaptane (ODM) self-assembly monolayer on gold in a low pressure oxygen plasma can be detected. Moreover, plasma induced changes of the oxidation states of iron and the thickness and composition of its oxide or oxyhydroxide layer could be monitored. The presented applications of this new in-situ analytical device prove that the measurement of work function in combination with monolayer sensitive vibrational spectroscopy provide new insight in plasma induced surface modifications.

Tailoring of oxide chemistry on aluminum by means of low pressure water and argon plasma surface modification was performed to influence the kinetics of the self-assembly process of octadecylphosphonic acid monolayers. The plasma induced surface chemistry was studied by in-situ FTIR reflection absorption spectroscopy. Ex-situ IRRAS and X-ray photoelectron spectroscopy were applied for the analysis of the adsorbed self-assembled monolayers. The plasma induced variation of the hydroxide to oxide ratio led to different adsorption kinetics of the phosphonic acid from dilute ethanol solutions as measured by means of a quartz-crystal-microbalance. Water plasma treatment caused a significant increase in the density of surface hydroxyl groups in comparison to the argon plasma treated surface. The hydroxyl rich surface led to significantly accelerated adsorption kinetics of the phosphonic acid

with a time of monolayer formation of less than a minute. On the contrary decreasing the surface hydroxyl density slowed down the adsorption kinetics. These studies are detailed described in chapter 4.

Chapter 5 consists of the results of investigations on the plasma induced modifications on the $MgZn_2$ alloy. The chemical composition of the native oxide was compared to the surface state after sequences of Ar/H_2 and oxygen plasma treatments by means of in-situ IRRAS and ex-situ XPS. The native zinc oxide is known to be a n-type semiconductor, the corresponding change in the electronic structure was studied by in-situ Kelvin probe measurements and utilized for a significant decrease of de-adhesion rate of a polymer film applied to the surface by spin coating and investigated by means of ex-situ scanning Kelvin probe in humid atmospheres.

Silicon wafer treated by a plasma show better bonding behavior compared to the untreated state. In cooperation with the Institut für Oberflächentechnik of the university of Braunschweig the effects of a dielectric barrier discharge and ozone to hydrogen terminated and native oxide covered silicon wafer were studied by means of in-situ and ex-situ techniques. Chapter 6 includes the results obtained on hydrogen terminated silicon wafer, which were studied in-situ by means of mirror enhanced IRRAS and ex-situ XPS after modifications by DBD and ozone in the here described chamber. Oxide thicknesses of several nm could be achieved by a DBD treatment of few minutes, however the effect of pure ozone has also to be considered in case of SiH surfaces.

In the previous century the plasma physics and chemistry have been studied and discussed in the literature very extensively. The following first chapter simply consists of several for this work relevant topics summarized from educational books, lectures, and review articles. In the last section of the first

chapter an introduction to oxide film formation will be given.

Chapter 1

Plasma - a tool for material engineering

This chapter is devoted to general remarks on the plasma physics and chemistry, special attention is paid to the modifications of passive films on metal and semiconductor surfaces induced by a plasma treatment. The content should give an overview over the basic relations and selected current literature concerning these topics.

1.1 General remarks

Plasma processing is applied mostly for thin film deposition or etching of surfaces [7, 20, 30]. The aim of this work was to use the plasma surface interaction to induce a change of the surface chemistry with a significant effect for the following surface processes. Relevant basic principles of plasma chemistry and physics will be summarized in this section.

In spite of the fact, that plasma is actually the most common phase of matter, it was discovered by Sir William Crookes in 1879 as the last one, finally it was Irving Langmuir in 1928 who assigned the term "plasma" [18, 22]. Flame, lightning, interstellar nebulae, stars are all examples of the plasma

state of matter. The physical properties of plasmas are mainly influenced by free charge carriers, free electrons and ionized atoms or molecules, which exhibit collective behavior due to the long-range Coulomb forces. However, certain criteria have to be considered for the definition of a plasma. In spite of free charge carriers a plasma is in the absence of external disturbances macroscopically neutral. An important physical parameter to describe a plasma is the Debay length λ_D. It is the distance, over which the influence of the electric field of an individual charged particle is felt by other charged particles inside the plasma. In a sphere with the radius λ_D mobile charge carriers screen out the electric field of an individual charged particle. The Debey length is directly proportional to the square root of the temperature T and inversely proportional to the square root of the electron number density n_e:

$$\lambda_D = \left(\frac{\epsilon_0 k_B T}{n_e e^2} \right)^{1/2} \tag{1.1}$$

A characteristic dimension of a plasma L has to fulfill the condition:

$$L >> \lambda_D \tag{1.2}$$

Furthermore, a collective particle behavior inside a Debey sphere is only ensured, when the number of charge carriers inside is very large:

$$N_D = \frac{4\pi}{3} \lambda_D^3 n_e >> 1 \tag{1.3}$$

An other important parameter is the plasma frequency, which describes the frequency of oscillations of charged particles caused by external disturbance of the equilibrium condition. Since these are high-frequency oscillations, the heavy-mass ions are unable to follow the motion of electrons. Thus, the electrons oscillate collectively around the ions to hold the quasi-neutrality. Based on this consideration of the collectively oscillating electrons as a surface

charge, which is deflected by the stationary ions with a shift δ, the electric field can be written as

$$E = \frac{1}{\epsilon_0} e n_e \delta. \tag{1.4}$$

The plasma frequency ω_p results from the equation of motion of the electrons driven by this field to

$$\omega_p = \left(\frac{n e^2}{\epsilon_0 m} \right)^{1/2}. \tag{1.5}$$

In order to collisions between the electrons and neutral particles would damp the collective oscillations, it is necessary that the collision-frequency is smaller than the electron plasma frequency, this condition results in

$$\omega\tau >> 1, \tag{1.6}$$

where τ represents the average time between subsequent electron-neutral collisions. Equations 1.2, 1.3 and 1.6 represent the basic characteristics of various laboratory and cosmic plasmas [5, 29].

1.2 Glow discharge

Considering the thermal energy of a plasma E_{th} and introducing the Coulomb coupling constant $\Gamma = \frac{E_{pot}}{E_{th}}$ and the degeneracy parameter $\Theta = \frac{E_{th}}{E_F}$, where E_{pot} is the potential energy between two charged particles in a plasma and E_F the Fermi energy of the electrons, several categories of plasmas can be distinguished. The plasma is nearly ideal by $\Gamma \ll 1$ weakly non-ideal by $\Gamma \leq 1$ and strongly coupled by $\Gamma > 1$, furthermore the electron system is non-degenerate by $\Theta > 1$ or degenerate by $\Theta < 1$. Is the thermal energy even in the range of the rest mass of the corresponding particle, the plasma becomes relativistic. Some prominent examples for non relativistic plasmas are shown in figure 1.1 in terms of a density-temperature dependency. According to the definitions of Γ and Θ the border line between the the ideal

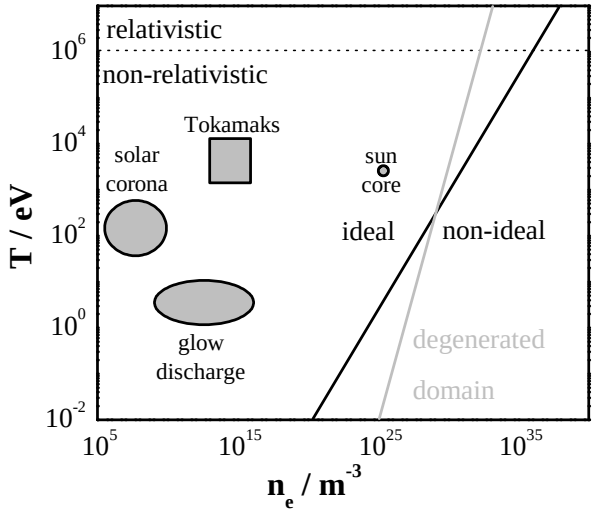

Figure 1.1: Density-temperature plane of plasmas, classified in domains depending on the thermal energy of the plasma, with some typical examples for the non-relativistic case [23, 29].

and non-ideal regime follows the relation $T \propto 1/n_e^{1/3}$ the corresponding relation for the border line between the degenerate and non-degenerate regimes is $T \propto 1/n_e^{2/3}$.

The region of glow discharges was highlighted in the picture, as these kind of plasmas has to be highly considered for the here presented work. Glow discharges are commonly described as discharges in which the cathode emits electrons, due to a bombardment of particles and photons from the gas volume [28]. Glow discharges represent the category of low temperature plasmas, where the temperature of the ions remains at the room temperature, while the temperature of the electrons is much higher (see the y-axis in figure 1.1). Furthermore, the degree of ionization in low temperature plasmas is signifi-

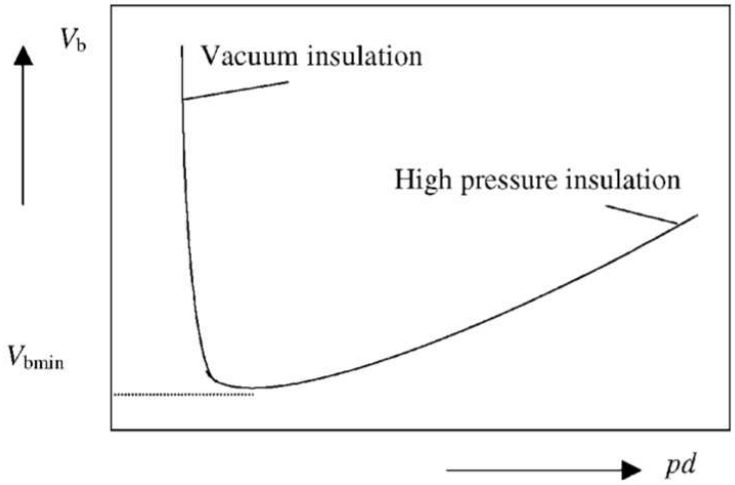

Figure 1.2: Schematic breakdown curve for a parallel plate (Paschen's law) [6].

cantly smaller than one. For the ignition of a self-sustained glow discharge in a gas filled volume the electrons have to be accelerated within the mean free path to a kinetic energy, which is high enough for ionization by colliding with neutrals. This requirement results in the Paschen's criterion for the breakdown voltage in a gas filled volume inside of a parallel plate configuration, dependent on the gas pressure p and distance d between the plates:

$$V_b = \frac{Bpd}{\ln Apd - \ln\left[\ln\left(1+\gamma^{-1}\right)\right]} \tag{1.7}$$

γ is the second Townsend coefficient, which describes the coupling of the ion-current to the generation of secondary electrons from the negative electrode, A and B are constants. The Paschen's law depends on on the gas species and the electrode material, more precisely on the work function of the used electrode material, since the work function affects the emission of secondary electrons.

Equation 1.7 results in the so called Paschen's curve as outlined in figure 1.2. At large pd, V_b increases due to the high-pressure insulation of the gas. At

some critical lower value of pd the value of V_b becomes infinite, due to the vacuum insulation. In between the relationship runs through a minimum [6, 29]. Contrary to the DC discharges described above, in plasmas at high-frequency (RF, 13.56 MHz) the electrode surface processes are of minor importance. The audio frequency plasma, as used in this work (4 kHz) is much more comparable to a pulsed DC discharge, than to a RF plasma. However, the breakdown conditions are comparable for DC and AC plasma excitation.

1.3 Plasma-solid interactions

As was denoted before, plasma-chemical process involving the interaction with a solid surface can be divided in three main categories. The first category is the plasma assisted removing of material from the surface, which can involve chemical etching or physical ablation (i.e. sputtering). The second category is the probably most widespread plasma enhanced chemical vapor deposition (PE-CVD). Here a solid surface becomes commonly covered with a very thin film formed due to an adsorption of molecules, which were activated in a discharge containing any kind of precursors and mostly an additional carrier gas. The third category of an interaction of a plasma with a solid is the modification of a surface without a noticeable removing of substrate material from the sample, or adding a different material to the treated surface. Here the outermost sample surface becomes slightly modified, by chemical reactions with reactive species from the plasma, due to exposure to the radiation, or by impact of particles with a certain momentum and kinetic energy. This third category of plasma-solid interactions is the most important for the here presented studies.

From the plasma physics point of view the modifications on surfaces caused by an interaction with a plasma are a special case and normally of course

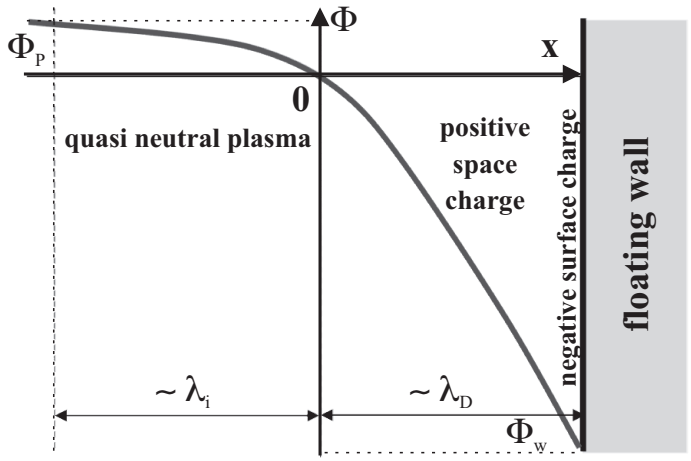

Figure 1.3: Potential structure in the plasma sheath, assuming a floating wall.

a desired effect of the broadly field of plasma-wall interactions. As mentioned above electrons are much more movable than the heavy-mass ions, therefore these hit surfaces exposed to the plasma first. Provided a floating surface, the conditions arrange as showed in figure 1.3. A positive space charge sheath occurs at the plasma-surface boundary. The dimension of this sheath is in the range of the Debey length λ_D (see section 1.1). To achive this space charge sheath, ions have to exceed a minimum velocity v_0, the so called Bohm-velocity v_B:

$$v_0 > \sqrt{\frac{k_B T_e}{M}} = v_B, \tag{1.8}$$

where k_B is the Boltzmann's constant, T_e the electron temperature, and M the mass of the ion. To achieve the Bohm-volocity the ions have to be accelerated in the adjoining sheath of quasi-neutral plasma with a dimension of the mean free path for the ions λ_i. Two characteristic potentials result from the conditions described above, the floating potential of the exposed

surface Φ_W, caused by equal ion and electron fluxes to the surface, and the plasma potential Φ_P resulting from the potential difference between the plasma volume and the border of the positive space charge sheath.

The flux of neutral atoms and molecules in exited states (e.g. radicals) is also important for the plasma-surface chemistry. The transport of neutrals in a plasma is determined by the diffusion processes. The density of neutrals in the vicinity of a surface depends strongly on the reactivity of the surface to the considered species.

1.4 Introduction to plasma induced oxide film formation on metals and semiconductors

One of the advantages of the plasma chemistry assisted modifications of surfaces is, that commonly the plasma processes happen at low temperature and therefore any thermal stress of the sample can be excluded. To understand the specific effect of an ionized gas to the oxide formation or to a further modification of an existing oxide film, an overview to the oxide film formation on semiconductors and metals will be given in the following section.
An summary of the more current studies on the plasma induced modifications of oxide films on materials relevant for the here presented work will be given in section 1.4.2.

1.4.1 Low temperature oxidation of metals and semiconductors

Fundamental studies concerning the oxidation of metals, in particular the formation thin films at low temperatures were done in the mid-20th century, supported by the further development of ultra-high vacuum techniques. Rep-

resentative for many groups, which have published results on special topics in this field, a couple of authors will be cited in this work, who have developed and reviewed the basic principles of the oxide film formation process. The following discussion is based on the book of Fehlner [11] and the review article of Lawless [19] concerning the oxidation of metals. In particular the work of Fehlner was focused on the low temperature oxidation.

Based on the assumption of the formation of a pure oxide film, the chemical reaction is very simple:

$$x\mathrm{Me} \; + \; \frac{1}{2}y\mathrm{O}_2 \; \rightleftharpoons \; \mathrm{Me}_x\mathrm{O}_y \tag{1.9}$$

The driving force for this reaction is the change of free energy, due to the formation of the oxide films. However, this free energy change does not directly determine the rate of the reaction. The kinetic of the oxide formation is determined by phase boundary reactions and diffusion processes. The diffusion of species across an already formed layer depends on an electric field established over the thin film, and on a chemical potential across the oxide as well.

Assuming a bare metal or semiconductor surface the first process, which occurs in the presence of a gas is the adsorption of molecules or atoms. Two types of adsorption have to be distinguished, physical adsorption and chemisorption. The latter is a chemical reaction and involves rearrangement of valence electrons. The physical adsorption depends on the rate of collisions of the gas molecules and the solid surface, as well as on the sticking probability. Among others, the rate of collisions is determined by the gas pressure. Assuming a sticking coefficient of unity and room temperature, a bare metal surface becomes covered by a monolayer of adsorbed gas at 10^{-6} mbar in approximately 1 s.

In case of oxygen as adsorbate, the chemisorption process consists of the

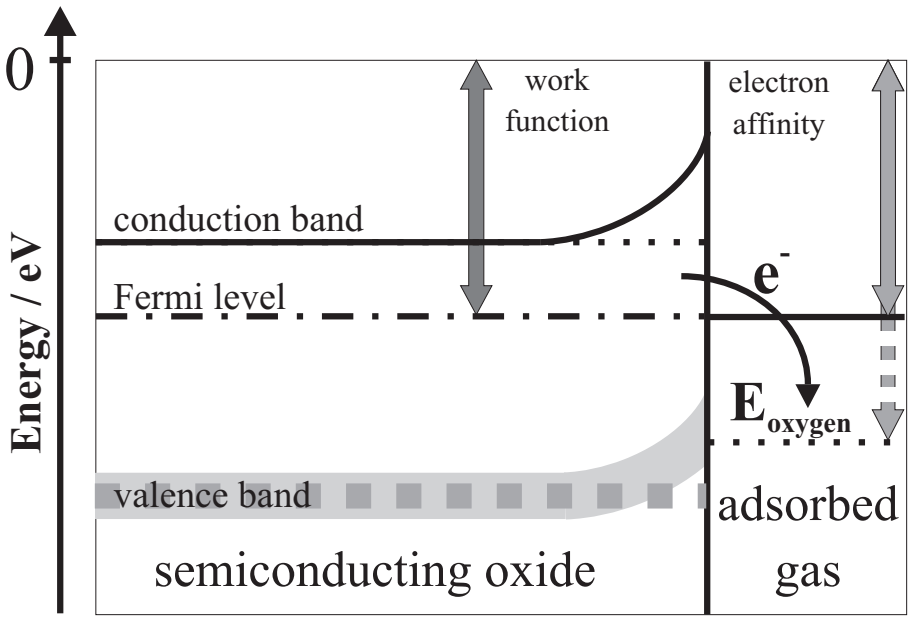

Figure 1.4: Schematic draw of the band bending of the electronic structure of a semiconducting oxide with a certain Fermi level and work function Φ, caused by the adsorption of a gas with a high electron affinity α (i.e. oxygen), dotted lines show the situation before, continuous after the electron transfer.

dissociation of the oxygen molecule and partial ionization of the atoms. Subsequently, the oxygen becomes incorporated in the outermost metal layer, possibly by a place exchange of metal and oxygen ions. The initial oxide growth is supposed to begin at surface defects in terms of oxide nuclei, which grow to oxide islands and finally to a closed oxide film. Ordered oxide structures are known to grow on iron, contrary to the amorphous oxides formed on aluminum, silicon and zinc [19, 27].

Since most oxides are semiconductors, the chemisorption of gas molecules or atoms on compact films becomes influenced by defects as sources for charge carriers. Figure 1.4 shows schematically the process for a n-type semiconductor with a certain Fermi level and work function Φ, and oxygen as adsorbing

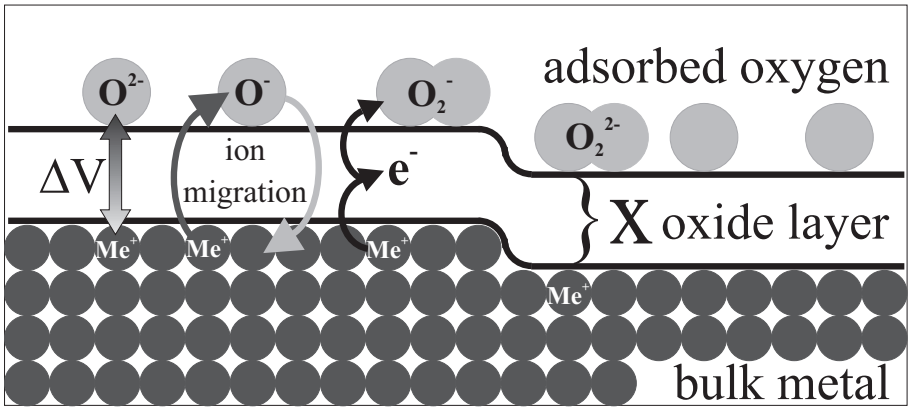

Figure 1.5: According to the Cabrera and Mott theory of the oxidation of metals, electron transfer from the metal atom to the oxide and from the oxide to the adsorbed oxygen (chemisorption), followed by a migration of the corresponding ions across the oxide layer, driven by the electrical field [21].

species. Due to the high electron affinity of oxygen α, an electron transfers from the conduction band of the semiconducting oxide to the adsorbed molecule or atom, if the molecule was dissociated. The electron depletion in a boundary layer with a certain length L induces a bending of the valence and conduction bands to higher energy levels in this surface near region. An energy barrier results and limits the chemisorption process.

Once a continuous oxide film has formed on the surface, the metal and gas ions become spatially separated by a barrier and the reaction can continue only, when ions and electrons diffuse to or through the formed oxide film. Figure 1.5 illustrates the processes for oxygen as adsorbate as were discussed by Mott [21] . The adsorbed oxygen becomes dissociated to some extend and ionized. The resulting potential difference ΔV induces electron transfer to the conducting layer of the oxide and ion migration. Notably migration of cations from the bulk metal or anions from the adsorbed species across the oxide layer depends on the materials, a table with so called ionic transport

numbers can be found by Fehlner [11] (table 4.1, page 68) for some metal oxides. The thermal oxidation of copper is fully determined by the cation migration, on the contrary the anodic oxidation of silicon occurs by over 95 % migration of the anions, low temperature oxide formation on zinc surfaces is as well determined by the anion migration [27]. In case of anodic oxidation of aluminum the ratio of cation and anion migration is balanced.

Assuming an energy barrier $W(x)$, which has to be overcome by the migrating species, and that the potential difference ΔV results in an electric field F, which lowers the energy barrier, the oxide growth rate can be expressed by

$$\frac{dx}{dt} = N\nu\Omega exp\left(-\left|\frac{W(x) - \frac{1}{2}|q|aF(x)}{k_B T}\right|\right), \tag{1.10}$$

where ν is the phonon frequency, Ω the volume of oxide created per oxidizing species, with the charge q and the jump distance a.

Following the extension of the Cabrera-Mott theory developed by Fehlner and Mott [12], the anion and cation migration leads to two different solutions of time dependent oxide thickness growth as described by equation 1.10. The migration of cations leads to a constant potential across the oxide film, due to fixed oxygen anions at the oxide/gas interface, which are responsible for the build-up of the field. Contrary, the anion transport leads to a constant field inside the oxide. When cation migration prevails an inverse logarithmic kinetic law results for the oxide growth, following the integration of Ghez [13] of the Cabrera-Mott equation. In case of anion migration, it is assumed that an incorporated oxygen ion at the oxide/gas interface first crosses an energy barrier, which decreases in the presence of an electric field. The electric field across the oxide is considered to remain constant, and an increase of activation energy for ion transport has to be assumed. This results in an

increasing barrier for ion entry into the oxide and a direct logarithmic law for oxide growth follows:

$$x = x_0 \log((t/\tau) + 1). \tag{1.11}$$

It should be mentioned at this point, that in practice both laws for the oxidation rate, direct and inverse logarithmic, are very difficult to distinguish.

1.4.2 Formation and modification of thin oxide films by means of plasmas

Already in the early fifties of the 20th century studied Engell and Hauffe the chemisorption of oxygen on nickel oxide [10] and found out, that the chemisorption process was promoted by using of an ionized gas [9]. The explanation of this behavior was given by the assumption of an increased chemical potential of oxygen due to the excitation in the plasma and associated to this a significantly higher electron affinity, which implicates the possibility of the build-up of a larger space charge region as discussed in the previous section.

According to the considerations reviewed in section 1.4.1, in particular the dependence of oxide formation on the oxidation state of the oxygen and the electrical field adjusted across the already formed layer, it becomes obvious to apply plasmas to control and to intensify the oxide modification processes. More recently Grundmeier and co-workers have studied the modification of native oxide films on iron and zinc samples by oxygen and argon plasmas as pretreatment methods to adjust a certain surface chemistry before further surface treatments were performed [15, 17, 1]. The complementary application of in-situ (IRRAS, QCM) and ex-situ (SKP, XPS) techniques allowed the observation and characterization of an oxide growth on iron during an

oxygen plasma treatment at room temperature, as well as a further modification of the formed oxide layer by a subsequent argon plasma without an observable decrease of oxide thickness, but with a considerable change of the ratio of the density of the oxidation states of iron Fe^{2+}/Fe^{3+} across the oxide layer. The developed dependence of the Volta potential difference to the activities of the corresponding oxidation states after certain plasma treatment

$$\Delta(\Delta\Psi_{\mathrm{Ox}}^{\mathrm{Ref}}) = \frac{RT}{F} \ln\left(\frac{a_{Fe^{2+}}(\text{plasma 1})}{a_{Fe^{2+}}(\text{plasma 2})}\right), \tag{1.12}$$

could be proved by SKP measurements [16]. The effects of the plasma pretreatment to the chemistry and electronic structure of the modified iron oxide, as well as the cleaning effect of the discharge to the surface, were used in other studies to obtain a strong adhesion of thin plasma polymers to the iron surface and to demonstrate excellent properties of the system with regard to electrochemical corrosion resistance.

Comparable experiments on zinc surfaces have shown, that all studied kinds of plasmas are able to remove the hydrocarbon contamination layer from a native zinc oxide, but water, oxygen, carbon dioxide and hydrogen plasmas led to slightly different modifications of the oxide chemistry [24]. Further studies on plasma modified and subsequent plasma polymer coated zinc substrates have shown that delamination rates of coatings were significantly decreased, therefore these systems were identified to be promising for design of highly stable polymer/metal interfaces [14, 26]. Bellakhal et al. investigated the influence of humid-air plasma in comparison to pure oxygen plasma treatment on brass and pure zinc samples and found by means of electrochemical methods a complex oxidation mechanism, involving a first formation of a precursor copper oxide Cu_xO and ZnO with a subsequent formation of Cu_2O and CuO. The resulted oxide composition was comparable to those resulting

from thermal treatments [8, 3, 2].
The corrosion resistance of an industrial magnesium alloy (AZ31B) could be significantly increased by plasma oxidation in oxygen and water plasmas. Corresponding electrochemical studies, Rutherford backscattering spectrometry and X-ray diffractometry at grazing incidence results were published by Tian and co-workers [25].
Bertrand et al. have studied the influence of a hydrogen plasma excited by means of microwaves at 2.45 GHz to native oxide films on stainless steel and aluminum. Using in-situ IR-ellipsometry it could be shown, that the native oxide on the stainless steel was almost completely reduced in a hydrogen plasma. In contradiction to this, the aluminum surface was more resistant and only the outermost hydroxylated part of the oxide layer could be reduced. It was also observed, that a dense oxide layer could be grown on the pretreated steel surface by a subsequent oxygen plasma [4].

The composition of the oxide layer covering the base metals and semiconductors is crucial for the behavior of the system during subsequent processing of the surface, in particular with regard to adhesion of any kind of coatings. All studies, presented above demonstrate the ability of a significant modification of the oxide chemistry on the corresponding materials by means of low temperature plasmas. Due to the undefined influence of the ambient atmosphere on the often very sensible conditions on plasma modified surfaces, the applying of in-situ techniques is essential for a deep understanding of the oxidation mechanism in a plasma.

1.5 References

[1] V. Barranco, P. Thiemann, H. K. Yasuda, M. Stratmann, and G. Grundmeier. Spectroscopic and electrochemical characterisation of thin cathodic plasma polymer films on iron. *Applied Surface Science*, 229(1-4):87–96, 2004.

[2] N. Bellakhal and M. Dachraoui. Electrochemical investigation of the oxides formed at the surface of brass (Cu-10Zn) by a humid-air plasma treatment. *Materials Chemistry and Physics*, 82(2):484–488, 2003.

[3] N. Bellakhal, K. Draou, and J. L. Brisset. Plasma and wet oxidation of (63Cu37Zn) brass. *Materials Chemistry and Physics*, 73(2-3):235–241, 2002.

[4] N. Bertrand, P. Bulkin, B. Drevillon, S. Lucas, and S. Benayoun. In situ infrared ellipsometry study of plasma processing of metallic surfaces. *Surface & Coatings Technology*, 94-5(1-3):362–367, 1997.

[5] J. A. Bittencourt. *Fundamentals of plasma physics*. Pergamon Press, Boston, 1986.

[6] N. S. J. Braithwaite. Introduction to gas discharges. *Plasma Sources Science & Technology*, 9(4):517–527, 2000.

[7] R. D'Agostino. *Plasma deposition, treatment, and etching of polymers*. Acad. Press, Boston, 1990.

[8] K. Draou, N. Bellakhal, B. G. Cheron, and J. L. Brisset. Preparation of zinc oxide films by oxygen plasma treatment of zinc foils. *Materials Chemistry and Physics*, 51(2):142–146, 1997.

[9] H. J. Engell and K. Hauffe. Der Einfluss einer Gasentladung auf die Chemisorption von Sauerstoff an Nickeloxyd - (Zur Randschichttheorie der Chemisorption-II). *Zeitschrift für Elektrochemie*, 57(8):773–775, 1953.

[10] H. J. Engell and K. Hauffe. Die Randschichttheorie der Chemisorption - ein Beitrag zur Deutung von Vorgangen an der Grenzfläche Festkörper Gas. *Zeitschrift für Elektrochemie*, 57(8):762–773, 1953.

[11] F. P. Fehlner. *Low Temperature Oxidation: The Role of Vitreous Oxides*. John Wiley & Sons, New York, 1986.

[12] F. P. Fehlner and N. F. Mott. Low-temperature oxidation. *Oxidation of Metals*, 2(1):59–99, 1970.

[13] R. Ghez. Mott-Cabrera oxidation rate equation and inverse-logarithmic law. *Journal of Chemical Physics*, 58(5):1838–1843, 1973.

[14] G. Grundmeier, M. Brettmann, and P. Thiemann. In situ spectroscopic and corrosion studies of ultra-thin gradient plasma polymer layers on zinc. *Applied Surface Science*, 217:223–232, 2003.

[15] G. Grundmeier, E. Matheisen, and M. Stratmann. Formation and stability of ultrathin organosilane polymers on iron. *Journal of Adhesion Science and Technology*, 10(6):573–588, 1996.

[16] G. Grundmeier and M. Stratmann. Influence of oxygen and argon plasma treatments on the chemical structure and redox state of oxide covered iron. *Applied Surface Science*, 141(1-2):43–56, 1999.

[17] G. Grundmeier and M. Stratmann. Interfacial processes during plasma polymer deposition on oxide covered iron. *Thin Solid Films*, 352(1-2):119–127, 1999.

[18] I. Langmuir. Oscillations in ionized gases. *Proceedings of the National Academy of Sciences of the United States of America*, 14:627–637, 1928.

[19] K. R. Lawless. Oxidation of metals. *Reports on Progress in Physics*, 37(2):231–&, 1974.

[20] M. A. Lieberman and A. J. Lichtenberg. *Principles of plasma discharges and materials processing.* John Wiley & Sons, New York, 1994.

[21] N. F. Mott. The theory of the formation of protective oxide films on metals – 3. *Transactions of the Faraday Society*, 43(7):429–434, 1947.

[22] H. M. Mott-Smith. History of plasmas. *Nature*, 233(5316):219–&, 1971.

[23] R. Redmer. Physical properties of dense, low-temperature plasmas. *Physics Reports-Review Section of Physics Letters*, 282(2-3):36–157, 1997.

[24] N. J. Shirtcliffe, M. Stratmann, and G. Grundmeier. In situ infrared spectroscopic studies of ultrathin inorganic film growth on zinc in non-polymerizing cold plasmas. *Surface and Interface Analysis*, 35(10):799–804, 2003.

[25] X. B. Tian, C. B. Wei, S. Q. Yang, R. K. Y. Fu, and P. K. Chu. Water plasma implantation/oxidation of magnesium alloys for corrosion resistance. *Nuclear Instruments & Methods in Physics Research Section B-Beam Interactions with Materials and Atoms*, 242(1-2):300–302, 2006.

[26] T. Titz, F. Hörzenberger, K. Van den Bergh, and G. Grundmeier. Influence of ultra-thin plasma polymer films on the interfacial electrode potential and the corrosion resistance of polymer coated zinc. In preparation.

[27] W. H. J. Vernon, E. I. Akeroyd, and E. G. Stroud. Tie direct oxidation of zinc. *Journal of the Institute of Metals*, 65:301–329, 1939.

[28] A. von Engel. *Ionized Gases*. AIP Press, Woodbury, 1994.

[29] A. von Keudell. *Vorlesungsskript: Einführung in die Plasmaphysik*. Ruhr-Universität Bochum, 2005.

[30] H. Yasuda. *Plasma Polymerization*. Academic Press, Orlando, 1985.

Chapter 2

Experimental

2.1 Setup of the plasma chamber

For the in-situ studies of changes on surfaces treated by low-temperature plasmas, as presented in this work, a special experimental setup was developed. Informations concerning the gas supply, gas mixture, set of electrodes, samples etc. used for the different experiments are discussed in the respective chapter. General remarks independent of the special experiments will be presented in the following.

A schematic of this experimental setup is shown in figure 2.1. It consists of a vacuum chamber with moveable sample holder inside. At one position an electrode holder is located while at a second position the sample can be analyzed by Fourier transform infrared reflection-absorption spectroscopy (FT-IRRAS) and a Kelvin probe (KP). Different sets of electrodes allow the generation of low pressure remote and direct plasmas as well as atmospheric pressure dielectric barrier discharges in defined atmospheres. The pumping system consists of a rotary vane pump in combination with a turbo molecular pump. Prior to any vacuum processing of samples the chamber was evacuated to a base pressure of about 10^{-4} mbar. A commercial high volt-

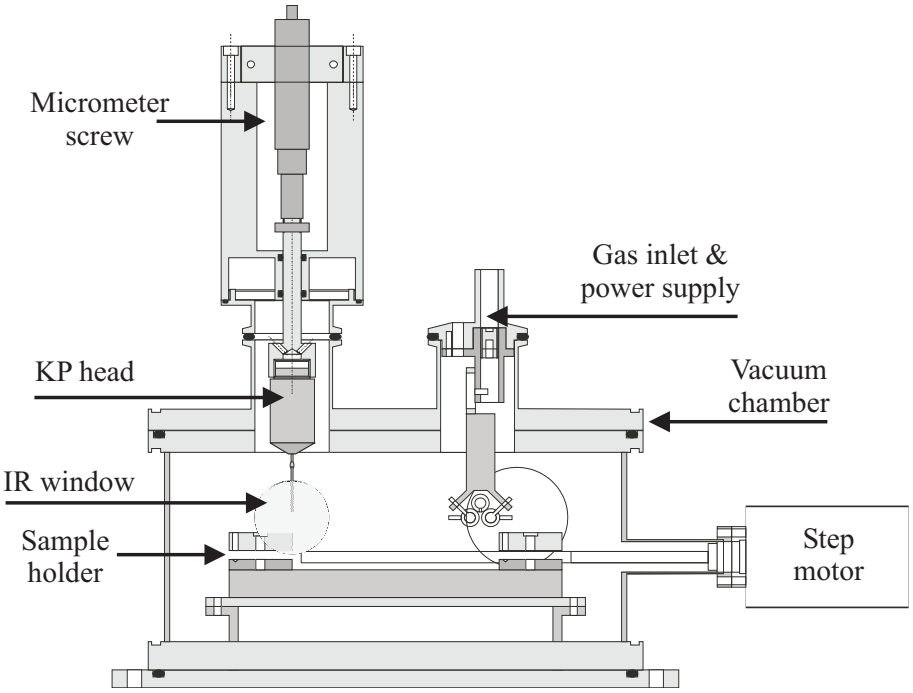

Figure 2.1: Experimental set-up for the application of in-situ FT-IRRAS and work function measurements subsequent to a plasma modification of a sample surface.

age power supply was used to apply an alternating, pulsable, and adjustable voltage with a frequency of 30.7 kHz to both electrodes in case of ignition of a plasma in the volume between electrodes and sample for so called direct modification of the sample surface. One electrode can be connected to ground for ignition of the plasma in the volume between the electrodes (rotated 90°, placed face to face), this configuration allows the so called remote plasma treatment of the sample surface. The high voltage pulse generator G2000 (Redline Technologies) supplies a sinewave voltage to a capacitive load. Frequency and amplitude of the output voltage can be adjusted independently. The output voltage can be periodically blanked by means of pulse packet modulation. The generator has an intermediate DC circuit with

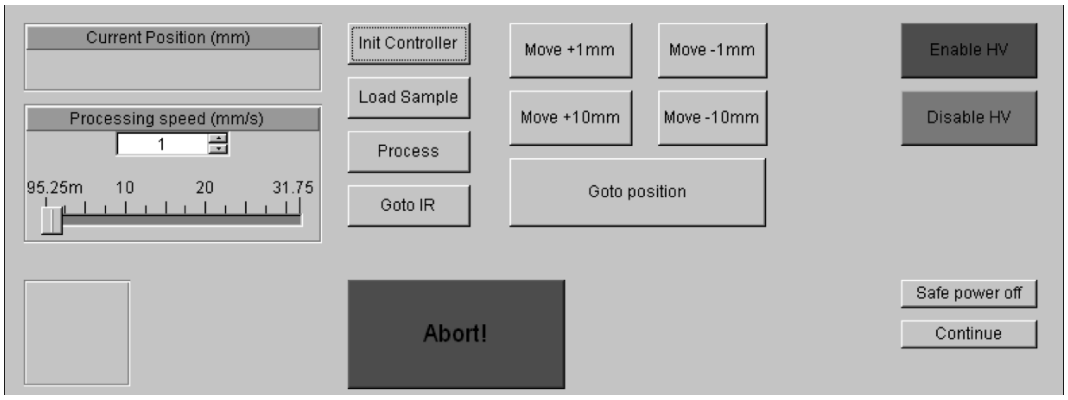

Figure 2.2: Screenshot of the input mask for the software based process control of the position and velocity adjustment of the sample along the chamber axis.

an adjustable voltage between 0 and 300 V (DC). The DC voltage feeds a short-circuit proof inverter which can be freely adjusted in pulse width and frequency. Thus the frequency can be set near to the resonance frequency of the load to achieve a maximum output voltage. For an accurate adjustment of the sample holder along the chamber axis at defined positions and in particular a adjustable velocity of moving through the plasma zone, a fine tunable step motor was implemented to the setup. Furthermore an appropriate computer process control was realized by a self-made simple software control over the RS232 interface. A screenshot of the input mask is shown in figure 2.2. The software was developed by means of Agilent VEE Pro 6.0 [9]. The sample can be moved with defined velocities between 0.1 and 30 mm/s through the plasma region to the diagnostic position, as well as positioned at any position along the traverse path. The software controls the interlock for the release of the power on modus of the power supply and is able to interrupt the high voltage in case of emergency.

2.2 In-situ polarization modulated FT-IRRAS

The diagnostic position of the chamber is centered between two ZnSe windows, which are part of the custom-designed optical path for the external infrared beam of a FTIR spectrometer (Biorad Excalibur 3000). The IR-beam is guided by a set of mirrors and transmitted through the ZnSe window onto the sample, reflected under 80° to the surface normal (so called grazing incidence), finally guided through the second window and by further mirrors to the LN_2 cooled mercury cadmium telluride (MCT) detector (see figure 2.3). Behind the second ZnSe window a linear polarizer is placed. This setup allows a discrete measurement of the polarization modes of the reflected infrared radiation. IRRAS of adsorbates at near grazing incidence on metals takes advantage of the fact that p-polarized light (parallel to the plane of incidence) is preferentially absorbed upon reflection, whereas s-polarized light is virtually unabsorbed, caused by a different phase shifts for s- and p-components of the incident radiation as a function of incident angle. At grazing incidence the phase shifts result in a node for s-polarized (electric field is zero) and an antinode for the p-polarized radiation. The absorption of the molecules of the surrounding medium is independent of the orientation of the electric field vector, due to the random orientation of the molecules in the gas (or liquid) phase. The application of polarization modulation allows to distinguish between the molecules like water and carbon dioxide in the gas phase and the change in the surface chemistry. Spectra are recorded in parallel (I_{lp} with adsorbed layer, I_{0p} without adsorbed layer) and perpendicular (I_{ls} and I_{0s}, respectively) polarizations. This results in two absorption spectra according to

$$A_p \;=\; -log_{10}\left(\frac{I_{lp}}{I_{0p}}\right) \tag{2.1}$$

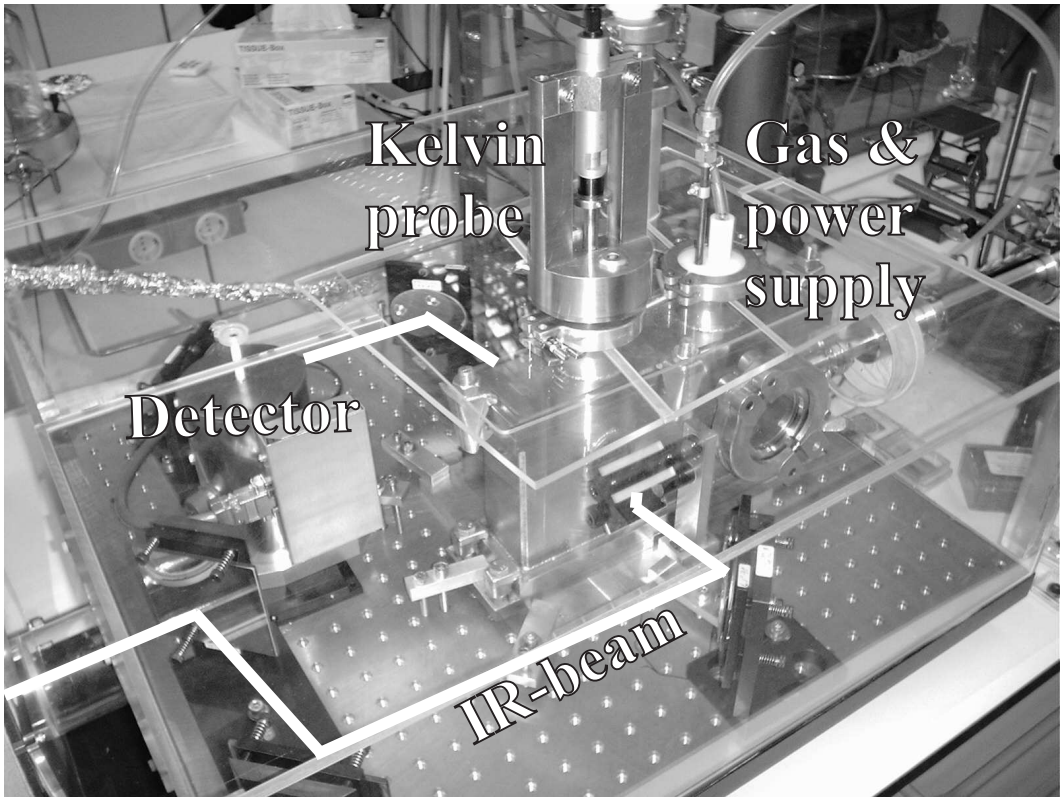

Figure 2.3: Picture of the plasma chamber placed in the optical path of the external IR-beam of a FTIR spectrometer.

and

$$A_s \;=\; -log_{10}\left(\frac{I_{ls}}{I_{0s}}\right) \tag{2.2}$$

where A_p is the absorption for parallel polarized light and A_s is the absorption for perpendicular polarized light (referred to the plane of incidence). The reflected radiation with parallel polarization vector consists the information of both the gas phase and the film absorption, while for the perpendicular part of the radiation the latter information is missing. The difference

$$A \;=\; A_p - A_s \tag{2.3}$$

therefore contains only the information of the absorption of the surface layer. Usually the polarization modulation is realized by means of a photoacustic modulator and switching the analyzed polarization plane with a frequency one order of magnitude higher than the frequency of the FTIR spectrometer. A more simple method is the discrete polarization modulation. Here, the spectra A_p and A_s are measured one after the other and will be subtracted subsequently [4]. A detailed description of the fundamentals of FT-IRRA spectroscopy can be found monographs and review articles [7, 14, 10, 11].

2.3 In-situ Kelvin probe

In the developed chamber, measurements of the plasma induced changes of work function by means of a Kelvin probe (KP) can be applied simultaneously to the FTIR analysis of the surface chemistry. The Kelvin probe is a non-contact, non-destructive vibrating capacitor device used to measure the work function difference, or for non-metals, the surface potential, between a conducting specimen and a vibrating tip [6]. The Kelvin probe is extremely sensitive to changes in the top-most atomic layers, such as those caused by absorption, corrosion and surface reconstruction. In some cases it can detect less than one-thousandth of an absorbed layer. The principle of the operating mode of a Kelvin probe is shown schematically in figure 2.4. The flat frontal area of the KP tip and the sample surface create a simple capacitor, with the capacitance

$$C = \frac{Q}{V} = \epsilon\epsilon_0 \frac{A}{d + \Delta d \sin \omega t}, \tag{2.4}$$

where ϵ and ϵ_0 are the dielectric constant and the permittivity of free space, A is the frontal area of the tip, d the distance between the surface and the tip and ω the frequency of the tip vibration. If an external contact is made

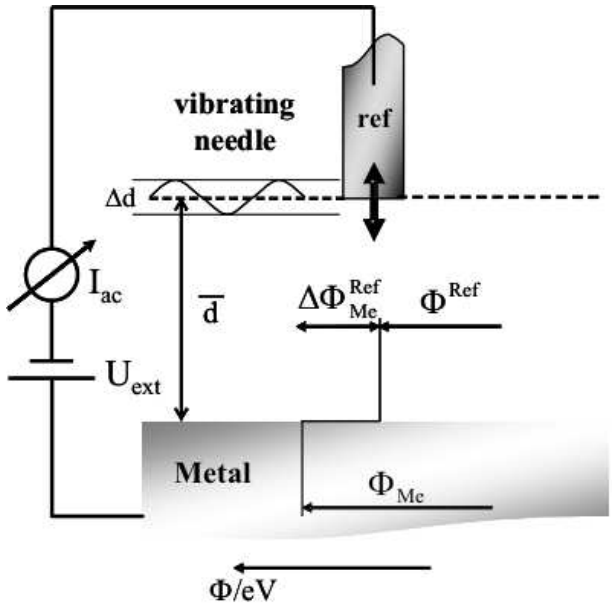

Figure 2.4: Schematic principle of the Kelvin probe technique, Φ represents the work function of the corresponding material.

between the two different materials of tip and sample, their Fermi levels equalize and the resulting flow of electrons from the metal with the lower to the metal with the higher work function (Φ) produces a contact potential difference V_{CPD}, between the electrodes

$$V_{CPD} \;=\; (\Phi_{Ref} - \Phi_{Me})/e \;=\; \Delta\Phi_{Me}^{Ref}/e. \tag{2.5}$$

This contact potential combined with the vibrating needle result in a current flow through the external contact, due to the periodical change of the capacitance with Δd and ωt (see eq. 2.4). By the substraction of an external voltage U_{ext} the resulting current I_{ac} can be expressed by

$$I_{ac} = (V_{CPD} - U_{ext}) \cdot \frac{dq}{dt}. \tag{2.6}$$

For the determination of V_{CPD} an $I_{ac} = 0$ has to be obtained, in this case is $V_{CPD} = U_{ext}$ [2, 3, 8]. Proper measurements of the contact potential differ-

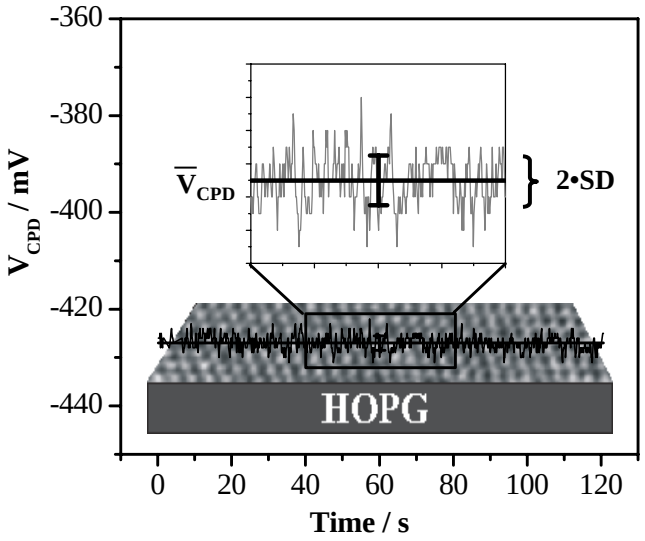

Figure 2.5: Contact potential difference of a graphite Kelvin probe tip and a HOPG surface measured over 120 s.

ences are possible only by using a tip material with a work function, which is stable under the measurement conditions, as becomes evident from the equation 2.6. Furthermore, determining work functions requires a known external reference for calibration of the Kelvin probe signal for each experiment. Highly ordered pyrolythic graphite (HOPG) was reported to be suitable as reference material for Kelvin probe measurements in air and vacuum as well [5]. The advantages of HOPG are to be a solid with no contaminating vapor, which is crucial for vacuum applications and to have a very weak tendency to build up adsorbate layers in air. For this reasons graphite seems to be appropriate to be used as external reference for calibration and as tip material as well. However, it is very difficult to produce tips with a diameter smaller than 0.5 mm with the required stiffness by using HOPG, therefore a previously heat treated graphite pencil lead (Staedler 2B marsmicro) with a diameter of 0.5 mm was used as KP tip. For all experiments 12 mm $\times$ 12 mm $\times$ 2 mm

samples of high quality HOPG with the lowest commercial available mosaic spread of 0.4° ± 0.1° were used (SPI supplies, Plano GmbH). Figure 2.5 shows a Kelvin probe signal obtained by a measurement with the pencil lead over a freshly cleaved HOPG surface. The measured Volta potential difference was stable over the measurement time of 120 s with a high signal to noise ratio represented by a standard deviation (SD) of 1.5 mV by a mean value of $V_{CPD} = -427$ mV. To illustrate the signal to noise ratio, a section of the signal was expanded to larger scale (small window in fig. 2.5). The x- and y-axis scales of the expanded diagram correspond to the lengths of the sides of the expanded section on the main figure axis. Furthermore, the graphite tip was measured versus a HOPG sample during an atmosphere change from nitrogen to oxygen and the behavior was compared to an evaporated gold surface. Figure 2.6 shows the result of these measurements. From this measurement of the HOPG surface it becomes evident, that the signal is stable over a much longer time than discussed above. For measurements on different surfaces presented in the following chapters relevant time scales are in the range of 60-120 s. The stability of the work function during the change of atmospheres by flushing the chamber by nitrogen first and oxygen subsequent is demonstrated in figure 2.6. No shift of the contact potential difference between the tip and the HOPG could be observed neither at time point of atmosphere change (450 s) nor afterwards. A compensation of opposing effects due to using graphite as tip material as well as measured surface could be excluded. The measured surface is graphite of highest purity and crystalline order, while the tip material is an amorphous mixture of graphite, clay and further additives. A comparable adsorption behavior of oxygen cannot be expected. In contradiction to the behavior of HOPG a potential drop of 600 mV was observed on a gold surface immediately after

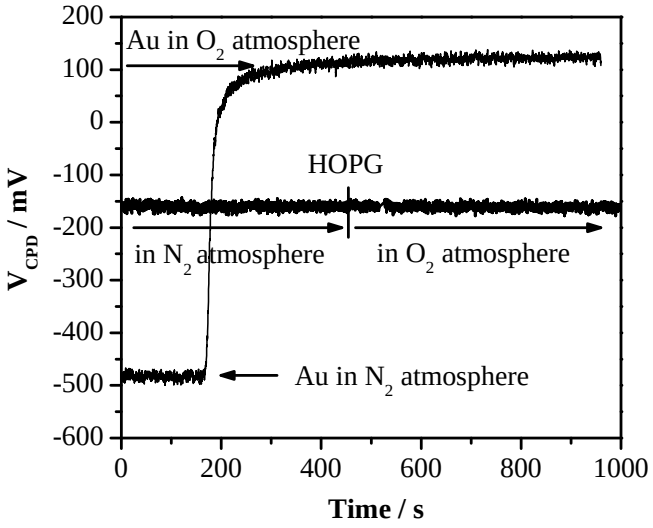

Figure 2.6: Contact potential difference of a graphite Kelvin probe tip and a HOPG surface compared to the signal of a graphite tip over a gold surface during an atmosphere change from N_2 to O_2.

the switch of the gas flow at 170 s. This potential shift is in accordance to the difference of the work functions of gold measured in vacuum and in air, as was reported in the literature [5]. Furthermore, it can be concluded based on the till now presented results, that the graphite pencil tip was proved to behave like HOPG with no tendency to build up adsorbate layers, due to atmosphere change from nitrogen to oxygen and seems to be the suitable tip material for the Kelvin probe.

The measured potentials shown in figures 2.5 and 2.6 were not corrected by the true value of the HOPG work function, due to the characteristic of the potential over the measurement time was in the focus of interest not the absolute values of work functions. Focus of the KP studies presented in the

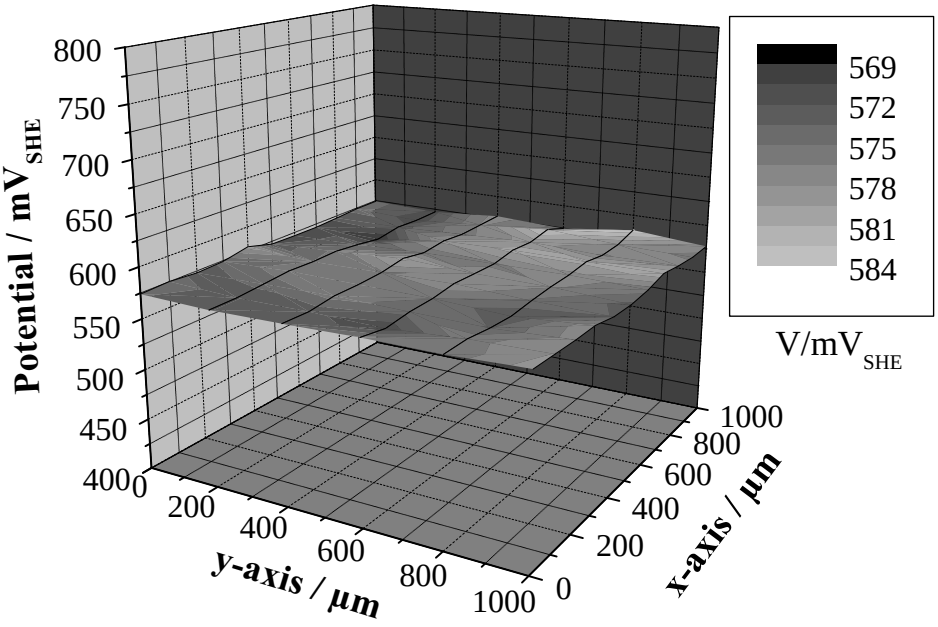

Figure 2.7: Scanning Kelvin probe measurement of the contact potential difference to a NiCr/Ni tip in a dry nitrogen atmosphere.

chapters 3 and 5 lies on the potential of the analyzed surfaces vs. the potential of a standard hydrogen electrode (SHE), due to the comparability of the results to other surface corrosion studies. Thus, the surface potential of the used HOPG sample was measured by means of the scanning Kelvin probe, which is calibrated by the standard electrode potential of a saturated Cu^{2+} solution in a Cu cup. The Cu/Cu^{2+} system is known to have the standard electrode potential value of 0.34 V vs. SHE [1]. The SKP measurement of the HOPG surface in a dry nitrogen a atmosphere by means of NiCr/Ni tip gives a potential difference of 0.575 V as is shown in figure 2.7. A calibration measurement of the tip over the Cu/Cu^{2+} system gives a V_{CPD} value of 0.455 V. The resulting standard potential of HOPG vs. SHE is 0.46 V. The homogene-

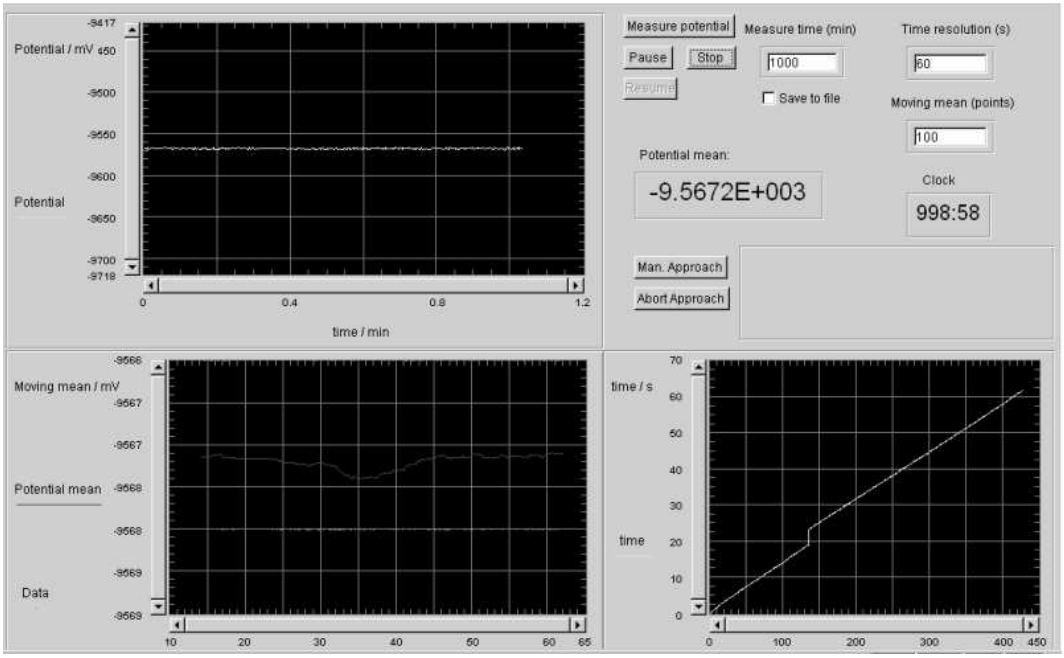

Figure 2.8: Screenshot of the input mask for the software based process control of the in-situ Kelvin probe measurements.

ity of potential mapping over a surface area of 1000 μm $\times$ 1000 μm on the HOPG sample (with a distance between the scanning lines of 200 μm) shown in figure 2.7 underlines the previous statement of the suitability of HOPG as reference material for Kelvin probe measurements. Before the end of the Kelvin probe section a remark concerning the measurement control should be given. Figure 2.8 shows a screenshot of the self-developed software, by using Agilent VEE Pro 6.0 (same as for the step motor control). The software processes data delivered by the control system of the Kelvin probe consisting of a lock-in amplifier, integrating circuit, and power supply unit. The output screen displays the measured V_{CPD} value over the measurement time, the moving mean value over the measurement time, and a mean value of the V_{CPD} over a defined time range. The input mask allows to adjust the mea-

surement time, the number of measurement points for calculating the moving mean, and the time resolution for the mean value calculation. The measured data can be saved as ASCII files for further processing and reporting. Details concerning the control system of the KP mentioned above were reported by Wapner et al. for a more advanced hight-regulating scanning Kelvin probe for atmospherical corrosion studies, but the principle of the KP operating mode is the same [13, 12].

All conclusions based on the results obtained by using the in-situ techniques as described in this section were additionally confirmed by applying complementary ex situ techniques. The different methods (e.g. XPS, SKP, etc.) will be mentioned for each experiment in the experimental details sections of the respective chapter.

2.4 References

[1] P. W. Atkins. *Physikalische Chemie*. VCH Verlagsgesellschaft mbH, Weinheim, 1996.

[2] I. D. Baikie and P. J. Estrup. Low cost PC based scanning Kelvin probe. *Review of Scientific Instruments*, 69(11):3902–3907, 1998.

[3] I. D. Baikie, U. Peterman, B. Lagel, and K. Dirscherl. Study of high- and low-work-function surfaces for hyperthermal surface ionization using an absolute Kelvin probe. *Journal of Vacuum Science & Technology A*, 19(4):1460–1466, 2001.

[4] G. Grundmeier, E. Matheisen, and M. Stratmann. Formation and stability of ultrathin organosilane polymers on iron. *Journal of Adhesion Science and Technology*, 10(6):573–588, 1996.

[5] W. N. Hansen and G. J. Hansen. Standard reference surfaces for work function measurements in air. *Surface Science*, 481(1-3):172–184, 2001.

[6] Lord Kelvin. *Philosophical Magazine*, 46:82–120, 1898.

[7] Y. P. Song, M. C. Petty, and J. Yarwood. Effects of polarization of infrared-spectra collected in reflection at grazing-incidence. *Vibrational Spectroscopy*, 1(3):305–309, 1991.

[8] N. A. Surplice and R. J. Darcy. A critique of Kelvin method of measuring work functions. *Journal of Physics E-Scientific Instruments*, 3(7):477, 1970.

[9] Agilent Technologies. http://www.agilent.com. 2004.

[10] V. P. Tolstoy. *Handbook of infrared spectroscopy of ultrathin films*. John Wiley & Sons, 2003.

[11] M. W. Urban. *Vibrational spectroscopy of molecules and macromoleules on surfaces*. John Wiley & Sons, 1993.

[12] K. Wapner. *Grenzflächenchemische und elektrochemische Untersuchungen zur Haftung und Enthaftung an modifizierten Klebstoff/Metall-Grenzflächen*. PhD thesis, Ruhr-Universität Bochum, 2006.

[13] K. Wapner, B. Schoenberger, A. Stratmann, and G. Grundmeier. Height-regulating scanning Kelvin probe for simultaneous measurement of surface topology and electrode potentials at buried polymer/metal interfaces. *Journal of the Electrochemical Society*, 152(3):E114–E122, 2005.

[14] J. T. Yates. *Vibrational spectroscopy of molecules on surfaces*. Plenum Pr., 1987.

Chapter 3

Combination of FTIR spectroscopy and work function measurements for in-situ studies of plasma modification of model polymer and iron surfaces

3.1 Introduction

In recent years cold plasmas have been used to modify polymer and metal substrates in different ways to achieve functional properties on material surfaces [11, 6, 1]. In most cases ultra-thin surface layers determine the properties of the modified system. In case of surfaces of engineering materials such as iron, aluminium or zinc ultra-thin metal oxide or hydroxide films cover the metal. The chemical composition and the electronic properties of the surface oxides strongly influence the corrosion behaviour of the metal as well as their interaction with organic molecules and water [5]. In case of polymeric substrates, the chemical composition, density and orientation of

polar groups which are introduced in non-polar substrate surfaces by means of plasma modification are of interest [2]. In most cases, surface chemical changes induced by plasma modification are investigated ex-situ; that means that the reactive surface is exposed to undefined environments which contain organic molecules (e.g. long chain aliphates) water, oxygen and carbon dioxide. These species lead to a change in the surface chemistry and ex-situ FTIR spectroscopy, x-ray photoelectron spectroscopy (XPS) or time-of-flight secondary ion mass spectrometry (ToF-SIMS) are thus not really showing the surface situation directly after the plasma modification. This has led to few works on the investigation of plasma processes in-situ [10, 7, 14] in which in-situ FTIR-spectroscopy was applied. The Kelvin probe (KP) technique was employed to measure changes of oxidation states of plasma modified passive films on iron [5]. However, in-situ measurements after plasma modification were not yet possible. In the here presented work, the newly developed system was applied to investigations of iron oxidation and the introduction of polar groups in self-assembly films of octadecylmercaptane on gold.
Parts of the here presented results were published in 2005 by Raacke, Giza, and Grundmeier in Surface Coatings Technology [8].

3.2 Experimental details

The experimental setup for the plasma modification and subsequent in-situ FT-IRRAS and KP studies was already described in chapter 2. Gold coated glass samples (250 nm Au / 2 nm Cr / Tempaxglass) were used as substrates. The adsorption of the ODM was performed from a $2{\cdot}10^{-3}$ M ethanol solution. The gold surface was flame annealed before the self-assembly monolayer was adsorbed to obtain mono-atomically flat terraces with Au(111) orientation. For the in-situ investigation of plasma induced reactions on iron surfaces, a

250 nm thin iron layer was evaporated on top of the gold surface. All plasma treatments were done at 0.3 mbar partial pressure. The polycrystalline iron film was first treated with a reducing hydrogen plasma to at least partially remove its native oxide layer. The sample was moved with a velocity of 0.1 mm/s through the plasma zone, what results in a treatment time of 380 s. Subsequently, the surface was exposed to an oxygen plasma and finally to an argon plasma. To be able to compare the water plasma effect with the oxygen effect, the sample was reduced again in hydrogen plasma before the water plasma was applied. After each of these steps an infrared spectrum was recorded and the surface potential was investigated with the Kelvin probe.

3.3 Results and discussion

3.3.1 Surface oxidation of iron

In figure 3.1 the surface oxidation process on evaporated iron is investigated in pure oxygen and water plasmas at 0.3 mbar by means of in-situ IRRAS. Since an iron surface consists of a native iron-oxyhydroxide with a thickness of about 2–3 nm, it was removed at least partially by the hydrogen plasma. In the case of a pure oxygen plasma, a strong positive peak of Fe_2O_3 is observed after the plasma modification accompanied by negative peaks in the $CH_{2,3}$-stretching region which indicates a removal of residual organic surface contaminations. Additionally, some smaller signals of FeOOH are visible, mainly because of desorbed water from the walls of the chamber. This was proven by treating the sample with a water plasma. This produces dominantly oxyhydroxide films and results in stronger absorption bands around 1100 and 1630 cm^{-1}. A subsequent argon plasma application leads to negative absorption bands in the spectrum. Furthermore, the shape of the band

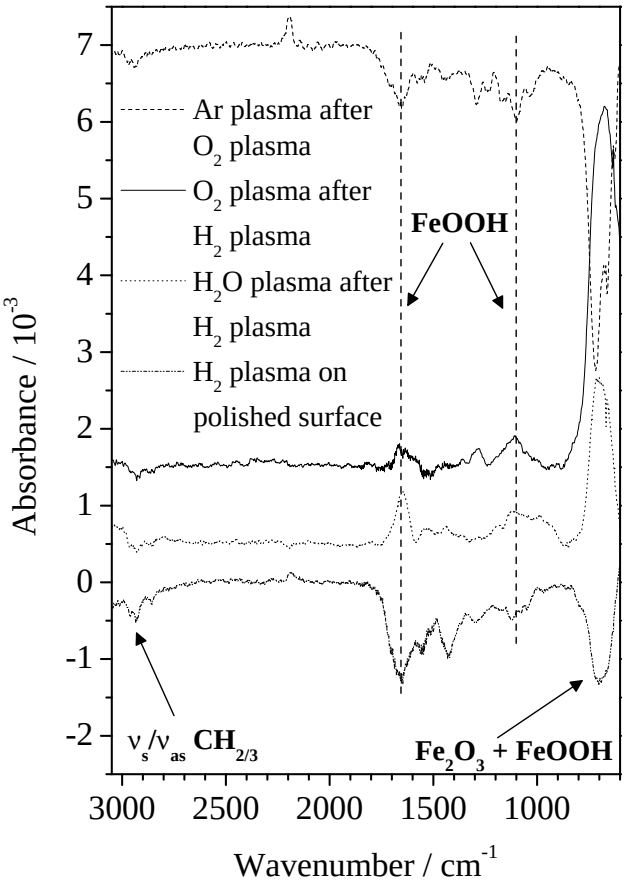

Figure 3.1: In-situ FT-IRRAS measurements of plasma modifications on iron

at 670 cm^{-1} is changed. Several different bands of Fe_2O_3 and FeOOH in this range are reported in the literature [4].

Simultaneously, Volta potential changes were recorded by Kelvin probe measurements. The resulting values are shown in 3.2. The removal of the native oxide layer results in a decrease of the measured potential of about 450 mV. Since the oxygen plasma generates an oxide with higher thickness and higher oxidation state than the native layer, the potential is shifted about 780 mV

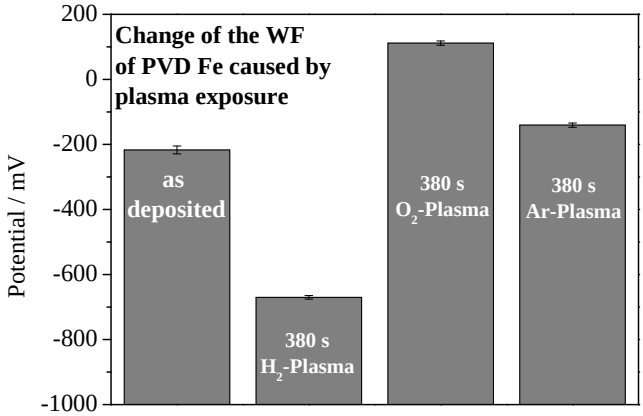

Figure 3.2: Potentials of an iron surface after different plasma treatments measured in-situ by the KP

positively. A subsequent argon treatment results again in a decrease of 250 mV due to the partial reduction of the oxide. The infrared spectrum suggests a sputtering effect of the argon plasma, while a second explanation could be the transformation of the surface layer to a different oxide structure. Since the characteristic absorption bands of Fe_3O_4 are located below 600 cm^{-1}, this oxide cannot be detected with our MID IR MCT detector. The Kelvin probe measurements confirm the latter assumption, because the potential after argon plasma treatment ranges between the potential of the plasma oxidized and the hydrogen reduced surface. Grundmeier and Stratmann could show that the change of the Volta potential difference is determined by the ratio of Fe(II) to Fe(III) activities at the surface [5].

$$\Delta(\Delta\Psi_{\mathrm{Ox}}^{\mathrm{Ref}}) = \frac{RT}{F} \ln\left(\frac{a_{Fe^{2+}}}{a_{Fe^{3+}}}\right) \tag{3.1}$$

Thus the in-situ KP measurement provides complementary insight into the plasma induced structural changes of the iron oxide surface layer.

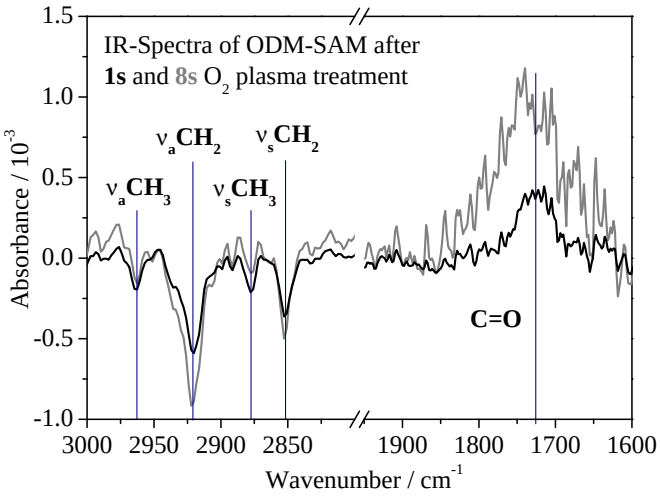

Figure 3.3: In-situ FT-IRRAS measurements of an oxygen plasma treated octadecylmercaptane self-assembly monolayer

3.3.2 Oxygen plasma treatment of model organic self-assembly films on gold

Organic self-assembly films have been employed as model systems for the investigation of surface functionalization of polymers by Friedrich et al. [3]. Moreover, a publication of Tatoulian et al. compares the etching rate of self-assembly films with those of amorphous polyethylene [12]. In the here presented work, octadecylmercaptane was adsorbed on flame annealed gold. The resulting self-assembly film was exposed repeatedly to an oxygen plasma. Figure 3.3 shows FT-IRRAS data after 1 s and 8 s plasma treatment relative to the untreated state. The oxygen plasma etches $CH_{2,3}$ groups (2850 – 2980 cm^{-1}) and builds up a layer of carbonyl functions (1720 cm^{-1}). Due to the ordering of the organothiols with a tilt angle of about 20 to 30° the CH_3 peaks contribute significantly to the spectrum. The CH_3/CH_2 peak ra-

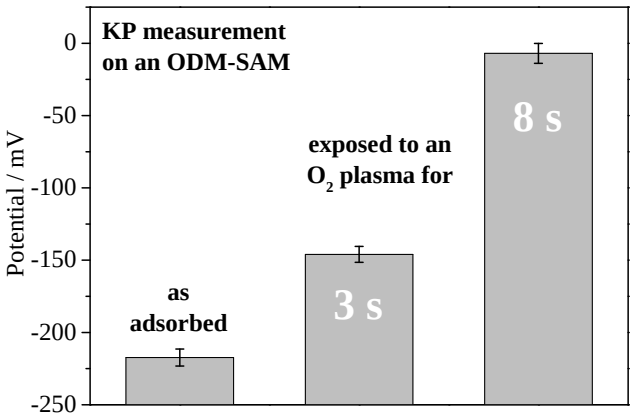

Figure 3.4: Influence of oxygen plasma treatment on the surface potential of an octadecylmercaptane self-assembly monolayer measured by in-situ KP

tio decreases significantly during the plasma treatment. This indicates that the etching process starts from the outer surface of the self-assembly monolayer (SAM) with the oxidative removal of the CH_3 functions. Obviously carbonyl groups are introduced at the end of the SAM chain. Parallel to this Kelvin probe measurements show an increase of the potential by about 85 mV after 3 s oxygen plasma and by further 125 mV after additional 5 s of plasma treatment, as is shown in figure 3.4. This behavior can be explained by an introduction and increase of the density of the carbonyl groups and can be modelled theoretically by assuming a floating dipole layer on top of the surface. The potential in a parallel plate capacitor changes upon the introduction of the dipole layer according to the Helmholz equation [13]:

$$\Delta V = \frac{\mu \cos\theta}{A\epsilon\epsilon_0} \tag{3.2}$$

where the numerator represents the dipole moment component perpendicular to the surface and the denominator includes the effective area of each dipole

as well as the dielectric constant of the layer.

An contribution of some gold oxides formed eventually due to the oxygen plasma treatment on top of the gold substrate, as was postulated by Ron et al. [9] to the Kelvin probe signal cannot be sure excluded.

3.4 Conclusions

With the set-up described here it is possible to modify model polymer and iron surfaces by plasma processes and to investigate the resulting surface composition by the combination of in-situ FT-IRRAS and in-situ KP. The chemical composition, thickness (if IRRAS measurements are calibrated by ellipsometric measurements) and the oxidation state of iron oxides and hydroxides can be measured with extremely high sensitivity and without interference from adsorbed contaminations. Thus, the structure of the outermost surface layers can be tailored by the plasma process based on an in-situ surface analysis in a sub-nanometer scale.

3.5 References

[1] R. D'Agostino. *Plasma deposition, treatment, and etching of polymers.* Acad. Press, Boston, 1990.

[2] J. Friedrich, W. Unger, and A. Lippitz. Plasma modification of polymer surfaces. *Macromolecular Symposia*, 100:111–115, 1995.

[3] J. Friedrich, W. Unger, A. Lippitz, S. Geng, I. Koprinarov, G. Kuhn, and S. Weidner. Modelling plasma-induced reactions on polymer surfaces using aliphatic self-assembling and LB layers. *Surface & Coatings Technology*, 98(1-3):1132–1141, 1998.

[4] G. Grundmeier. *Grenzflächenchemische und korrosionsanalytische Untersuchungen von Plasmapolymerbeschichtungen auf Stahl.* PhD thesis, Universität Erlangen-Nürnberg, 1997.

[5] G. Grundmeier and M. Stratmann. Influence of oxygen and argon plasma treatments on the chemical structure and redox state of oxide covered iron. *Applied Surface Science*, 141(1-2):43–56, 1999.

[6] G. Grundmeier, P. Thiemann, J. Carpentier, N. Shirtcliffe, and M. Stratmann. Tailoring of the morphology and chemical composition of thin organosilane microwave plasma polymer layers on metal substrates. *Thin Solid Films*, 446(1):61–71, 2004.

[7] J. Meichsner and K. Li. In situ characterisation of thin-film formation in molecular low-temperature plasmas. *Applied Physics a-Materials Science & Processing*, 72(5):565–571, 2001.

[8] J. Raacke, M. Giza, and G. Grundmeier. Combination of FTIR reflection absorption spectroscopy and work function measurement for in-situ

studies of plasma modification of polymer and metal surfaces. *Surface and Coatings Technology*, 200(1-4):280–283, 2005.

[9] H. Ron, S. Matlis, and I. Rubinstein. Self-assembled monolayers on oxidized metals. 2. Gold surface oxidative pretreatment, monolayer properties, and depression formation. *Langmuir*, 14(5):1116–1121, 1998.

[10] N. J. Shirtcliffe, M. Stratmann, and G. Grundmeier. In situ infrared spectroscopic studies of ultrathin inorganic film growth on zinc in non-polymerizing cold plasmas. *Surface and Interface Analysis*, 35(10):799–804, 2003.

[11] J. Song and W. J. Van Ooij. Bonding and corrosion protection mechanisms of gamma-APS and BTSE silane films on aluminum substrates. *Journal of Adhesion Science and Technology*, 17(16):2191–2221, 2003.

[12] M. Tatoulian, O. Bouloussa, F. Moriere, F. Arefi-Khonsari, J. Amouroux, and F. Rondelez. Plasma surface modification of organic materials: Comparison between polyethylene films and octadecyltrichlorosilane self-assembled monolayers. *Langmuir*, 20(24):10481–10489, 2004.

[13] D. M. Taylor. Developments in the theoretical modelling and experimental measurement of the surface potential of condensed monolayers. *Advances in Colloid and Interface Science*, 87(2-3):183–203, 2000.

[14] R. H. Turner and F. J. Boerio. Molecular structure of interfaces formed with plasma-polymerized silica-like primer films: Part I. characterization of the primer/metal interface using infrared spectroscopy in situ. *Journal of Adhesion*, 78(6):447–464, 2002.

Chapter 4

Adsorption kinetics of organophosphonic acids on plasma modified oxide covered aluminum surfaces

4.1 Introduction

The adhesion and interfacial corrosion resistance of organic coatings on oxide covered aluminum is of high importance and is mainly determined by the alloy composition, the surface chemistry of the alloy and the composition of the organic coating [8]. For a replacement of anodizing processes and chromate layers, adhesion promoting, ultra-thin films or even monomolecular layers like self-assembled monolayers of bi-functional organophosphonic acids have been recently investigated as new advanced interfacial layers for polymer coated aluminum alloys [17]. Maege et al. studied the adsorption of amino functionalized long-chain organo-phosphonic acids on pure aluminum substrates and have shown an equivalent corrosion protection and an improved adhesion to model coatings in comparison to chromated surfaces [13].

Pahnke and Rühe showed the effective coupling of benzophenone functionalized organophosphonates to oxide covered aluminum surfaces which opens the way of adhesion promotion to organic layers via a photochemical reaction [16]. Wapner and Grundmeier applied aminopropylphosphonic acids as short chain adhesion promoting molecules on aluminum alloy surfaces from dilute aqueous solutions and from a liquid adhesive film and showed excellent filiform corrosion resistance [24]. It is generally accepted that surface hydroxyl groups promote the adsorption of the organophosphonate and that the adhesion of the phosphonate group is based on an acid-base interaction. The driving force is assumed to be the formation of a surface salt as already described for long-chain carboxylic acids by Allara et al. [2] and recently by van den Brand et al. [20, 21]. Alexander et al. showed that an aluminum surface under atmospheric conditions is covered by a thin pseudo-boehmite layer. The passive film consists of the two main phases γ-Al_2O_3 and γ-Al(O)OH. The hydroxide to oxide ratio could be characterized by means of high resolution X-ray photoelectron spectroscopy XPS and appropriate curve fitting [15]. Low temperature plasma processes at reduced or atmospheric pressure recently are of high interest for the adjustment of surface chemistry on metals and polymers. In extremely short times the material surface can be changed in its chemical composition [5, 11]. Grundmeier et al. illustrated how oxide covered iron and zinc can be modified with regard to their surface chemistry and oxide thickness [10, 19]. However, for most technical applications the time required to form a functional monolayer is crucial for the applicability in a process chain, the most challenging being continuous lines for aluminum sheet surface technology. Adsorption times of few tens of seconds would allow the integration of self-assembly processes even in these high speed technologies. Up to now the study of the kinetics of adsorption

was not in the focus of the investigations. Most monolayers were formed within same hours of immersion in solution. The idea of the here presented work is to combine plasma modification of the passive film on aluminum with a self-assembly of a model organophosphonic acid to accelerate the adsorption process of the monolayers. The quartz crystal microbalance (QCM) was applied for the first time as a method for the determination of adsorption kinetics of the organophosphonic acid on aluminum. The plasma induced surface chemistry was studied by in-situ FTIR reflection– absorption spectroscopy (IRRAS). Ex-situ IRRAS and X-ray Photoelectron Spectroscopy were used for the analysis of the adsorbed self-assembled monolayers.
Parts of the results of the studies presented in this chapter were published in 2008 by Giza, Thissen, and Grundmeier in Langmuir [6].

4.2 Experimental details

4.2.1 Sample preparation

For the here presented studies two different types of aluminum samples were prepared by physical vapor deposition (PVD). Aluminum layers were deposited on commercial gold coated quartz crystals (Maxtek, Ø = 1 inch) for the in-situ IRRAS measurements and subsequent study of adsorption kinetics of phosphonic acids by a quartz crystal microbalance (QCM). The Al-films for the XPS analysis were prepared on glass. Both types of samples were coated with 250 nm aluminum layer (Al 99.99 %) using electron beam evaporation (Univex 450, Leybold AG). During the evaporation the layer thickness was monitored by a QCM (Inficon XTC). Prior to aluminum film deposition the samples were thoroughly cleaned in a mixture of hydrogen

peroxide and ammonia (1:1) for 60 minutes at 80 °C, afterwards rinsed with de-ionized water and dried in a nitrogen stream.

4.2.2 Surface chemistry

The experimental setup for the plasma modification is shown in figure 4.1a. The sample is mounted on a holder which can be moved by a stepper motor along the chamber axis. For an uniform modification of the surface the sample was moved through the plasma zone at a constant velocity, which determines the time of exposure. More detailed description of the plasma generation is given in chapter 2. The base pressure of the chamber before flushing with the working gases was ensured to be in the range of 10^{-4} mbar. The pressure of the corresponding gas atmosphere during all plasma modifications was adjusted to 0.3 mbar. Pure gases were used for the experiments, argon and hydrogen in the quality 5.0 by Air Liquid, for the water plasma modifications a closed flask with a high precision valve was filled with ultra pure water. Before using the water was frozen by dipping in liquid nitrogen and the residual gas content pumped down. For the adjustment of a defined water vapor atmosphere in the plasma chamber to 0.3 mbar the water partial pressure was fed by a fine valve and the pumping system was throttled. The gas phase compositions and relevant times during the different plasma treatments are given in table 4.1. The experimental setup for the adsorption experiments is shown in figure 4.1b. The QCM (Maxtek, RQCM) with a resonance frequency of 5 MHz is sensitive to mass changes down to nanograms (56.49 $\mathrm{Hz}\times\mathrm{cm}^2\times\mu\mathrm{g}^{-1}$). To minimize the QCM frequency drift associated with thermal fluctuations, the temperature of the solutions during adsorption was monitored over the complete measurement time and did not fluctuate more than 0.1 K. All adsorption measurements were performed

Table 4.1: Gas phase compositions and relevant times of the several plasma treatments.

Gas composition	Partial pressure/mbar	Treatment time/s
Ar/H_2	0.25/0.05	120
H_2O	0.3	120
Ar	0.3	120

in a 150 ml glass beaker. Total solution volume in the beaker was 100 ml for each measurement. Stirring was accomplished with a magnetic stirrer and a Teflon coated stir bar. The experiments were started first in pure ethanol (absolute for analysis, Merck) until the QCM was running with a stable baseline, without any oscillations or shifts. The phosphonic-acid (n-octadecylphosphonic acid $CH_3(CH_2)_{17}P(O)(OH)_2$, by Alfa Aesar) was then quickly introduced by a syringe. To achieve final concentration of 10^{-4}mol/l, the experiment was started with 99 ml of solvent. After equilibration, 1 ml of 10^{-2} mol of the phosphonic acid solution was introduced. The Sauerbrey equation assumes that an additional mass or film deposited on the crystal has the same acousto-elastic properties as the quartz [18]. This assumption results in a sensitivity factor C_f, which is a fundamental property of the QCM. It is important to note that under these assumptions, the change in frequency is a function of mass per unit area. Therefore, in theory, the QCM mass sensor does not require calibration. However, the Sauerbrey equation is only strictly applicable to uniform, rigid, thin-film deposits.

4.2.3 Surface analysis

The plasma chamber which is implemented in a FTIR spectrometer (Digilab, FTS 3000) allows an in-situ analysis of the modified surface by Fourier

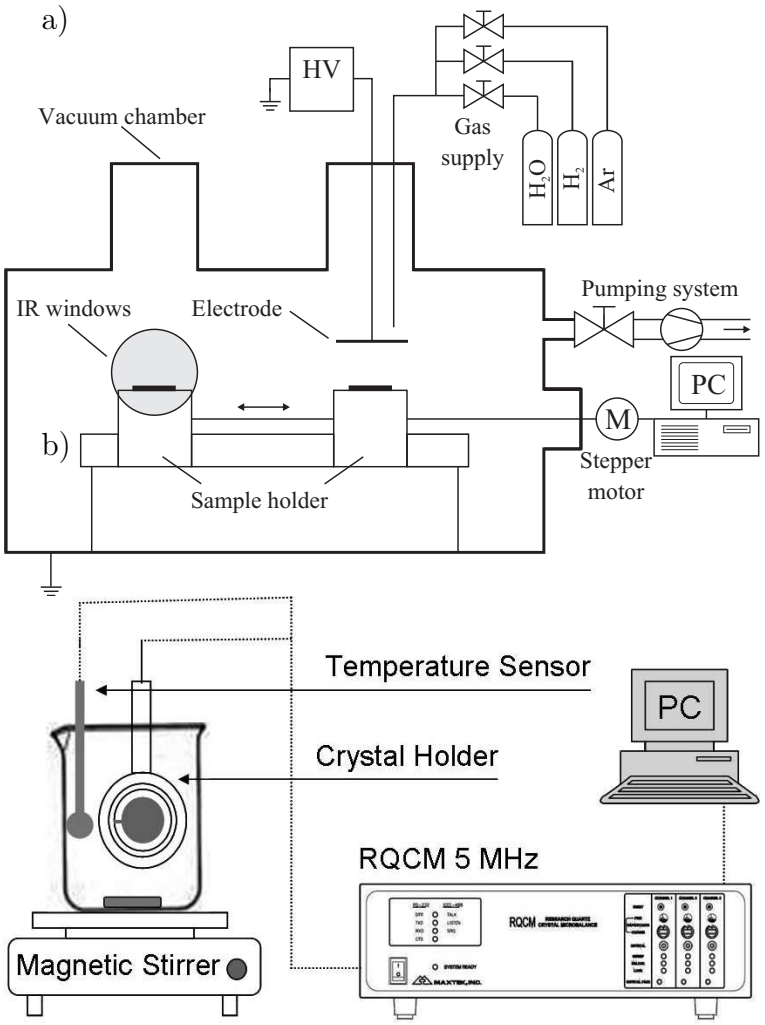

Figure 4.1: Schematic drawing of the experimental setups for a) plasma treatment and in-situ IRRAS and b) the measurements of the adsorption caused mass change on the surface by QCM.

transform infrared reflection absorption spectroscopy (FT-IRRAS). The mid infrared beam is guided by a set of mirrors and transmitted through ZnSe windows onto the sample and reflected under 80° to a liquid nitrogen cooled mercury cadmium telluride (MCT) detector. All presented spectra were recorded using a resolution of 4 cm^{-1} and originate from a co-addition of

256 single scans. To further enhance the sensitivity for the surface species and to eliminate the gas phase absorption of residual water and carbon dioxide in the spectrometer a discrete polarization modulation was performed [9, 7] (for details, see chapter 2). The results obtained from the FT-IRRAS measurements were additionally verified by means of X-ray photoelectron spectroscopy (XPS, Quantum 2000, Physical Instruments, USA) using a monochromated Al K_α X-ray source with a spot diameter of 100 μm. The take off angle of the detected photoelectrons was 45° to the surface normal. All spectra were calibrated using the C1s peak (binding energy, BE = 285 eV) as internal reference. Sputtering was performed with an argon ion beam energy of 2 kV on a 2 mm × 2mm spot. The sputter rate was 5.4 nm/min calibrated on a thermal oxide covered silicon wafer. The chemical composition of the oxide layer on freshly evaporated aluminum changes on the time scale of several days [22]. With regard to possible industrial in-line applications, deposited layers were used for each series of measurements within 24 hours after preparation and stored in an exsiccator before using. Furthermore, the time of exposure to ambient conditions of a sample after a surface modification did not exceed 15 minutes before XPS measurements, or monolayer adsorption studies were performed.

4.3 Results and discussion

4.3.1 Plasma surface chemistry

To achieve a carbon contamination free surface before the water plasma modification was performed, each sample was cleaned in an argon/hydrogen plasma. Figure 4.2 shows the corresponding infrared reflection absorption spectra of an aluminum coated quartz crystal surface after the cleaning step

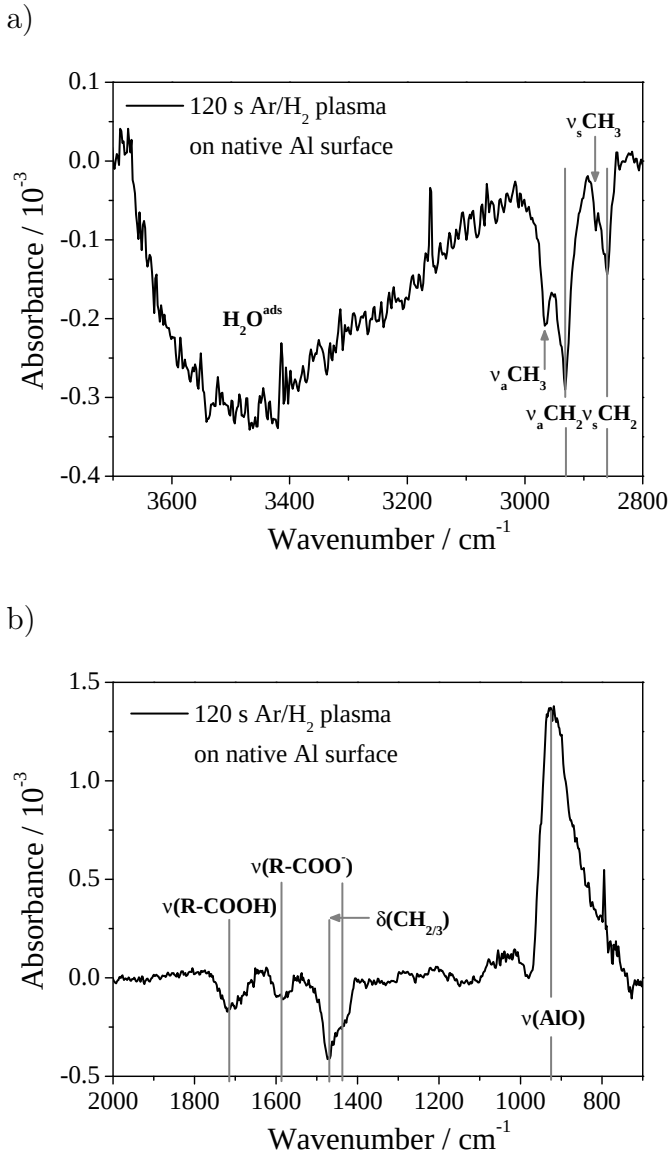

Figure 4.2: In-situ FT-IRRAS of an oxide covered aluminum surface after 120 s argon/hydrogen plasma modification with the surface of the PVD aluminum film as reference.

with a treatment time of 120 s. The resulting infrared absorption after the modification is related to the signal obtained from the native surface. The

cleaning procedure leads to a removal of hydrocarbon contaminations resulting in negative signals in the range of 2800–3000 cm^{-1} (see figure 4.2a) caused by the symmetrical and asymmetrical stretching vibrations of CH_2 and CH_3, and in a weak negative signal at 1420 cm^{-1} caused by the deformation vibrations of CH_2 and CH_3. The broad and asymmetrical negative band at 3500 cm^{-1} in figure 4.2a is assigned to a plasma induced removed of adsorbed water from the native oxide layer; the corresponding peak at 1650 cm^{-1} is very small (with an expected ratio of 6:1 [20]) and could be overlaid by the broad peak at 1720 cm^{-1} (see figure 4.2b). The negative absorption bands at 1720 cm^{-1}, 1590 cm^{-1} and 1475 cm^{-1} (see figure 4.2b) appear due to a removal of organocarboxylates. The dominant feature of the spectrum is located at 930 cm^{-1} and results from a first plasma induced formation of Al_2O_3 (see positive peak in figure 4.2b). The oxidizing species appear in the plasma due to a residual amount of water, oxygen, and carbon mono- and dioxide resulting as well from the vacuum conditions in the chamber ($p_{base} \approx 10^{-4}$ mbar) as from plasma induced desorption of adsorbates from the sample surface and from the walls of the chamber. Two processes interact here simultaneously, a formation of surface oxides and hydroxides due to the residual gases in the plasma volume and an additional transformation of aluminum hydroxide to aluminum oxide, due to the influence of the argon plasma. The other aspect will be discussed more detailed later. Figure 4.3 shows the infrared reflection absorption spectra of an aluminum coated quartz crystal surface after the Ar/H_2 plasma cleaning step and subsequent H_2O plasma modification (black line) and after an additional Ar plasma treatment (grey line). Both spectra were acquired in-situ immediately after the respective plasma modification and were related to a background measured immediately prior to the water plasma treatment. The interesting regions of the

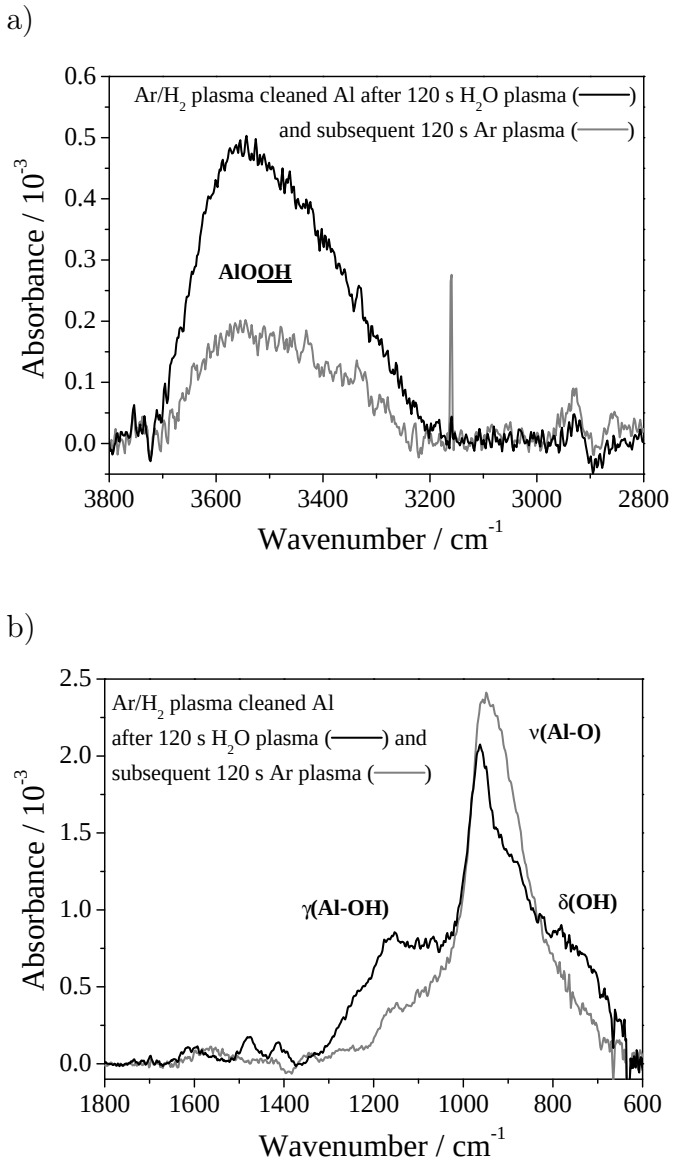

Figure 4.3: In-situ FT-IRRAS of an oxide covered Al surface after a water and subsequently argon plasma modification related to the background acquired after the cleaning step; a) the region of OH vibrations (3800 – 2800 cm^{-1}), and b) the region of Al-O, Al-OH and H_2O vibrations (1800 – 600 cm^{-1}).

spectrum are expanded to a larger scale. Spectrum 4.3a shows the region from 2800 cm^{-1} to 3800 cm^{-1}. This spectral region includes the vibration modes of terminal hydroxyls (3700–3800 cm^{-1}), bridging hydroxyls, hydrogen bonded hydroxyls and water (3200–3500 cm^{-1}). The broad asymmetric absorption band in the spectrum 4.3a has its maximum at 3500 cm^{-1}. The absence of the corresponding band at 1650 cm^{-1} for the water molecules is a hint for the lack of water in the formed film. An absorption band at 3700–3800 cm^{-1} is also absent, which indicates that the water plasma modification does not increase the density of terminal non-hydrogen bonded hydroxyls compared to the Ar/H_2 plasma cleaned native passive film. For these reasons the measured absorption band can be assigned to the symmetric and asymmetric vibration modes of bridging or hydrogen bonded hydroxyls in the formed layer. The exact wavenumber of these vibration modes depends on the local chemical environment of the hydroxyls [20]. The second important region from 600 cm^{-1} to 1800 cm^{-1} is shown in figure 4.3b. The water plasma treatment induced absorption bands within these range represent the vibration modes of AlOOH (1100 cm^{-1}), Al_2O_3 (950 cm^{-1}) and OH^- adsorbed on Al_2O_3 [23, 12]. There is a second possible outcome of the water plasma modification, which was observed under certain conditions. In this case the feature of the FTIR spectrum at 950 cm^{-1} does not appear and the vibration bands attributed to the hydroxides are detected only. The author suppose, that this behavior strongly depends on the thickness of the already air formed oxide film, which can not be furthermore increased by a plasma treatment. The observations and results described in the following are independent from the formation of this additional oxide layer, since the formation of aluminum hydroxides is the crucial process. To check a possible reversibility of the water plasma induced tailoring of the surface chemistry on oxide covered

aluminum an additional argon plasma treatment of the modified oxide layer was performed. This subsequent argon plasma treatment leads to an increase of the Al_2O_3 signal in the FTIR spectrum in figure 4.3b while the intensities of the AlOOH and of the OH-peaks decrease (see figure 4.3a+b). This can be explained with a partial transformation of hydroxides into oxides under argon ion bombardment. This is similar to the observation of Grundmeier and Stratmann, that an argon plasma treatment of an oxide film on iron, which was formed by an oxygen plasma, does not change the layer thickness but changes significantly the film chemistry [10]. The influence of the argon ion bombardment on the surface chemistry of aluminum was not discussed intensively in the literature until now. It is well known that an ion bombardment might change the surface chemistry depending on the substrate material e.g. during a sputter process [3]. McCafferty and Wightman used an argon plasma for cleaning of native aluminum surface from carbon contamination and did not observe any changes neither in the oxide thickness nor in the OH^-/O^{2-} ratio by XPS measurements [14]. This discrepancy in the results might be explained by the differences in the plasma conditions in the experiments. The presented work is the first, which shows the influence of plasma modifications on the chemistry of aluminum surfaces in particular on the change of OH^-/O^{2-} ratio in the layer by in-situ IRRAS.

To confirm the FT-IRRAS results, XPS spectra were measured on the non-modified and plasma modified aluminum surfaces. The XPS data analysis focused on the hydroxide to oxide ratio. For this reason the C1s peak of the aliphatic groups was shifted to a binding energy of 285 eV. Figure 4.4 shows the O1s core level spectra of a freshly evaporated aluminum surface (a), of a second sample cleaned by an Ar/H_2 plasma and subsequently modified by a H_2O plasma (b), and of a third aluminum surface (c) which was

Table 4.2: XPS analysis of the composition of the native PVD aluminum surface, after water plasma and after water plasma with subsequent argon plasma modification

	native PVD Aluminum			Al after 120 s H_2O plasma treatment			Al after 120 s H_2O and subsequent 120 s Ar plasma treatment		
El.	BE / eV	FWHM / eV	$at\%$ / $\pm 0.5\%$	BE / eV	FWHM / eV	$at\%$ / $\pm 0.5\%$	BE / eV	FWHM / eV	$at\%$ / $\pm 0.5\%$
Al 2p	71.7	0.9	14.3	71.3	0.9	9.3	71.6	0.9	8.4
	74.3	1.6	24.3	74.3	1.7	24.9	74.5	1.6	27.1
O 1s	531.3	1.87	39.6	531.1	1.81	31.5	531.2	1.78	38.0
	532.7	1.87	10.8	532.5	1.81	27.6	532.6	1.78	19.6
C 1s	285.0	1.5	7.4	285.0	1.5	4.2	285.0	1.4	5.2
	286.6	1.5	2.1	286.6	1.5	1.5	286.6	1.4	0.9
	288.9	1.5	1.5	289.4	1.6	1.0	289.3	1.7	0.8

modified like sample (b) but additionally Ar plasma treated. The measured O1s transition envelopes several peaks with different binding energies due to different chemical environments. The O^{2-} contribution of the oxide, the OH^- contribution of the hydroxide and the contributions of adsorbed water and oxygen as part of adsorbed carboxylic acid groups appear in the range of 530–534 eV. However the contribution of oxygen containing organic species is in the range of 1.7–3.6 at% (see table 4.2) and shows an opposite trend in comparison to the corresponding part of the O1s signal (≈533 eV). For this reason it can be neglected in these studies. In accordance to the literature an excellent curve fitting was obtained in all cases with symmetric components of equal full width at half maximum (FWHM) separated by 1.4 eV [1]. The component 1 around 531.2 eV corresponds to the oxide; the component 2 around 532.6 eV to the hydroxides in the formed layer. It becomes evident from the spectra in figure 4.4 and fitting results of the O1s photoelectron

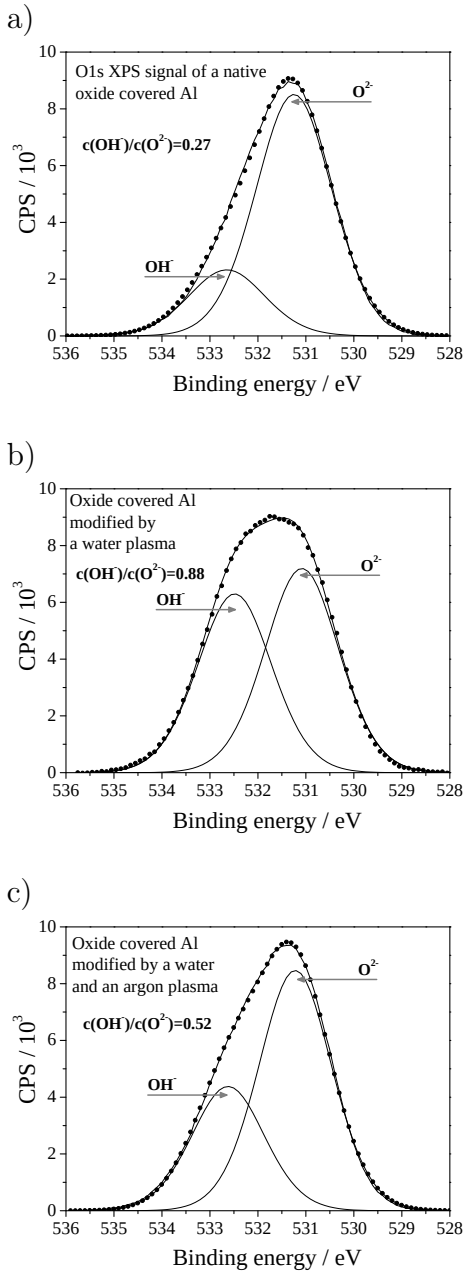

Figure 4.4: O1s XPS spectra of: a) the native oxide on a PVD Al-film; b) Al surface after a water plasma; c) Al surface after a water and subsequent argon plasma modification.

spectrum shown in table 4.2, that a water plasma treatment significantly increases the concentration of hydroxides in comparison to the native passive film. The ratio of the atomic concentration of hydroxide part to the oxide part of the oxygen signal is $c_{hydroxide}$ / c_{oxide} = 0.27 for the native passive Al film and $c_{hydroxide}$ / c_{oxide} = 0.88 for the water plasma treated Al surface. A further argon plasma modification partially reverses this trend to a value of $c_{hydroxide}$ / c_{oxide} = 0.52. The total surface concentration of oxygen increases from 50.4 at% on the native oxide covered aluminum to 59.1at% after the water plasma modification and to a comparable value of 57.6 at% after a subsequent argon plasma treatment, by a simultaneous decrease of the amount of oxygen containing organic species. Element spectra of Al2p peaks and sputter profiles of the elements listed in table 4.2 were measured as well and confirm also changes in the chemistry of the studied surfaces. Figure 4.5a shows the Al2p signals measured on native oxide on a PVD aluminum film, the corresponding surface after a water plasma modification and an aluminum film modified in a water plasma with a subsequent argon plasma treatment. The spectra consist of the metallic contribution at about 71.5 eV and of the oxidized part of aluminum at 74.3 eV (see table 4.2). The higher Al^{3+}/Al^{0} ratio after the plasma modification is caused by increasing oxide layer thickness during the process. The crucial hints provide the depth profiles of the O1s and the metallic part of the Al2p signals shown in figure 4.5b. It has to be kept in mind that the sputter rate was calculated from the calibration of the sputter time on a 100 nm thermal SiO_2 layer on a silicon wafer and the value for the sputter rate (5.4 nm/min) obtained in this way is not the same for an aluminum surface. On the other hand it is difficult to decide at which point of the profile the oxygen signal originates just from readsorption processes and not from the oxide anymore. For these reasons the

a)

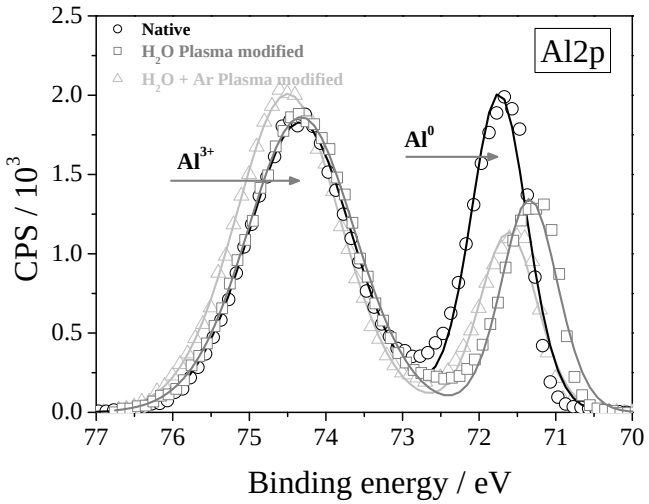

b)

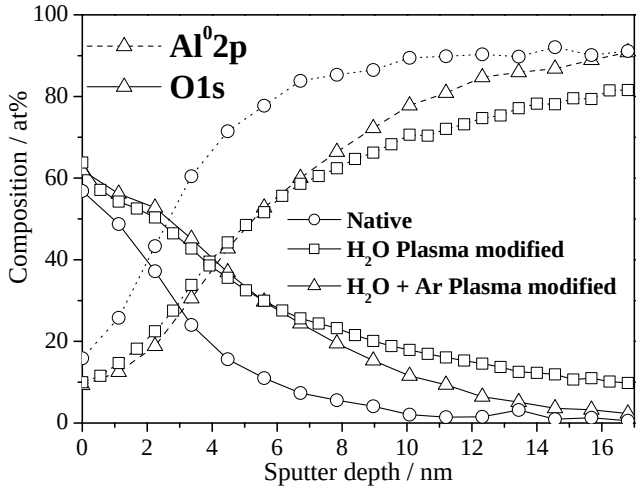

Figure 4.5: a) XPS Al2p signals of the native oxide on a PVD Al-film, the Al surface after a water plasma treatment and the Al surface after a water and subsequent argon plasma modification; b) XPS depth profile of the O1s and the metallic part of the Al2p signals.

quantitative determination of the oxide thickness is very difficult in this way. A good approach to handle this problem is to determine the crossing point of the several profiles. This assumption is not suitable to quantify the thickness values, but it is possible to discuss relative changes of oxide thickness in an appropriate way. However, in this study just the relative changes of the surface oxide chemistry and thickness due to the different plasma modifications are essential. Considering the crossing points of the depth profiles of the oxygen signal and the metallic part of the aluminum signal in figure 4.5b it was observed that the oxide thickness was increased by a factor of two due to the water plasma treatment. No further change of the thickness was detected after the subsequent argon plasma modification. These XPS results support the conclusions of the in-situ IRRAS measurements. The binding energy of the components of the O1s transition after different treatments varied in the range of 0.2 eV (see table 4.2), also the binding energy of the Al2p electrons varies in the range of about 0.4 eV after the different treatments. These shifts were not compensated by adjusting the C1s binding energy to 285 eV. This is in accordance with results in the literature. Cordier et al. observed that peak shifts in photoelectron spectra of differently pretreated aluminum surfaces can not be explained just by the assumption of charging effects and change of the chemical environment. As an additional effect, a shift of the Fermi level of the surfaces should be considered to explain independent shifts of O1s and Al2p, which cannot be compensated by adjusting the C1s binding energy of aliphatic compounds to 285 eV [4]. To ensure that the measured effects are caused by the changes in the surface chemistry, without any influence by changes of the surface morphology additional AFM measurements were performed on each type of samples. Table 4.3 shows the values of the surface roughness measured by AFM on two different areas (1 x 1 μm^2) on

Table 4.3: Surface roughness on native oxide covered aluminum and after H_2O and H_2O + Ar plasma treatments measured by AFM.

Surface state	RMS/nm
Native	7.1 ± 0.03
H_2O plasma treated	6.8 ± 0.4
H_2O + Ar plasma treated	7.3 ± 0.1

each sample. The plasma modifications did not change the surface roughness.

4.3.2 Adsorption of ODPA

IRRAS measurements were done after the phosphonic acid adsorption as well on native as on plasma pretreated samples. For the IRRAS studies the adsorption time was varied between 30 s and several hours. As an example the corresponding characteristic IR absorption bands of the adsorbed phosphonic acid on water plasma treated passive film on aluminum are shown in figure 4.6. In this case the adsorption time was chosen to be two hours. Part a of the spectrum shows the range of 2750–3050 cm^{-1} with the symmetric and asymmetric stretching vibrations of the CH_2 chains with a CH_3 head group. In part b the range of 700–1600 cm^{-1} with a broad line with a centre at 1100 cm^{-1} is shown, which can be assigned to a convolution of symmetric and asymmetric stretching bands of the phosphonate groups. As already discussed by Maege et al. [13] for long chain aliphatic phosphonates, salts of the alkylphosphonic acids give characteristic stretching vibrations at 1125–970 cm^{-1} and at 1000–960 cm^{-1}. Based on this argument the broad absorption at 1100 cm^{-1} indicates that bonding to the aluminum oxi-hydroxide surface occurs via a tridentate bonding. The position and intensity of all

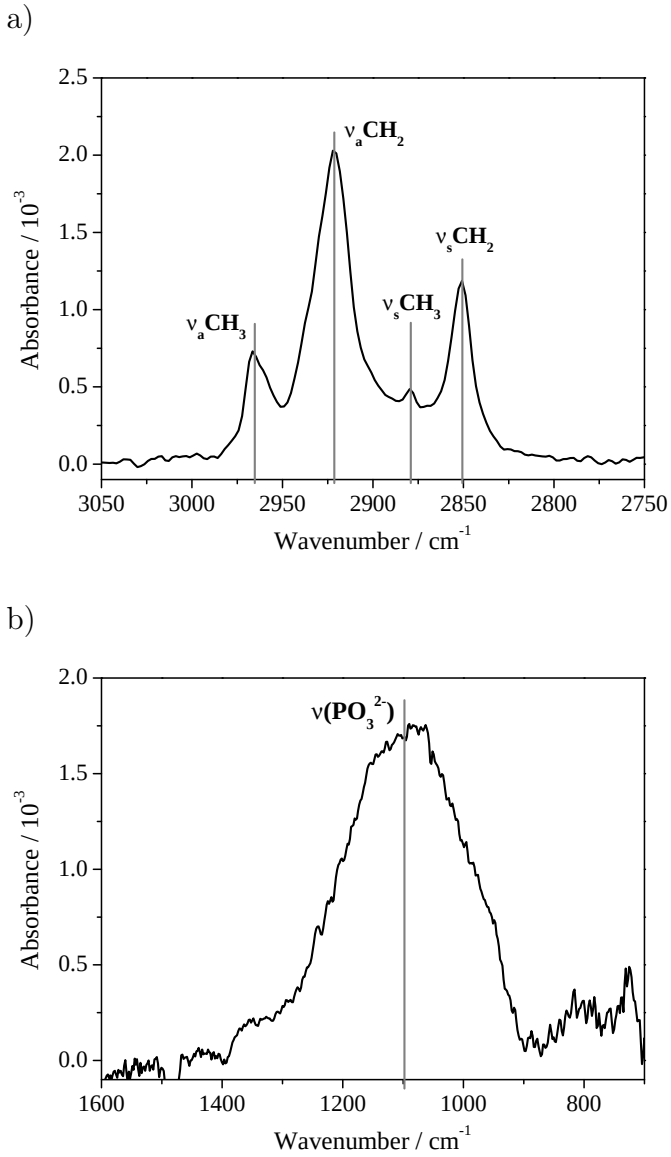

Figure 4.6: FT-IRRAS of an Al surface after 2 h rinsing in an ODPA solution, (a) range of the hydrocarbon vibrations and (b) vibration region of the phosphonates.

peaks assigned to the adsorbed organophosphonic acids were proven to be independent of the adsorption time and the respective plasma pre-treatment of the aluminum surface. On the ODPA covered Al surfaces XPS mea-

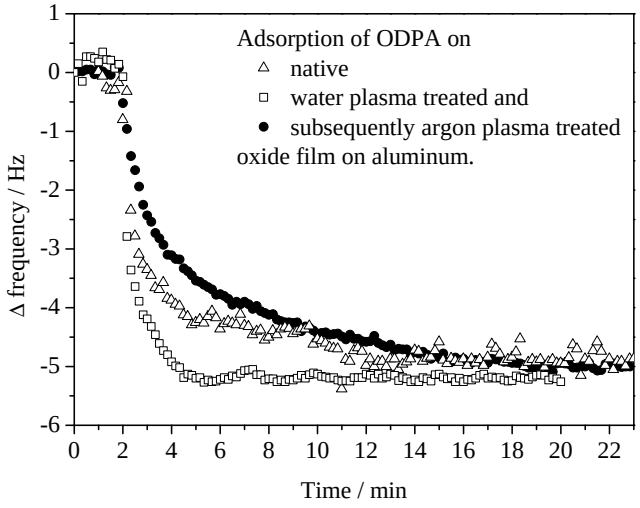

Figure 4.7: Frequency change of an aluminum coated quartz crystal due to the adsorption of ODPA on the native oxide film, on a water plasma modified oxide film and on a water and subsequently argon plasma treated passive film on aluminum measured by means of QCM.

surements were also performed. The surface concentrations of phosphorus and carbon are in the range of 1 at% and about 30 at% respectively. No detectable differences in the surface concentration of ODPA could be determined neither after different immersion times nor different pre-treatments. The amount of photoelectrons emitted from the phosphorus atoms located in the self assembled monolayer at the interface to the oxide film is very small and makes conclusions concerning differences in concentration of phosphorous difficult. To reveal the adsorption kinetics the QCM technique was applied. The frequency transients caused by adsorption of organophosphonic acids on different pretreated oxide films on PVD aluminum are shown in figure 4.7. The adsorption induced resulting frequency change, which was

achieved for long times of immersion on native and plasma treated oxide films on PVD aluminum surfaces was reproducible and did not vary significantly with the initial hydroxide to oxide ratio of the PVD deposited film. However, the transients show a remarkable dependence on the plasma treatment. Figure 4.7 shows the frequency changes after addition of ODPA for all discussed surface modifications. On the native oxide film on the aluminum surface an initial fast decrease of approximately -2 Hz with a further slower decay of the frequency down to a limiting value of -5 Hz takes place. After reaching this plateau value the adsorption was accepted as complete and the measurement was terminated. In the case of adsorption on a water plasma modified oxide on aluminum surface the time required for a frequency change of -5Hz was significantly shorter than in the case of the native passive film. The subsequent argon plasma treatment of a water plasma modified passive film on aluminum resulted in slower adsorption kinetics comparable with the adsorption kinetics on the native surface. The fast initial drop of the quartz frequency followed by a slower decrease in case of native passive film on the aluminum surface suggests either a two step process at different rates or the existence of at least two types of adsorption sites with different adsorption energies. For the H_2O-plasma treated surface with high hydroxyl density already no second regime with slower adsorption kinetics is observed. This can be explained by the high density of hydroxyl sites dominating the adsorption kinetics. For less hydroxyl rich surfaces it is likely, that the non hydroxyl terminated surface areas show slower adsorption kinetics. Especially, the argon plasma treatment creates a comparable clean surface but as previously mentioned leads to a partial transformation of the hydroxides to oxides and effectively leads to a decrease of the adsorption rate. These effects show that the assumption of a dependence of adsorption kinetics of phosphonates on

oxide covered aluminum from the density of hydroxyl functions on the surface is an appropriate way to explain the observed phenomena on plasma treated passive films on aluminum. Since the density of hydroxyl groups dominates the adsorption kinetics and as proven by the FTIR-data the chemisorbed molecule is deprotonated, a two step mechanism of the adsorption process can be assumed. The nucleophilic substitution of organophosphonic acids on hydroxide rich oxide covered aluminum surfaces is initiated by the formation of hydrogen bonds. The hydroxyl groups of the phosphonic acid interact with the hydroxylated aluminum oxide surface. This transition state is followed by a condensation reaction leading to stable acid-base interactions between the phosphonate and the aluminum oxide surface. As an explanation for the finally equal overall frequency shift after the full completion of adsorption process it might be assumed that the adsorption of the phosphonic acid group and the subsequent condensation reaction lead to the additional formation of hydroxides on the Ar-plasma treated oxide surface.

4.4 Conclusions

The water and subsequent argon plasma modification of native oxide covered aluminum was studied for the first time by in-situ IRRAS. These measurements in combination with ex-situ XPS showed that a water plasma treatment increases the density of hydroxides in the oxide surface layer while a subsequent argon plasma transforms the hydroxides to oxides. The combination of ex-situ IRRAS and XPS with QCM measurements of the adsorption process of ODPA as well on native oxide covered aluminum as on plasma modified films has shown a strong dependence of the adsorption kinetics on the density of hydroxyl functions on the oxide covered aluminum surface. With an increase in the surface hydroxyl density the adsorption kinetics can

be accelerated. Such an acceleration can be explained by the adsorption of the phosphonic acid via surface hydrogen bonds prior to the condensation reaction, leading to the finally adsorbed phosphonate.

4.5 References

[1] M. R. Alexander, G. E. Thompson, and G. Beamson. Characterization of the oxide/hydroxide surface of aluminium using X-ray photoelectron spectroscopy: a procedure for curve fitting the O1s core level. *Surface and Interface Analysis*, 29(7):468–477, 2000.

[2] D. L. Allara and R. G. Nuzzo. Spontaneously organized molecular assemblies. 1. Formation, dynamics, and physical-properties of normal-alkanoic acids adsorbed from solution on an oxidized aluminum surface. *Langmuir*, 1(1):45–52, 1985.

[3] D. Briggs. *Practical surface analysis.* Wiley, 1983.

[4] F. Cordier and E. Ollivier. X-ray photoelectron-spectroscopy study of aluminum surfaces prepared by anodizing processes. *Surface and Interface Analysis*, 23(9):601–608, 1995.

[5] R. D'Agostino. *Plasma deposition, treatment, and etching of polymers.* Acad. Press, Boston, 1990.

[6] M. Giza, P. Thissen, and G. Grundmeier. Adsorption kinetics of organophosphonic acids on plasma-modified oxide-covered aluminum surfaces. *Langmuir*, 24(16):8688–8694, 2008.

[7] G. Grundmeier, E. Matheisen, and M. Stratmann. Formation and stability of ultrathin organosilane polymers on iron. *Journal of Adhesion Science and Technology*, 10(6):573–588, 1996.

[8] G. Grundmeier, W. Schmidt, and M. Stratmann. Corrosion protection by organic coatings: electrochemical mechanism and novel methods of investigation. *Electrochimica Acta*, 45(15-16):2515–2533, 2000.

[9] G. Grundmeier and M. Stratmann. Nucleation and growth of plasma-polymerized hexamethyldisilazane on iron-substrates. *Berichte Der Bunsen-Gesellschaft-Physical Chemistry Chemical Physics*, 99(11):1387–1392, 1995.

[10] G. Grundmeier and M. Stratmann. Influence of oxygen and argon plasma treatments on the chemical structure and redox state of oxide covered iron. *Applied Surface Science*, 141(1-2):43–56, 1999.

[11] G. Grundmeier, P. Thiemann, J. Carpentier, N. Shirtcliffe, and M. Stratmann. Tailoring of the morphology and chemical composition of thin organosilane microwave plasma polymer layers on metal substrates. *Thin Solid Films*, 446(1):61–71, 2004.

[12] A. B. Kiss, G. Keresztury, and L. Farkas. Raman and IR-spectra and structure of boehmite (gamma-AlOOH) - evidence for the recently discarded D-2h(17) space group. *Spectrochimica Acta Part a-Molecular and Biomolecular Spectroscopy*, 36(7):653–658, 1980.

[13] I. Maege, E. Jaehne, A. Henke, H. J. P. Adler, C. Bram, C. Jung, and M. Stratmann. Self-assembling adhesion promoters for corrosion resistant metal polymer interfaces. *Progress in Organic Coatings*, 34(1-4):1–12, 1998.

[14] E. McCafferty and J. P. Wightman. Determination of the concentration of surface hydroxyl groups on metal oxide films by a quantitative XPS method. *Surface and Interface Analysis*, 26(8):549–564, 1998.

[15] C. K. O'Sullivan and G. G. Guilbault. Commercial quartz crystal microbalances - theory and applications. *Biosensors & Bioelectronics*, 14(8-9):663–670, 1999.

[16] J. Pahnke and J. Ruhe. Attachment of polymer films to aluminium surfaces by photochemically active monolayers of phosphonic acids. *Macromolecular Rapid Communications*, 25(15):1396–1401, 2004.

[17] M. Rohwerder, G. Grundmeier, and M. Stratmann. Corrosion protection by organic monolayers and thin polymer films. In J. Oudar P. Marcus, editor, *Corrosion Mechanisms in Theory and Practice*, pages 479–527. Marcel Dekker, New York, 2002.

[18] G. Sauerbrey. Verwendung von Schwingquarzen zur Wägung dünner Schichten und zur Mikrowägung. *Zeitschrift Für Physik*, 155(2):206–222, 1959.

[19] N. J. Shirtcliffe, M. Stratmann, and G. Grundmeier. In situ infrared spectroscopic studies of ultrathin inorganic film growth on zinc in non-polymerizing cold plasmas. *Surface and Interface Analysis*, 35(10):799–804, 2003.

[20] J. van den Brand, O. Blajiev, P. C. J. Beentjes, H. Terryn, and J. H. W. de Wit. Interaction of anhydride and carboxylic acid compounds with aluminum oxide surfaces studied using infrared reflection absorption spectroscopy. *Langmuir*, 20(15):6308–6317, 2004.

[21] J. van den Brand, O. Blajiev, P. C. J. Beentjes, H. Terryn, and J. H. W. de Wit. Interaction of ester functional groups with aluminum oxide surfaces studied using infrared reflection absorption spectroscopy. *Langmuir*, 20(15):6318–6326, 2004.

[22] J. van den Brand, S. Van Gils, P. C. J. Beentjes, H. Terryn, and J. H. W. de Wit. Ageing of aluminium oxide surfaces and their subsequent reac-

tivity towards bonding with organic functional groups. *Applied Surface Science*, 235(4):465–474, 2004.

[23] S. Van Gils, C. A. Melendres, and H. Terryn. Quantitative chemical composition of thin films with infrared spectroscopic ellipsometry: application to hydrated oxide films on aluminium. *Surface and Interface Analysis*, 35(4):387–394, 2003.

[24] K. Wapner, M. Stratmann, and G. Grundmeier. Structure and stability of adhesion promoting aminopropyl phosphonate monolayers at polymer/oxide/aluminium interfaces. *International Journal of Adhesion and Adhesives*, 28(1-2):59–70, 2008.

Chapter 5

Combination of FTIR reflection absorption spectroscopy and work function measurements for in-situ studies of plasma modified passive films on $MgZn_2$

5.1 Introduction

New Zn-alloys with improved corrosion resistance are of increasing importance for the protection of steel sheets [21, 18]. Moreover, for organically coated zinc alloy substrates or coatings one would like to avoid the need to perform a wet chemical conversion process between the synthesis of the alloy and the organic coating process. If a strong adhesion and high corrosion resistance could be achieved by forming a polymer/zinc alloy oxide/zinc interphase the wet chemical processes could be completely avoided.
Mg containing Zn and ZnAl-alloy coatings showed superior corrosion resistance in the painted and non-painted state as reported in the literature [14].

Recently, Hausbrand et al. observed, that the slow de-adhesion kinetics of organic films on the oxide covered $MgZn_2$-alloy is due to an electrode potential at the polymer/oxide/metal alloy interface that is more negative than the free corrosion potential of the alloy. Grinding was done to prepare the surface of the alloy. The resulting oxide was shown to be mixture of Zn and Mg-oxyhydroxides. The resulting electrode potential was a result of the immediate atmospheric passivation after the grinding process [11, 12, 13].

In the here reported work, the author aims at the introduction of a plasma chemical step that allows the adjustment of the oxide composition and thereby the interfacial electrode potential. Such a dry plasma induced passive film formation would perfectly fit to a continuous production of zinc alloy coatings either by hot-dip galvanizing or physical vapor deposition. As reducing and oxidizing low temperature plasmas, an audio frequency plasma at reduced pressure was performed in hydrogen or oxygen atmospheres. The plasma chemistry on the alloy surface was studied by means of combined in-situ IRRAS and work function measurement in combination with ex-situ XPS. The observed change of passive film chemistry and work function were correlated with interfacial electrode potentials as measured by means of a scanning Kelvin probe at the interface between a model polymer film and the plasma modified alloy surface in humid atmospheres. The resulting de-adhesion kinetics could be well correlated to the oxidation state and the chemical composition of the interfacial oxide.

The results presented in this chapter will be published soon by Giza and Grundmeier, the manuscript is in preparation [5].

5.2 Experimental details

5.2.1 Sample preparation

The $MgZn_2$ samples were produced by stoichiometric melting down of the pure components Mg (99.9 %, Good Fellow) and Zn (99.999 %) in a MgO crucible at $2{\cdot}10^{-2}$ mbar and casting under Ar at 650 °C in a mold. The molding blank was cut in samples with a size of 20 x 20 x 5 mm^3, each sample was grinded with abrasive paper 4000 which corresponds to a grain size of 5 μm and compares to a coarse polishing. Afterwards the samples were ultrasonically cleaned in absolute ethanol (99.8 %, Merck, Darmstadt, Germany) and dried in a stream of nitrogen prior to the plasma modifications. The stoichiometry of the $MgZn_2$ samples was verified by energy-dispersive x-ray spectroscopy (EDX) by means of a FE-SEM (LEO 1550VP) and a combined EDX unit (Oxford Instruments). The measurements were performed at an accelerating voltage of 15 kV and a working distance of 8 mm, which results in a panetration depth of electrons higher than 1 μm.

5.2.2 Tailoring of the surface chemistry

The experimental setup for the plasma modification is shown in figure 5.1. The sample is mounted on a holder which can be moved by a stepper motor along the chamber axis. For a uniform modification of the surface the sample was moved through the plasma zone at a constant velocity which determines the time of exposure. More detailed description of the plasma generation is given in chapter 2. The base pressure of the chamber before flushing with the working gases was ensured to be in the range of 10^{-4} mbar. The pressure of the gas atmosphere during all plasma modifications was adjusted to 0.3 mbar, by opening the suitable gas valve till a partial pressure of 0.05 mbar was

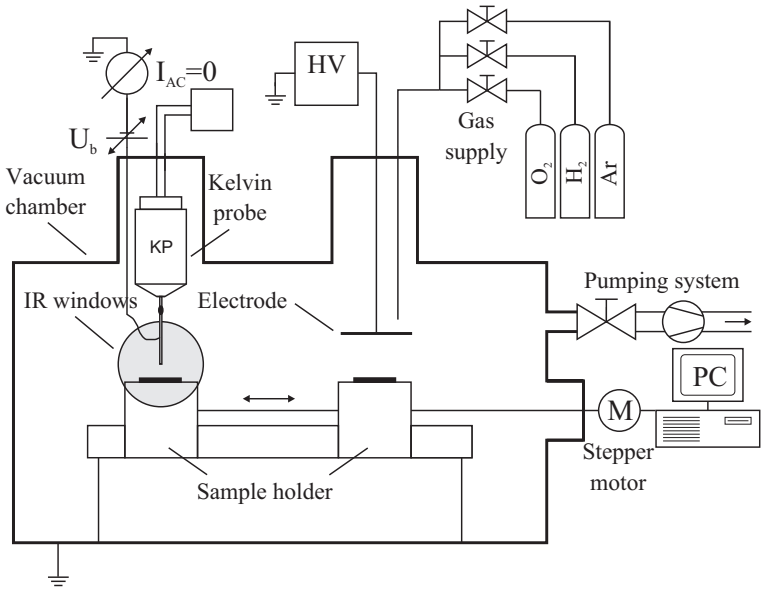

Figure 5.1: Experimental set-up of the combination of in-situ FT-IRRAS and KP with a plasma cell for detection of plasma induced modifications on $MgZn_2$.

reached, which was proven to correspond to a gas flow of 1.5 sccm argon, and by throttling the pump system. Pure gases were used for the experiments, argon and hydrogen in the quality 5.0, oxygen in the quality 4.5 by Air Liquid. The gas phase compositions and relevant times during the different plasma treatments are given in table 5.1.

To compare the different plasma induced effects on the samples directly, it was helpful to prepare the samples as suggested in figure 5.2. Independent

Table 5.1: Gas phase compositions and relevant times of the several plasma treatments.

Gas composition	Partial pressure/mbar	Treatment time/s
Ar/H_2	0.25/0.05	380
O_2	0.3	380

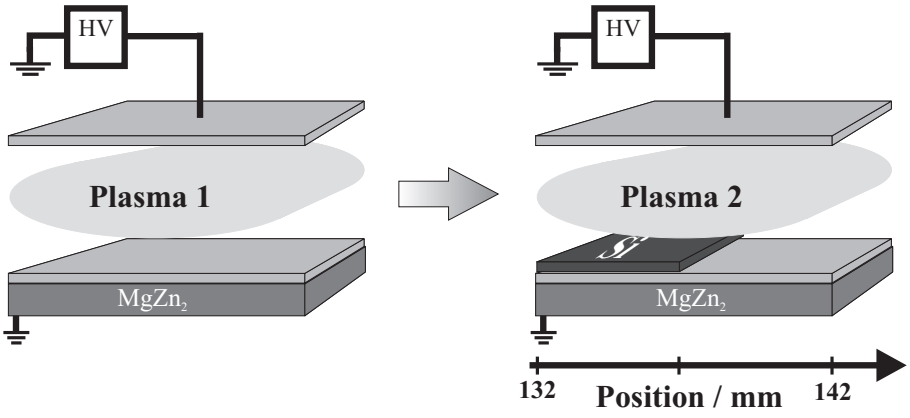

Figure 5.2: Procedure of treatment for direct comparisons of different plasma modified zones on the same $MgZn_2$ sample.

from the number of plasma modification steps, the final modification was performed on a partially covered sample, masked by an adapted piece of silicon wafer. This procedure results in a half-side modification by the very last plasma treatment with a sharp transition from region modified by plasma 1 to the part modified by plasma 2. The position scale drawn in the bottom of figure 5.2 corresponds to the scales drawn in later figures for in-situ Kelvin probe studies on the modified $MgZn_2$ samples.

5.2.3 Methods applied for surface analysis

The plasma chamber which is implemented into the optical path of a FTIR spectrometer (Digilab, FTS 3000) allows an in-situ analysis of the modified surface by Fourier transform infrared reflection absorption spectroscopy (FT-IRRAS). The mid infrared beam is guided by a set of mirrors and transmitted through ZnSe windows onto the sample and reflected under 80 °C to a liquid nitrogen cooled mercury cadmium telluride (MCT) detector. All presented spectra were recorded using a resolution of 4 cm^{-1} and originate

from a co-addition of 256 single scans. To further enhance the sensitivity for the surface species and to eliminate the gas phase absorption of residual water and carbon dioxide in the spectrometer a discrete polarization modulation was performed [7, 8]. For FTIR measurements of the kinetic of plasma modification the sample holder and the electrode were placed on the IR measurement position. By a decrease of resolution to 8 cm^{-1} and simultaneous decrease co-added number of scans to 18, it was possible to measure the change of the spectra with a time resolution of 5 s during the plasma treatment with an acceptable signal to noise ratio.

At the same position the work function can be measured by replacing the electrode with a Kelvin probe. A previously heat treated graphite pencil lead (Staedler 2B marsmicro) with a diameter of 0.5 mm was used as KP tip. Highly ordered pyrolythic graphite (HOPG) was reported to be suitable as a vacuum reference material for Kelvin probe measurements [10]. The graphite tip was measured versus a HOPG sample in different atmospheres and has proven to behave like HOPG (see chapter 2).

The results obtained from the FT-IRRAS measurements were additionally verified by means of X-ray photoelectron spectroscopy (XPS, Quantum 2000, Physical Instruments, USA) using a monochromated Al K_α X-ray source with a spot diameter of 100 μm. The take off angle of the detected photoelectrons was 45 ° to the surface normal. All spectra were calibrated using the C1s peak (binding energy, BE = 285 eV) as internal reference. Sputtering was performed with an argon ion beam energy of 2 kV on a 2 mm x 2 mm spot. The sputter rate was 7.8 nm/min calibrated on a thermal oxide covered silicon wafer. For a detailed analysis of the components of the measured XPS signals peak fitting was applied. All fits were performed by means of the CasaXPS software [17].

Height regulated scanning Kelvin probe (SKP) measurements were performed using a self-designed height regulated probe which is described explicitly in [25, 26]. The samples were measured in a cleaned gas atmosphere by using air with 95% relative humidity. A plane-ended, electrochemical etched Ni/Cr cylindrical wire (diameter approximately 80 μm) was used for the scanning of the sample surface in x, y and z direction. The calibration of the NiCr probe was done by measuring and referring to $Cu/CuSO_4$. All potentials measured by the SKP are given with respect to Standard Hydrogen Electrode (SHE). For the corrosive de-adhesion studies obtained by SKP, a commercial two component lacquer (Glasurit®) with an isocyanate derivative as a hardener (MS-Clear 923-155, BASF Coatings AG, Germany) was applied by spin coating at 2000 rpm for 20 s producing a film thickness of about 10 μm on the surface modified $MgZn_2$ substrate. Afterwards, the polymer films were cross-linked for 30 min at 60 °C.

5.3 Bulk composition of the alloy

The stoichiometry of the $MgZn_2$ alloy was calculated from the EDX measurements as shown in table 5.2. The measured surface near volume of the specimen consists of the elements carbon, oxygen, magnesium and zinc, no further elements could be detected during the analysis. The values given in table 5.2 are mean values with the respective standard deviations resulting from measurements on four different points on the used sample. The amount of carbon (2.8 at%) and oxygen (1.4 at%) is very small and results primarily from the passive film and the top carbon contamination. The information depth of more than 1 μm is much higher than the thickness of the native oxide layer of few nm. Thus the EDX measurement is suitable to characterize the bulk composition. The resulting ratio of the atomic concentrations of zinc

Table 5.2: Chemical composition of the bulk material of the produced MgZn alloy measured by means of EDX.

Element	Mass %	at %
C K	0.7 ± 0.1	2.8 ± 0.6
O K	0.5 ± 0.1	1.4 ± 0.2
Mg K	15.2 ± 0.3	**31.5** ± 0.4
Zn L	83.6 ± 0.4	**64.3** ± 0.8

and magnesium is $c_{Zn}/c_{Mg} = 2.04$. However, considering the uncertainty of the measurements this result is in accordance to the estimated stoichiometry of the $MgZn_2$ phase.

5.4 Surface chemistry

5.4.1 Native oxide on $MgZn_2$

The chemical composition of the native oxide film and the carbon contamination layer, which is unavoidable due to the transport of samples in ambient conditions were measured by means of XPS and summerized in table 5.3. The values of the atomic concentration of all measured species (in bold) were obtained by calculating the mean value of two measured points on each sample. The given uncertainty of the measurements of 0.5 at% results from an estimation given for the used equipment by the manufacturer. Furthermore the measured signals were fitted by peaks of possible oxidation states for each element as listed in column three of the table. Additionally the fitting parameters binding energy and full width at half maximum were given in column four and five. The relative percentage of different oxidation states of each element, obtained from the fitting procedure complete the informations

Table 5.3: Chemical composition of the $MgZn_2$ surface in the native state analyzed by means of XPS with fitting parameters used for the determination of the contributions of species with different oxidation states to the element signals.

Element	Conc./at%	Component	B.E./eV	FWHM/eV	Percentage
C1s	**18.4** ±0.5	C–C	285.0	1.6	38.5
		C–OH	286.6	1.6	23.4
		C–OOH	288.4	1.6	12.0
		CO_3^{2-}	289.9	1.6	26.1
Mg2p	**16.9** ±0.5	$Mg^{0/2+}$	50.0	1.7	100
O1s	**52.8** ±0.5	O^{2-}	530.0	1.9	12.7
		OH	531.8	1.9	87.3
Zn2p$_{3/2}$	**11.9** ±0.5	Zn^0	1020.4	1.1	9.2
		Zn^{2+}	1022.1	1.7	90.8

contained in table 5.3. The dominant species at the native $MgZn_2$ surface are oxygen with 52.8 at% and carbon with 18.4 at%. The O1s signal consists of two components, which were fitted by symmetrical profiles with a resulting FWHM of 1.9 eV and an energy gap between the peaks of 1.7 eV. The component at the binding energy of 530.0 eV resulting from the O^{2-} oxidation state of oxygen in the oxide bond. The component at 531.8 eV consist of the contributions of hydroxide and of the oxygen containing organic adsorbates at the surface. The chemical composition of these organic adsorbates becomes identified by the components of the carbon components in table 5.3. Another important information, which was already mentioned in the context of the bulk composition of the $MgZn_2$ samples is the Zn to Mg concentration ratio. For the native oxide of a grinded sample this ratio has a value of $c_{Zn}/c_{Mg} = 0.70$. This value differs significantly from the bulk composition, due to the magnesium enrichment in the oxide layer as was also reported by

Hausbrand et al. [11]. A further splitting of the Zn and Mg signals and a detailed assignment to the oxide, hydroxide and carbonate components is very difficult due to the small binding energy differences between the considered oxidation states and is irrelevant for the results discussed later on. The outermost native oxide layer, which determines the electrochemical properties of the alloy and which should be modified by the plasma treatments consist of a solid solution of magnesium-zinc hydroxide with a small amount of oxide [13].

5.4.2 Argon/hydrogen plasma cleaning step

The detailed chemical composition of the native oxide film depends strongly on the pretreatment and storage conditions of the sample [13]. For this reason a plasma treatment in a mixture of argon and hydrogen was chosen as a first step to obtain a carbon contamination free surface and at least partially remove its native carbonate layer before any further modification was performed. Fig. 5.3 shows the corresponding infrared reflection absorption spectra of a grinded $MgZn_2$ surface after the cleaning step with a treatment time of 380 s. The resulting infrared absorption after the modification is related to the signal obtained from the native surface. The full range of the measured FTIR spectrum (4000–600 cm^{-1}) is shown and the dominant features of the spectrum are labeled. The cleaning procedure by an Ar/H_2 plasma leads to a removal of hydrocarbon contaminations (2800–3000 cm^{-1}), a removal of carbonates or organocarboxylates (1000–1700 cm^{-1}), and to a decrease of the hydroxide density in the native oxide layer (see broad negative band at 3000–3600 cm^{-1}) [22, 4]. The positive band at 2204 cm^{-1} can be attributed to adsorbed carbon monoxide species, which might be created by the plasma enhanced dissociation of the removed carbonates and carboxy-

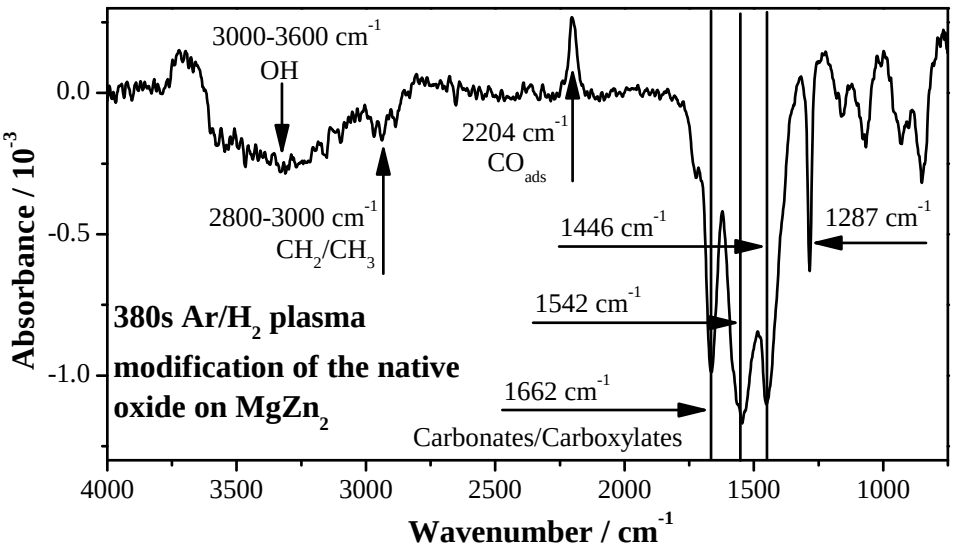

Figure 5.3: In-situ IRRA spectrum of a 380 s long Ar/H_2 plasma modification of the native passive layer on a grinded $MgZn_2$ sample, the measurement is related to a spectrum obtained from the unmodified surface.

lates, the exact wavenumber of the corresponding vibration depends on the adsorbent and on the pressure [2].

Complementary XPS measurements were performed on the Ar/H_2 modified samples as well. The list of measured elements with the corresponding chemical composition, the binding energy of the identified components with the FWHM value and the corresponding percentage are summarized in table 5.4. The XPS measurements had to be performed ex-situ, with a transfer time to the equipment of up to thirty minutes. This time is long enough for a re-adsorption of the removed carbonate and carboxylate layer on the very reactive $MgZn_2$ surface. However, the amount on organic adsorbates was reduced significantly from 18.4 to 10.6 at% due to the plasma cleaning process.

Table 5.4: Chemical composition of the $MgZn_2$ surface after an Ar/H_2 plasma modification analyzed by means of XPS with fitting parameters used for the determination of the contributions of species with different oxidation states to the element signals.

Element	Conc./at%	Component	B.E./eV	FWHM/eV	Percentage
C1s	**10.6** ±0.5	C–C	285.0	1.6	50
		C–OH	286.5	1.6	14.2
		C–OOH	288.8	1.6	8.5
		CO_3^{2-}	290.0	1.6	27.3
Mg2p	**24.5** ±0.5	$Mg^{0/2+}$	50.1	1.7	100
O1s	**53.8** ±0.5	O^{2-}	530.2	1.9	16.9
		OH	531.7	1.9	83.1
Zn2p$_{3/2}$	**11.1** ±0.5	Zn^0	1020.4	1.0	7.2
		Zn^{2+}	1022.0	1.8	92.8

The absolute oxygen content did not change significantly, but the hydroxide to oxide ratio decreased slightly from $c_{OH}/c_{O^{2-}} = 6.87$ on the native surface to $c_{OH}/c_{O^{2-}} = 4.92$ on the Ar/H_2 plasma modified surface. The content of zinc stays stable, but an increased content of magnesium leads to a decrease of the $c_{Zn}/c_{Mg} = 0.45$ compared to the untreated surface $c_{Zn}/c_{Mg} = 0.70$ (see above). This fact indicates a further plasma induced enrichment of magnesium in the outermost oxide layer. Two mechanisms might be responsible for this behavior, an preferential sputtering of zinc during the bombardment of argon ions, or a chemical induced diffusion of magnesium due to the formation of a new carbonate, carboxylate and oxi–hydroxide layer.

5.4.3 Oxygen plasma modification

Subsequently, the effect of an oxygen plasma to the $MgZn_2$ was studied. Figure 5.4a shows the corresponding IRRA spectrum of a grinded $MgZn_2$ surface

after the Ar/H_2 plasma cleaning step and a subsequent O_2 plasma modification (both 380 s). The background spectrum is the one obtained after the Ar/H_2 plasma cleaning step, both spectra were acquired in-situ immediately after the respective plasma modification. The oxygen plasma induces positive absorption bands within the range from 1000 cm^{-1} to 1400 cm^{-1}, thus the part of the FTIR spectrum from 1450–800 cm^{-1} was enlarged and the dominant features of the spectrum were labeled. In comparison to the modification of the $MgZn_2$ sample, pure magnesium and zinc samples were prepared and modified in the exact same manner. The resulting IRRA spectra are shown in figures 5.4b and 5.4c, the spectra were enlarged similarly. The dominant features of the spectra are located around 1160 cm^{-1} and 1305 cm^{-1} after the modification of all three samples, whereas the intensity ratio of the two peaks differs in case of modified magnesium from the zinc and ZnMg-alloy samples. According to earlier studies by Shirtcliffe et al. and Grundmeier et al. on the plasma modification of zinc surfaces the strong asymmetric peak around 1160 cm^{-1} can be assigned to the formation of oxy-hydroxides with the composition given as $Zn(OH)_\delta O_{(2-\delta)/2}$ [22, 6]. Another possible explanation for the appearance of the here discussed peaks, in particular the feature at 1306 cm^{-1} in the spectrum obtained from the modified magnesium sample, might be the formation of hydroxycarbonates as was suggested by Neufeld and Cole [19], due to observations made during the corrosion of zinc; or the formation of carboxylates, due to the presence of magnesium as observed by Fotea et al. on freshly evaporated magnesium subsequently exposed to ambient conditions [4]. Both interpretations of the here discussed spectra seem to be improbable, because of the absence of any further absorption bands typical for the carbon containing species mentioned above. The assignment of the peaks to the formation of oxy-hydroxides, as

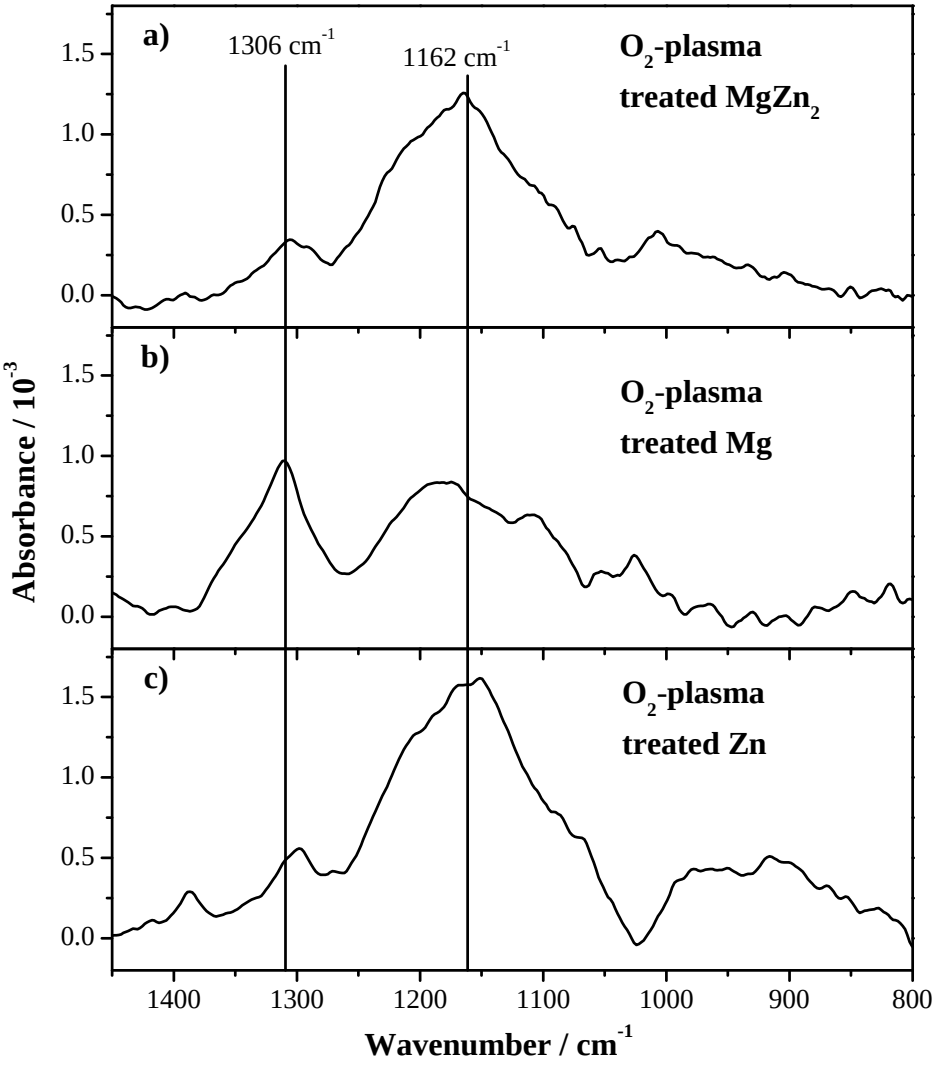

Figure 5.4: In-situ IRRA spectra on O_2 plasma treated passive films on grinded $MgZn_2$ (a), Mg (b), and Zn (c) substrates, related to the corresponding measurement after the respective cleaning step in an Ar/H_2 plasma.

supposed above appears more plausible. To leave no doubt on this conclusion XPS measurements were complementary performed and will be discussed

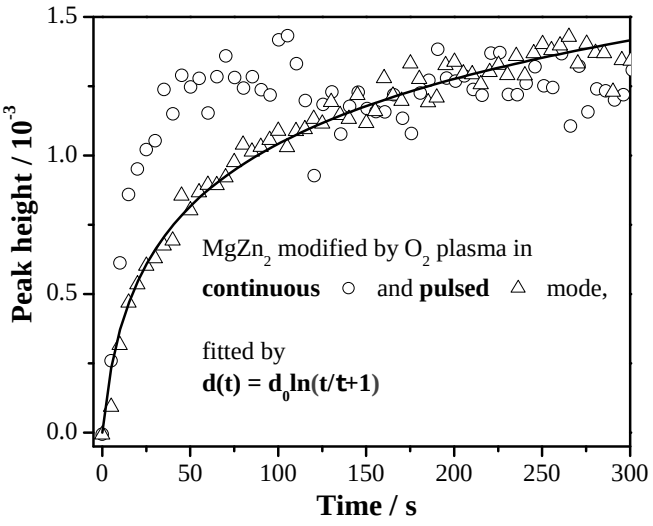

Figure 5.5: FTIR kinetic measurement during O_2 plasma modification of the passive layer on a Ar/H_2 plasma pretreated $MgZn_2$ sample.

beneath. For any kind of an industrial continuous process the duration of the surface modification plays a decisive role. For this reason real time in-situ FT-IRRAS measurements during plasma oxidation were performed to reveal the kinetics of oxyhydroxide growth, by a slight modification of the experimental setup described in the experimental section. Fig. 5.5 shows the corresponding evolution of the integral of the absorption band at 1162 cm^{-1} depending on the time during the oxygen plasma modification, from the start of the plasma treatment at 0 s to its stop after 300 s. The measurement plotted by circles correspond to the common parameters of applied plasmas and is called as continuous mode. It is characterized by a fast initial increase and reaching a plateau region within the first 50 s. To reveal the characteristic of dependance of the increase of the peak intensity over the treatment time

a pulsed mode was performed. This process slows down the oxidation significantly. The result of the measurement is plotted as triangles in figure 5.5. Results on the oxidation of silicon presented in chapter 6 and the work of Cui et al. [3] have shown that there is a linear dependence of the measured IR peak intensity and the formed oxide thickness at least in the range of few nanometers. Therefore a direct correlation of the peak height plotted on the y-axsis to the formed oxide thickness on the $MgZn_2$ surface can be assumed. The trend can be fitted by using an empirical direct logarithmic law

$$d(t) \;=\; d_0 \ln(t/\tau + 1), \tag{5.1}$$

which is in accordance to the low temperature oxidation model of zinc given by Vernon et al. [24]. d_0 represents a thickness constant and τ is a time constant. This low temperature oxidation model is based upon the consideration of a thickness-independent surface charge, leading to a thickness-independent electrical field across the oxide as the driving force for anion movement to the metal/oxide interface (for details, see section 1.4.1). Contrary to the low temperature oxidation without a plasma, here the oxygen anions are formed at the oxide surface by dissociation of oxygen molecules in the discharge. Therefore, as well a constant charge density at the surface, as a constant electrical field across the oxide layer, caused by the adjacent plasma can be assumed.

However, two conclusions result from this kinetic measurements. On the one hand it becomes evident from the comparison of the continuous and the pulsed mode, that the oxidation rate strongly depends on the presence of the electrical field. On the other hand the maximum effect of the plasma treatment is achieved after a view tens seconds, which is very promising for a possible industrial continuous process.

To confirm the conclusions on the composition of the formed layer mea-

sured by means of in-situ IRRAS, complementary XPS studies of the oxygen plasma treated $MgZn_2$ samples were performed as well. Table 5.6 shows the summarized informations from the XPS measurement of the detected species as discussed above. The modification by an Ar/H_2 plasma with a subsequent oxygen plasma treatment results in a further slight decrease of the concentration of carbon containing species (8.5 at%) and a significant increase of the oxygen concentration (59.7 at%). At the same time the hydroxide to oxide ratio decreases to the value $c_{OH}/c_{O^{2-}} = 4.38$. The concentrations of zinc and magnesium fall both by around 2 at% by a almost unchanged ratio of $c_{Zn}/c_{Mg} = 0.39$. To examine the depth of the effect of the oxygen plasma modification across the oxide layer sputter profiles were performed. First of all figure 5.6 gives an insight to the surface chemistry beneath the top layer of contaminations. The shown element spectra of magnesium (Mg2p), carbon (C1s), oxygen (O1s), and zinc (Zn2p) were obtained from the $MgZn_2$ surface

Table 5.5: Chemical composition of the $MgZn_2$ surface after an Ar/H_2 and subsequent O_2 plasma modification analyzed by means of XPS with fitting parameters used for the determination of the contributions of species with different oxidation states to the element signals.

Element	Conc./at%	Component	B.E./eV	FWHM/eV	Percentage
C1s	**8.5** ±0.5	C–C	285.0	1.5	58.8
		C–OH	286.6	1.5	10.6
		C–OOH	288.7	1.5	7.1
		CO_3^{2-}	290.0	1.5	23.5
Mg2p	**22.9** ±0.5	$Mg^{0/2+}$	50.2	1.8	100
O1s	**59.7** ±0.5	O^{2-}	530.3	1.9	18.6
		OH	532.0	1.9	81.4
Zn2p$_{3/2}$	**8.9** ±0.5	Zn^0	1020.5	1.1	6.7
		Zn^{2+}	1022.2	1.9	93.3

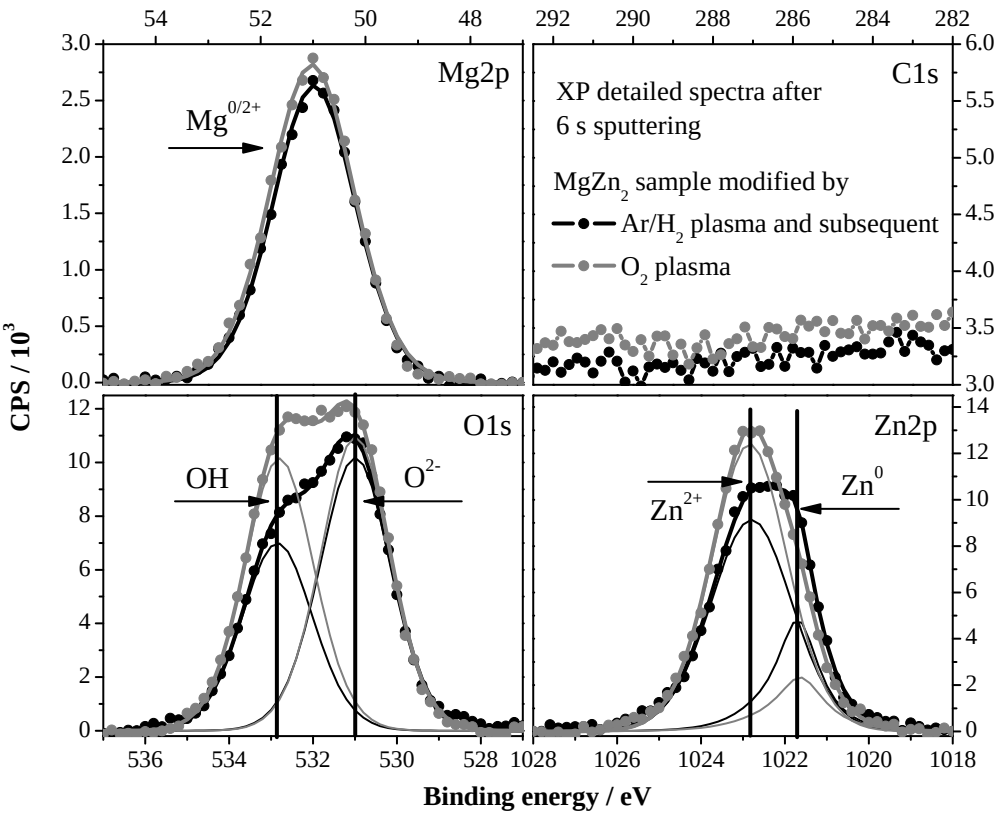

Figure 5.6: Element XP spectra of Mg, C, O, and Zn after the removal of the contamination layer on the Ar/H_2 (black lines) and on the subsequent O_2 plasma modified $MgZn_2$ sample (grey lines).

after a sputtering time of 6 s, which corresponds to a removed layer with a thickness on the reference sample (thermal oxidized silicon) of about 0.8 nm. Spectra measured on the surfaces after the cleaning step in an Ar/H_2 plasma (black lines) and after the subsequent modification in an O_2 plasma (grey lines) are compared in figure 5.6. Furthermore in reasonable cases the different oxidation states of the respective elements are highlighted, dots represent

the measured data, thin lines indicate the profiles used for the peak fitting and thick lines are the convoluted component profiles. All element spectra were fitted by symmetrical Gaussian/Lorentzian profiles, except for the metallic part of the zinc signal, which is asymmetrical [13, 15]. The values of FWHM, binding energies, and resulting percenteges of the considered components are given in tables 5.4 and 5.6. The element spectra after removing of the contamination layers underline the effects of the plasma modifications discussed above. Due to the disappearance of any carbon containing species from the surface after the short sputtering, it becomes clear, that the carbonate and carboxylate spectra measured on top of the surfaces origin from adsorbed atmospheric contamination. The magnesium content of the layer seems to be unaffected at this point, unlike the zinc signal, which shows a significantly higher amount of Zn in the oxidation state +2 and a smaller metallic contribution after the oxygen plasma treatment. The oxygen signal on the oxidized sample compared to the signal on the Ar/H_2 plasma cleaned surface differ as well, the hydroxide and oxide contents increase both due to the oxidation, but in a non-uniform manner.

It should be kept in mind, that a sputtering process as well as any other kind of plasma treatment alters the surface chemistry. However, it can be assumed that the sputter process alters the surfaces in the same manner independent from the prior plasma modification, so it should be possible to draw qualitative conclusions from this kind of measurements.

Moreover, the distribution of magnesium and zinc, in particular the oxidic and the metallic contributions of these elements, as well as the oxygen concentration within the oxide layer are very important informations for the characterization of the plasma induced changes of the native film. Figure 5.7 shows the correspondent comparison of sputter profiles on the Ar/H_2 plasma

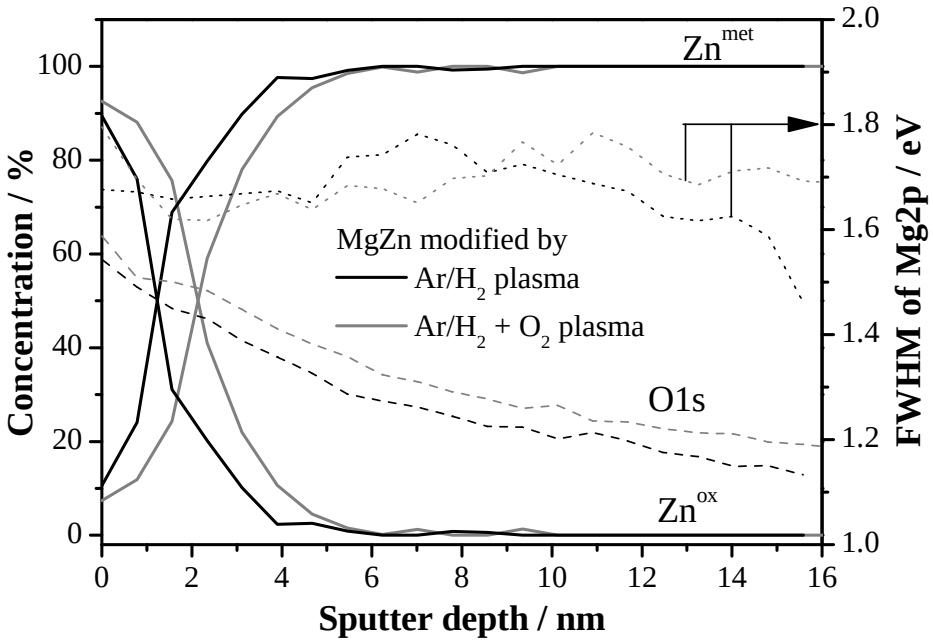

Figure 5.7: Sputter profiles of the Ar/H_2 (in black) and subsequent O_2 (in grey) plasma modified passive layers on a $MgZn_2$. Trends of the metallic and oxidic part of the Zn2p signal (solid lines), as well as the oxygen content relating to the zinc and magnesium concentration (dashed lines) are shown. Additionally the trend of the FWHM of the Mg2p signal over the sputter depth is overlaid (dotted lines).

cleaned (black line) and O_2 plasma oxidized (grey line) samples. As already discussed in chapter 4 associated with the XPS studies of the surface chemistry on plasma modified aluminum samples, the crossing point of the profile of metallic zinc with the oxidic part of the signal (solid lines) will be considered for qualitative conclusions on the oxide thickness changes. An increase of the thickness of the zinc oxide containing layer on the $MgZn_2$ samples by a factor of approximately two can be observed in the considered profile, caused

by the oxygen plasma modification of the surface. This result is in accordance to earlier studies from Shirtcliffe et al. on pure zinc samples [22] and comparable studies of plasma treatment of iron surfaces by Grundmeier et al. [9]. Unfortunately, similar examination of the magnesium signal proved to be impossible due to the difficult deconvolution of the measured signal to the correspondent metallic and oxidic components. Therefore, a much simpler method was applied to analyze the magnesium profile. The trend of the full width at half maximum (FWHM) of the Mg2p signal is plotted in figure 5.7 over the sputter depth (dotted lines). It is assumed that the transition of the Mg2p signal from oxidic to metallic lead to a significant decrease of the FWHM value. The measured FWHM values are shown on the right y-axis of figure 5.7. The FWHM value of the Mg2p signal on the Ar/H_2 plasma treated sample stays on a nearly constant level of 1.70 eV (with a standard deviation of 0.04 eV) over the thickness of 9 nm, followed by a continuous slow decrease of the FWHM value. Contrary to this behavior, the FWHM value of the Mg2p signal on the O_2 plasma modified sample stays on the same constant level of 1.70 eV (with a standard deviation of 0.05 eV) over the whole sputter depth shown here. A comparable decrease of the FWHM value on the oxidized $MgZn_2$ sample starts beyond the depth of 18 nm (outside of the in figure 5.7 shown range). The depth profile of the oxygen concentration is also shown in figure 5.7 (dashed lines). A higher oxygen content over the whole oxide layer could be observed.

The thickness of the magnesium oxide containing part of the passive layer on $MgZn_2$ is much higher than the zinc oxide film thickness, this is in accordance to the observations done by Hausbrand et al. [13]. The measured profiles of oxygen concentration and the FWHM value of the Mg2p signal lead to the conclusion, that the thickness of the magnesium oxide containing layer on

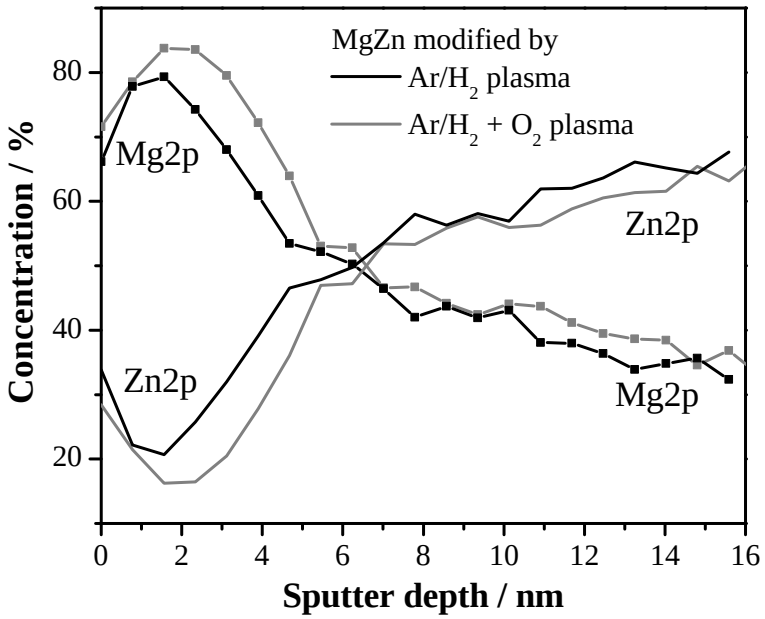

Figure 5.8: Sputter profiles of the Ar/H_2 (black lines) and subsequent O_2 (grey lines) plasma modified passive layers on a $MgZn_2$. Trends of the zinc and magnesium concentrations over the sputter depth are compared.

the $MgZn_2$ surface becomes also increased by an oxygen plasma treatment. Furthermore, the comparison of the absolute zinc and magnesium contents inside of the passive film over the oxide thickness is of high interest. Figure 5.8 shows the corresponding profile. The passive film on the $MgZn_2$ sample is rich on magnesium, the magnesium concentration starts on the surface with a significant higher value than the zinc concentration (see discussed ratios above). This relation inverses with increasing depth until the appropriate stoichiometric bulk ratio Mg to Zn of 1:2 is reached (here approximately at 16 nm compared to the SiO_2 reference). The change of the concentration

ratio c_{Zn}/c_{Mg}, as discussed above for the outermost surface is similar for the situation within the oxide layer. In case of the Ar/H_2 plasma cleaned surface (black lines) the zinc concentration within the passive film is significant higher and the magnesium concentration lower than within the subsequent oxygen plasma modified (grey lines) passive film on the $MgZn_2$ surface.

5.4.4 Second argon/hydrogen plasma treatment

To check the reversibility of the effects of the oxygen plasma treatment on the $MgZn_2$ surface a final modification by another Ar/H_2 was performed subsequent to the oxidation step and analyzed in-situ by IRRAS as well. The resulting FTIR spectrum is shown in figure 5.9. The relevant regions

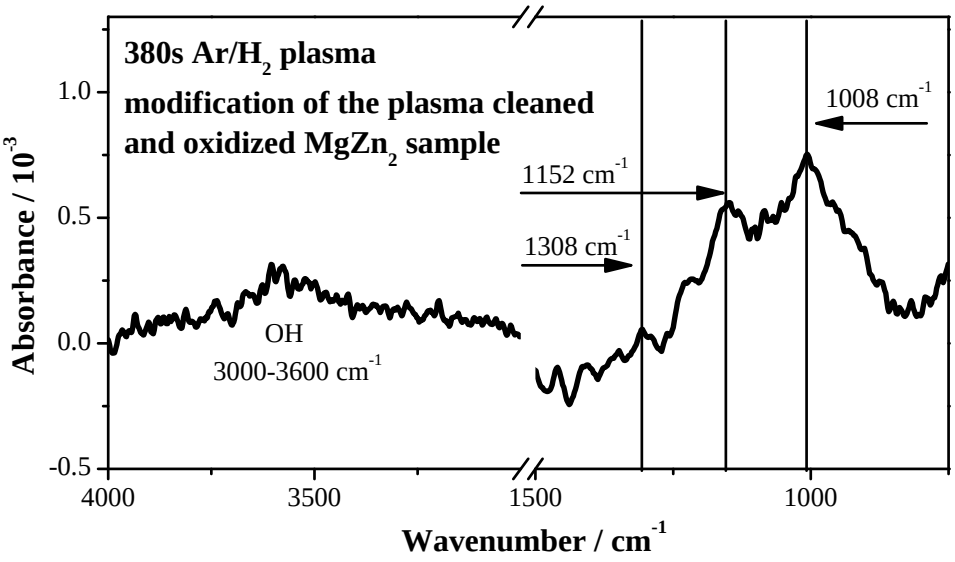

Figure 5.9: In-situ IRRA spectra of the final Ar/H_2 plasma modification of the plasma cleaned and oxidized passive layer on a grinded $MgZn_2$ sample referred to the cleaning step.

Table 5.6: Chemical composition of the $MgZn_2$ surface after a final Ar/H_2 plasma treatment analyzed by means of XPS with fitting parameters used for the determination of the contributions of species with different oxidation states to the element signals.

Element	Conc./at%	Component	B.E./eV	FWHM/eV	Percentage
C1s	**9.8** ±0.5	C–C	285.0	1.6	63.3
		C–OH	286.7	1.6	9.2
		C–OOH	289.0	1.6	9.2
		CO_3^{2-}	290.0	1.6	18.3
Mg2p	**28.3** ±0.5	$Mg^{0/2+}$	50.2	1.7	100
O1s	**54.3** ±0.5	O^{2-}	530.4	1.9	16.8
		OH	531.8	1.9	83.2
Zn2p$_{3/2}$	**7.6** ±0.5	Zn^0	1020.5	1.4	6.6
		Zn^{2+}	1022.2	1.8	93.4

of the spectrum were expanded. After the 380 s Ar/H_2 plasma modification of the oxidized surface the feature of the spectrum at 1152 cm^{-1} decreases. In contrast to this, the intensity of the peak at 1008 cm^{-1} increases. This peak was already present in the spectra of figure 5.4a and 5.4b, but here it becomes dominant. Furthermore, a small absorption band at approximately 3600 cm^{-1} appears in the spectrum, which can be assigned to the vibration of surface hydroxyl groups. However, it can be assumed in accordance to the discussion of the effects of argon plasma treatment of oxidized aluminum surfaces in chapter 4, that the Ar/H_2 plasma treatment alters the surface chemistry from more oxide like to hydroxide rich, without any further changes of the oxide thickness. This assumption is also comparable to the results on iron plasma modified surfaces discussed by Grundmeier et al. [9]. Complementary ex-situ XPS measurements on the in this way modified samples were done as well. The corresponding results are summarized in

table 5.6. A further magnesium enrichment was observed. The Zn to Mg ratio was reduced to a value of $c_{Zn}/c_{Mg} = 0.27$. The oxygen content on the surface falls back to the value before the oxidation step, but the oxide thickness, which was determined in the same way as before did not change anymore. The hydroxide to oxide ratio of $c_{OH}/c_{O^{2-}} = 4.95$ also changed to the value before the plasma oxidation.

5.5 Electronic structure of the modified ultra-thin oxide films

5.5.1 In-situ work function measurements

Complementary to the in-situ IRRAS and ex-situ XPS analysis of the changes in the passive film chemistry, the in-situ work function analysis allowed the correlation of the oxide film chemistry and thickness with the resulting Volta potential difference.

No calibration of the Kelvin probe signal is necessary, if changes of the Volta potentials, caused by different treatments of the surface are measured. Here the measured signals will be compared to the corrosion potential of pure zinc. Therefore an appropriate calibration was done by measuring the well defined Volta potential difference between the Kelvin probe tip and a freshly cleaved HOPG surface as was discussed in chapter 2. Due to this calibration procedure the measured Volta potential differences can be given as surface potential versus standard hydrogen electrode (V_{SHE}).

Figure 5.10 shows the comparison of several potential values, which are important for the further discussion. To obtain a direct comparison of the potentials after the corresponding plasma treatments, they were measured at different positions on two zones of one sample which was prepared in different

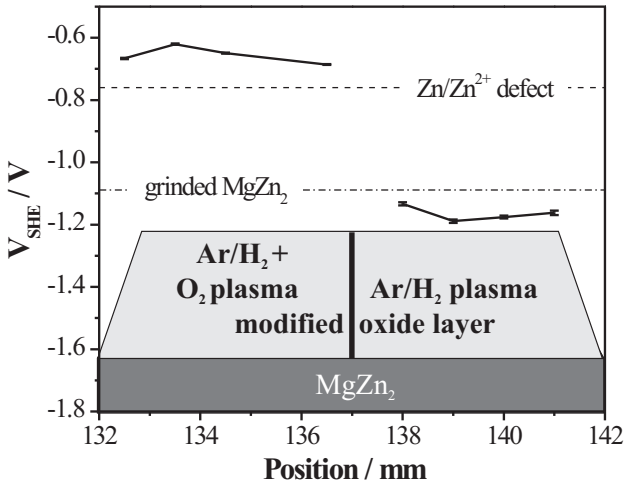

Figure 5.10: Comparison of in-situ measured surface potentials of the native $MgZn_2$ surface with the same surface after a reducing and oxidizing plasma treatment.

ways, as described in the experimental details above (see figure 5.2). The dashed line at -760 mV represents the corrosion potential of the Zn/Zn^{2+} system [1], which is given in a defect with zinc dissolution as dominant process, as will be discussed later. While the native $MgZn_2$ surface after preparation showed a potential in dry atmosphere that was about 50–300 mV (depending on the preparation and aging state of the surface) more negative as the free corrosion potential of Zn (dotted/dashed line, own measurements), the Ar/H_2-plasma treatment leads to a significant negative potential shift to a value of about -1200 mV. The oxidizing plasma leads to a positive potential shift of about +550 mV to a value of about $V_{SHE} \approx$ -650 mV, that is over 100 mV more positive than the free corrosion potential of zinc.

Figure 5.11 shows a similar sample setup as discussed above, but here a sub-

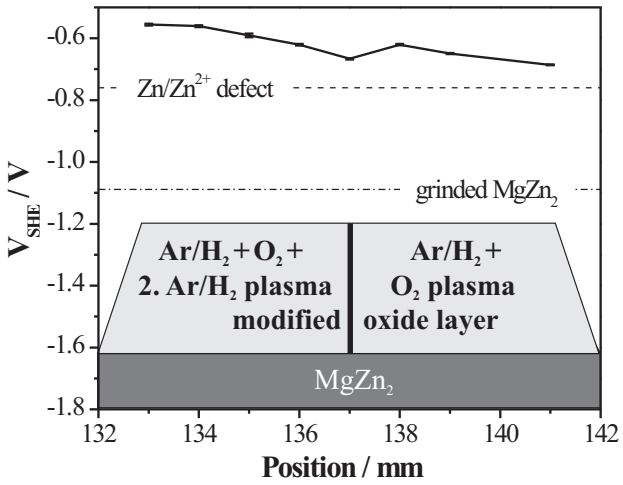

Figure 5.11: Comparison of in-situ measured surface potentials of the native $MgZn_2$ surface with the same surface after an oxidizing and a subsequent second reducing plasma treatment.

sequent reducing treatment of the oxidized part of the sample by a second Ar/H_2 plasma was performed. This second reducing plasma treatment does not change the surface potential significantly.

5.5.2 Ex-situ SKP delamination study on a model system

The in-situ measured potentials were reflected in the established interfacial electrode potentials after the application of an organic model coating as shown in figure 5.12. The sample was prepared as described before, by a full size cleaning in an Ar/H_2 plasma and a half side modification by an oxygen plasma (see experimental part, figure 5.2). After all plasma treatments the model lacquer system was applied to the surface and a defect area was

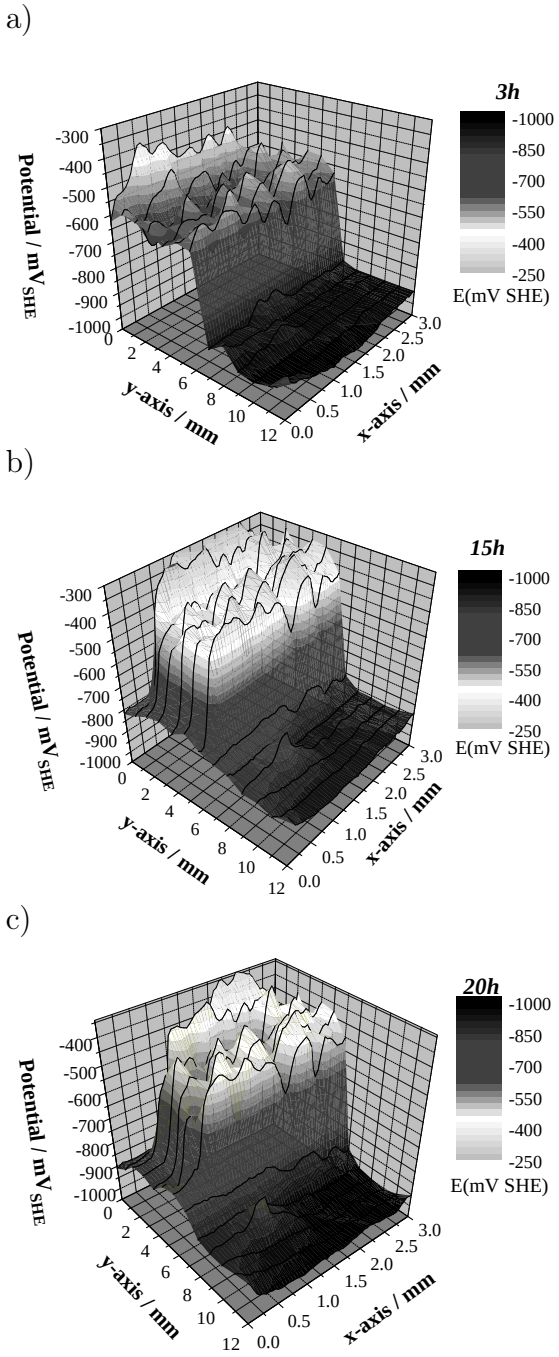

Figure 5.12: Delamination of a lacquer in humid atmosphere on $MgZn_2$ after Ar/H_2 (right) and subsequent oxygen (left) plasma modification.

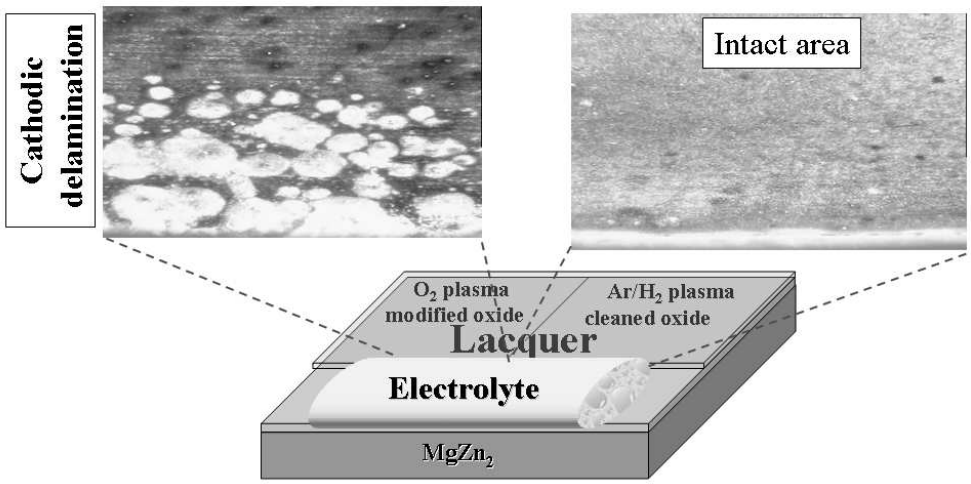

Figure 5.13: Pictures of different pre-treated areas on $MgZn_2$ after the delamination experiment, right picture show the Ar/H_2 and left picture the subsequent oxygen plasma modified area.

prepared (see the lower part of figure 5.13). Figure 5.12 shows the Volta potential difference mapping, resulting from line scans with a distance of 1 mm and a length of 3 mm. The scanner head of the SKP was aligned to start every measurement at the defect and to scan along the boundary line between the two areas treated in different ways. The plasma treated interface proved to be stable even during the coating application and curing process, thereby leading to an interfacial potential which is some tens mV more negative that the free corrosion potential of the alloy at the Ar/H_2 plasma cleaned area, whereas the oxidized part is still some hundreds mV higher. The development of the potential maps over time in figure 5.12a–c show that indeed the

delamination process occurs fast in the area where the interfacial potential was more positive than the defect potential while no delamination was observed in the plasma reduced interface. To prove the difference in interfacial stability, optical microscopy was performed on the two areas was. Clearly, corrosion products formed at the interface between the clear coat and the plasma oxidized alloy surface. The extension of the corroded interfacial area agrees well with the potential profile as measured by means of the SKP (see figure 5.12).

5.6 Discussion

Native oxides formed on the pure metals zinc and magnesium are n-type semicondutcors. This applies also to the passive film on the MgZn alloy. Figure 5.14 shows the comparison of the band gaps of these semiconducting oxide films [13]. This schematic diagram contains the informations about the positions of the corresponding valence and conducting bands (E_v and E_c), as well as the intrinsic Fermi levels ($E_{F(i)}$) and real Fermi levels caused by the donor density (E_F). It becomes clear, that the energy value of the band gap increase with the content of magnesium. Furthermore, the position of the Fermi levels is straight beneath the conducting bands of the semiconducting oxide films, what is typical for n-type semiconductors with a high density of donor states due to oxide defects in form of interstitial metal atoms or cations as well as oxygen vacancies, as was found for zinc oxide depending on the oxygen partial pressure [16, 23], or prevalent oxygen vacancies in case of magnesium oxide [20].

The plasma treatment causes several effects, which occur simultaneously, as was worked out in section 5.4 devoted to the surface chemistry of $MgZn_2$. In addition to the removal of hydrocarbon contaminations and carbonates from

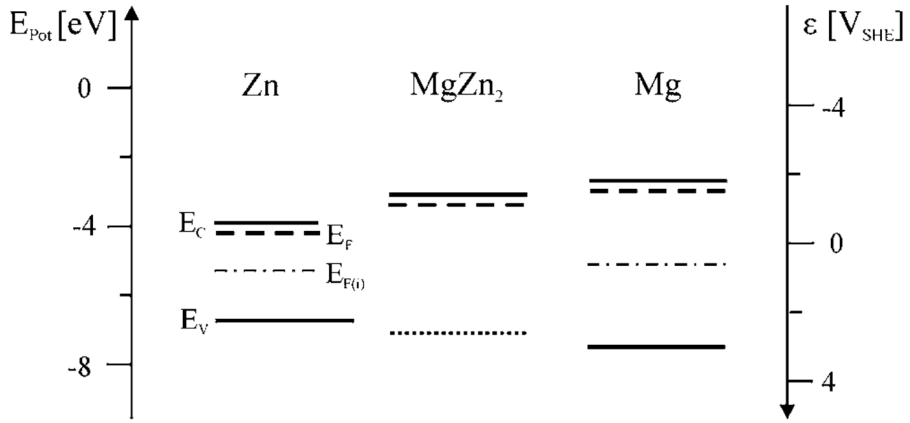

Figure 5.14: Schematic diagram of the electronic band structure of the passive films on zinc, MgZn alloy, and magnesium, with the corresponding valence and conducting level (E_v and E_c), as well as the intrinsic Fermi levels ($E_{F(i)}$) and real Fermi levels caused by a high donor density (E_F) [13].

the surface, the plasma treatments lead to a significant decrease of the zinc to magnesium concentration ratio in the oxide film, compared to the native oxide on the $MgZn_2$ sample. The values of the surface concentration ratio of zinc to magnesium c_{Zn}/c_{Mg} in the passive film on $MgZn_2$ depending on the plasma modification were calculated from the XPS data by fitting the corresponding element spectra in section 5.4 for the native sample and for each plasma modification step. The results are summarized in figure 5.15. The first Ar/H_2 plasma cleaning step shows here the highest effect, accompanied by a decrease of the hydroxide to oxide ratio (see section 5.4.2), without a significant increase of oxygen concentration and oxide thickness. This results in an increased band gap and a higher density of defects within the oxide layer on the $MgZn_2$ alloy. Hence, the Fermi level shifts to higher values, the work function falls and with this, according to the equation 2.5 in chapter 2 falls the contact potential difference, measured by the Kelvin probe,

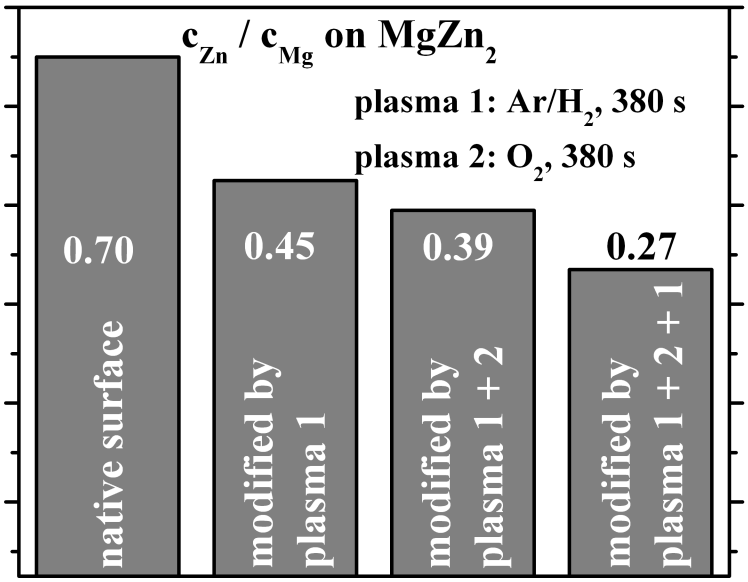

Figure 5.15: Change of the surface concentration ratio of zinc and magnesium c_{Zn}/c_{Mg} in the passive film on $MgZn_2$ depending on the plasma modification, calculated by fitting of the XPS element spectra.

as well. The subsequent oxygen plasma modification significantly increases the oxide thickness on the $MgZn_2$ surface. Thereby increase simultaneously the thickness of the zinc oxide and magnesium oxide containing layers of the passive film. The logarithmic kinetics of the oxidation process, as was described before, indicates the migration of oxygen anions through the oxide. The driving force for the anion migration to the metal/oxide interface is the high electric field caused by the plasma treatment. Moreover, the oxygen content of the oxide film on the $MgZn_2$ sample is significantly higher after the oxygen plasma modification than before. This is equivalent to the healing of oxide defects and with it to a shift of the Fermi level to lower energy values. According to the former argumentation the lowering of the Fermi level results in an increase of the contact potential difference, or equivalent

to this an increase of the Volta potential difference referred to the SHE, as was shown in the previous section.

This model of the potential development for semiconducting $MgZn_2$ oxide is in agreement with the studies of Grundmeier and Stratmann on oxide covered iron [9]. Equation 5.2 suggests an increase of the Volta potential difference between the non-modified and plasma modified state due to the lowering of the Me^+-density in the passive film.

$$\Delta(\Delta\Psi_{\mathrm{Ox}}^{\mathrm{Ref}}) = \frac{RT}{F} \ln\left(\frac{a_{Me^+}(\text{plasma 1})}{a_{Me^+}(\text{plasma 2})}\right) \tag{5.2}$$

$\Delta\Psi_{\mathrm{Ox}}^{\mathrm{Ref}}$ is the Volta potential difference between the vibrating reference electrode and the oxide surface and a_{Me^+} is the Me^+ activity respectively in the plasma 1 or plasma 2 modified metal or alloy oxide surface.

The sample after the cleaning step by an Ar/H_2 plasma with subsequent O_2 plasma oxidation and an additional treatment by another Ar/H_2 plasma shows a further decrease of the c_{Zn}/c_{Mg} ratio without any further change of the oxide thickness. The Volta potential difference of this sample remained at the same level as the oxidized surface. This indicates an increased band gap caused by the changed c_{Zn}/c_{Mg} ratio without a formation of further defects in the oxide layer, which is equivalent to an unchanged Fermi level compared to the oxidized surface of $MgZn_2$.

The electrode potential of a sample covered by a model lacquer is comparable to the potential of the passive film, since the polymer does not react with the oxide and no significant dipole potentials are formed at the oxide/polymer interface. Usually, a fast cathodic delamination was observed to proceed from defects on polymer coated oxide covered zinc. The driving force for this behavior is the potential difference between the intact area and the generally more cathodic corrosion potential of the defect. In case of the MgZn alloy the corrosion potential of the defect is determined by the dis-

solution of zinc and the resulting corrosion potential of the alloy is close to the thermodynamic potential of the Zn/Zn^{2+} electrode. A contact potential results in the vicinity to the defect, on the oxidized sample part the typical bend bending of a n-type semiconductor becomes inverted due to an electron excess, caused by the electron transfer from the defect to the intact area, when the Fermi levels equal. For this reason oxygen reduction at the oxide surface is supported and the corrosion proceeds. Contrary behavior can be observed on the Ar/H_2 plasma cleaned surface area. Here the Volta potential difference is more cathodic than on the native untreated surface and first of all more cathodic than the corrosion potential of the defect. The resulting contact potential and, linked to it, the alignment of the Fermi levels leads to a depletion of electrons at the interface and any oxygen reduction process is inhibited (see figure 1.4 in section 1.4.1).

5.7 Conclusions

Plasma modifications, as presented in this work open the possibility to a selective band gap and Fermi level engineering of the semiconducting passive film on the $MgZn_2$ alloy. By an appropriate plasma cleaning procedure in an Ar/H_2 atmosphere the surface chemistry became changed in a way resulting in an electronic structure of the oxide layer with lowered surface potential. This provide an excellent protection against the corrosive de-adhesion along the metal oxide / polymer interface, caused by the appropriate Volta potential difference between the intact area and a electrolyte filled defect. However, an oxidation of the surface in an oxygen plasma led to a healing of the oxide defects and to a significant increase of this Volta potential difference. The resulting surface potential was more anodic than the corrosion potential of the defect and the driving force for an accelerated delamination process was

given. A subsequent treatment of the oxidized $MgZn_2$ surface by a further reducing Ar/H_2 plasma affected the surface chemistry slightly by changing the oxide to hydroxide ratio, but it did not lead to an increase of the donor site density within the oxide layer and in consequence it did not inverse the effect of the oxygen plasma modification.

5.8 References

[1] P. W. Atkins. *Physikalische Chemie*. VCH Verlagsgesellschaft mbH, Weinheim, 1996.

[2] F. Boccuzzi, A. Chiorino, S. Tsubota, and M. Haruta. FTIR study of carbon monoxide oxidation and scrambling at room temperature over gold supported on ZnO and TiO_2. *Journal of Physical Chemistry*, 100(9):3625–3631, 1996.

[3] Z. J. Cui and C. G. Takoudis. Characterization of ultrathin silicon oxide films with mirror-enhanced polarized reflectance Fourier transform infrared spectroscopy. *Journal of Applied Physics*, 89(9):5170–5176, 2001.

[4] C. Fotea, J. Callaway, and M. R. Alexander. Characterisation of the surface chemistry of magnesium exposed to the ambient atmosphere. *Surface and Interface Analysis*, 38(10):1363–1371, 2006.

[5] M. Giza and G. Grundmeier. Combination of FTIR reflection absorption spectroscopy and work function measurements for in-situ studies of plasma modified passive films on $MgZn_2$. *In preparation.*

[6] G. Grundmeier, M. Brettmann, and P. Thiemann. In situ spectroscopic and corrosion studies of ultra-thin gradient plasma polymer layers on zinc. *Applied Surface Science*, 217:223–232, 2003.

[7] G. Grundmeier, E. Matheisen, and M. Stratmann. Formation and stability of ultrathin organosilane polymers on iron. *Journal of Adhesion Science and Technology*, 10(6):573–588, 1996.

[8] G. Grundmeier and M. Stratmann. Nucleation and growth of plasma-polymerized hexamethyldisilazane on iron-substrates. *Berichte*

der Bunsen-Gesellschaft – Physical Chemistry Chemical Physics, 99(11):1387–1392, 1995.

[9] G. Grundmeier and M. Stratmann. Influence of oxygen and argon plasma treatments on the chemical structure and redox state of oxide covered iron. *Applied Surface Science*, 141(1-2):43–56, 1999.

[10] W. N. Hansen and G. J. Hansen. Standard reference surfaces for work function measurements in air. *Surface Science*, 481(1-3):172–184, 2001.

[11] R. Hausbrand. *Elektrochemische Untersuchungen zur Korrosionsstabilität von polymerbeschichtetem Zink-Magnesiumüberzug auf Stahlband*. PhD thesis, Department of Chemistry, Ruhr-University Bochum, 2003.

[12] R. Hausbrand, M. Stratmann, and M. Rohwerder. Delamination resistant zinc alloys: Simple concept and results on the system zinc-magnesium. *Steel Research International*, 74(7):453–458, 2003.

[13] R. Hausbrand, M. Stratmann, and M. Rohwerder. The physical meaning of electrode potentials at metal surfaces and polymer/metal interfaces: Consequences for delamination. *Journal of the Electrochemical Society*, 155(7):C369–C379, 2008.

[14] N. C. Hosking, M. A. Strom, P. H. Shipway, and C. D. Rudd. Corrosion resistance of zinc-magnesium coated steel. *Corrosion Science*, 49(9):3669–3695, 2007.

[15] H. P. Hughes and J. A. Scarfe. Lineshapes in core-level photoemission from metals. 1. Theory and computational analysis. *Journal of Physics-Condensed Matter*, 8(10):1421–1438, 1996.

[16] A. F. Kohan, G. Ceder, D. Morgan, and C. G. Van de Walle. First-principles study of native point defects in ZnO. *Physical Review B*, 61(22):15019–15027, 2000.

[17] Casa Software Ltd. CasaXPS version 2312, 2005.

[18] A. R. Marder. The metallurgy of zinc-coated steel. *Progress in Materials Science*, 45(3):191–271, 2000.

[19] A. K. Neufeld and I. S. Cole. Usind Fourier transform infrared analysis to detect corrosion products on the surface of metals exposed to atmospheric conditions. *Corrosion*, 53(10):788–799, 1997.

[20] G. Pacchioni. Ab initio theory of point defects in oxide materials: structure, properties, chemical reactivity. *Solid State Sciences*, 2(2):161–179, 2000.

[21] B. Schuhmacher, W. Muschenborn, M. Stratmann, B. Schultrich, C. P. Klages, M. Kretschmer, U. Seyfert, F. Forster, and H. J. Tiller. Novel coating systems and surface technologies for continuous processing of steel sheet. *Advanced Engineering Materials*, 3(9):681–689, 2001.

[22] N. J. Shirtcliffe, M. Stratmann, and G. Grundmeier. In situ infrared spectroscopic studies of ultrathin inorganic film growth on zinc in non-polymerizing cold plasmas. *Surface and Interface Analysis*, 35(10):799–804, 2003.

[23] D. G. Thomas. Interstitial zinc in zinc oxide. *Journal of Physics and Chemistry of Solids*, 3(3-4):229–237, 1957.

[24] W. H. J. Vernon, E. I. Akeroyd, and E. G. Stroud. Tie direct oxidation of zinc. *Journal of the Institute of Metals*, 65:301–329, 1939.

[25] K. Wapner and G. Grundmeier. Scanning Kelvin probe measurements of the stability of adhesive/metal interfaces in corrosive environments. *Advanced Engineering Materials*, 6(3):163–167, 2004.

[26] K. Wapner, B. Schoenberger, A. Stratmann, and G. Grundmeier. Height-regulating scanning Kelvin probe for simultaneous measurement of surface topology and electrode potentials at buried polymer/metal interfaces. *Journal of the Electrochemical Society*, 152(3):E114–E122, 2005.

Chapter 6

Investigations of the effect of a dielectric barrier discharge on silicon surfaces

6.1 Introduction

Since, silicon wafer bonding is one of the important processes for the electronic industry. It was found that the bonding temperature can be significantly lowered to about 200 °C by a plasma pretreatment of wafers [10], with a dramatical advantage for involved materials like aluminum (melting point by 660 °C).

Despite numerous publications, which already appeared on this topic, explanations for the improved low-temperature bond behavior still leave plenty of room for discussion. However, a consensus can be drawn from the literature, that several reasons have to be taken in consideration, which in sum are supposed to lead to the beneficial effect. First of all, the modification of the covering oxide layer by energetic ions impinging from the plasma are claimed to play an important role. The oxygen ions are supposed to penetrate 1-2 nm deep into the oxide layer, where they cause a subsurface modification in a way

that leads to increased porosity and increased reactivity [1]. Both, increased porosity and reactivity, are believed to be responsible for the dramatical enhanced dynamics and strength of bond formation especially at low annealing temperatures. The high reactivity origins from the increase of the number of OH groups at the surface in the cleaning step after plasma activation and the porosity leads to an improved diffusivity of water and gaseous species away from the interface [18].

In contrast to the low pressure plasma activation described so far, wafer activation with atmospheric pressure plasma (i.e. dielectric barrier discharge (DBD)) is comparably new. The DBD activation method is highly interesting for industrial use due to the simplicity of the hardware setup and the increased throughput. In 2004, first experiments were done at the Fraunhofer IST in cooperation with the Max-Planck-Institut für Mikrostrukturphysik [8]. Bond strengths up to 2.5 Jm^{-2} could be obtained upon annealing at 200 °C. However, very little has been published on the surface modifying effect of DBD treatment for silicon wafers as pre-treatment method for enhanced low-temperature bonding, yet. Furthermore, it is well known, that ozone has a high oxidizing potential and is the main component of the gas species generated by the dielectric barrier discharge [6]. Thus the influence of the pure ozone on the oxidation process of a hydrogen terminated silicon wafer was studied in comparison, by means of the setup allowing plasma modifications and in-situ FT-IRRA spectroscopy.

The results presented in this chapter are part of a publication with additional studies on the dielectric barrier discharge effects on the roughness, cleaning, and further oxidation of the native oxide layer of a silicon sample [12].

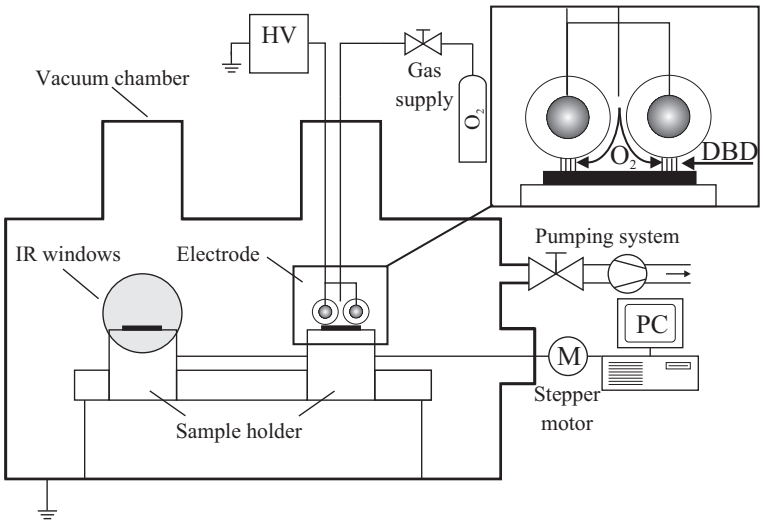

Figure 6.1: Experimental setup for ozone treatment and in-situ mirror enhanced infrared reflection absorption spectroscopy [14].

6.2 Experimental details

For the here presented in-situ studies n-type phosphorus doped silicon <111> wafers (Si-Mat, Germany) with a resistivity of 1–50 Ωcm were used. The wafers (diameter: 100 mm, thickness: 500 μm) were cut to samples of 20 x 20 mm^2, RCA 1 cleaned with 30% hydrogen peroxide, 28 – 30 % ammonium hydroxide and ultra pure water (Elga Purelab Plus, Germany) (1:1:5 in volume) at 353 K for 15 minutes, rinsed with ultra pure water and stored in ultra pure ethanol. Each sample was dried in a nitrogen stream before it was dipped in a 40 % NH_4F solution for 8 minutes to remove the native oxide and terminate the surface by hydrogen. For the experiments the vacuum sealed chamber (shown in figure 6.1, see also chapter 2), was flushed with oxygen at atmospheric pressure (quality 4.5 by Air Liquide). A set of two copper electrodes shielded by a 1 mm Al_2O_3 cylindrical shell was placed directly over a sample holder with a gap size of approximately 1 mm. The

application of a high voltage at a frequency of 30.7 kHz results in a filamented barrier discharge between the electrodes and the grounded sample holder. For a homogeneous DBD treatment of a sample the holder can be moved with an adjustable velocity from 0.1 to 30 mm/s through the plasma zone. Following to the plasma treatment the holder was automatically adjusted to the optical path of a FTIR spectrometer (Digilab, FTS 3000). The mid infrared beam was guided by a set of mirrors, transmitted through ZnSe windows onto the sample and reflected under 80° to the surface normal to a LN_2 cooled mercury cadmium telluride (MCT) detector. Due to the optical transmittance of silicon in this spectral range a gold coated mirror was placed at the backside of the sample with a gap of approx, 30 μm by adding two stripes of commercial aluminum foil between the sample and the mirror. This so called mirror enhanced Fourier transform infrared reflection absorption spectroscopy (ME-FT-IRRAS) was proven to be sensitive for detection of ultra thin oxides formed on silicon wafer [4]. This unique combination of the described plasma chamber with the ME-FT-IRRAS method provides in-situ studies of DBD induced changes of the surface chemistry. All presented spectra of final states were recorded using a resolution of 4 cm^{-1} and originate from a co-addition of 256 single scans. Ozone is known to be a product of the DBD chemistry on atmospheric pressure [6]. A slight modification of the setup described above allowed in-situ online studies of the influence of this long life molecule to the hydrogen terminated silicon surface by means of the ME-FT-IRRAS. For these measurements the sample holder was fixed to the optical path of the FTIR spectrometer and a second holder was fixed beneath the electrodes. The on-line measurements of the oxide growth kinetics have to be done much faster and were recorded using a resolution of 8 cm^{-1}, by a co-addition of 18 scans this results in a time resolution of ap-

prox. 5 s. The results obtained from the ME-FT-IRRAS measurements were additionally verified by means of X-ray photoelectron spectroscopy (XPS, Quantum 2000, Physical Instruments, USA) using a monochromated Al K_α X-ray source with a spot diameter of 100 μm. The take off angle of the detected photoelectrons was 45° to the surface normal. The calibration of the spectra was performed using the C 1s peak (binding energy, BE= 285 eV) as internal reference.

6.3 Results and discussion

The dipping of native oxide covered silicon samples into the NH_4F solution leads to an ultra hydrophobic and oxide free hydrogen terminated Si surface. The quality of the resulting passive surface was checked via the water contact angle measurement and by means of XPS. Figure 6.2 shows the corresponding detail spectrum of Si2p after an 8 minutes NH_4F treatment and a few minutes exposure to the ambient air due to the transport to the XPS equipment. The spectrum shows well resolved the spin-orbit coupling with an energy difference of 0.6 eV. No higher oxidation states of silicon could be observed. A further analysis of detected elements on the surface shows a contamination by carbon species in the range of about 14 at%. After the DBD experiments as described in the experimental section, the XPS measurements of modified silicon surfaces have shown a formation of an ultra-thin oxide layer on the non treated backside of the sample. This might be caused by the formation of long life oxidizing species in the discharge, in particular ozone [6], which is distributed over the whole volume of the chamber and to attain to the backside of the sample through the gap formed by the sample and the mirror. Before any discussion of effects of a DBD treatment on a silicon surface attention should be paid to the influence of ozone to the hydrogen termi-

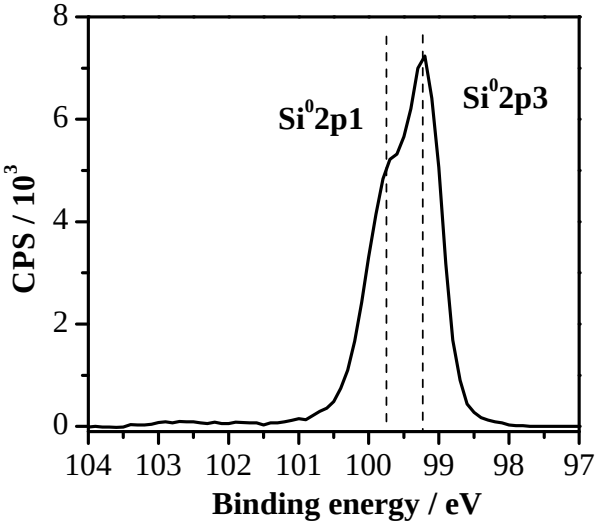

Figure 6.2: XPS element spectrum of hydrogen terminated silicon surface.

nated silicon surface. The influence of ozone at room temperature on an oxide covered wafer can be neglected as was discussed by Michel and Giza in [12]. This cannot be applied to the hydrogen terminated wafers, as is shown in figure 6.3 by means of ME-FT-IRRAS. The region between 2000 cm^{-1} and 3000 cm^{-1} (see figure 6.3a) includes the peaks of CH_2 and CH_3 groups which confirm the ultra-thin contamination layer observed by XPS and a sharp peak at 2080 cm^{-1}. This transition belongs to the absorption of the silicon monohydride, which typically forms during the NH_4F etching of the Si (111) surface due to the one dangling bond per Si atom at this surface orientation [2]. The negative appearance of these vibration modes in the spectrum clearly indicates the ozone induced oxidizing of the contamination layer as well as the removal of Si-H bonds at the surface. Moreover, the spec-

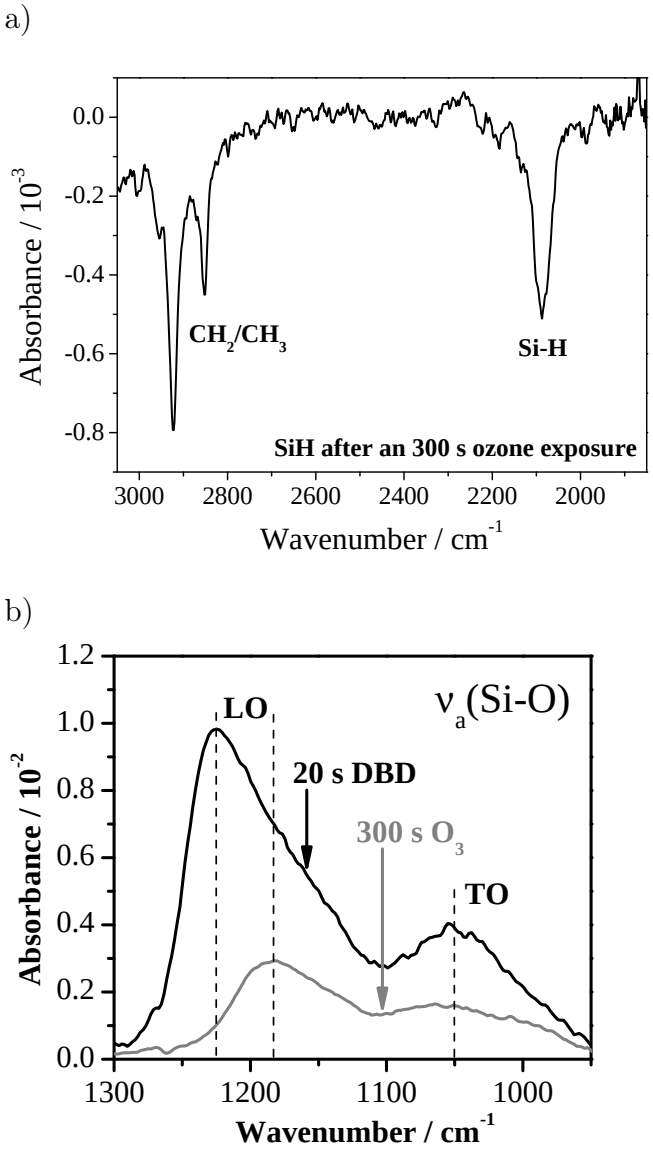

Figure 6.3: ME-IRRAS of the oxidation process of a H-terminated silicon surface, a) spectral range of the $CH_{2/3}$, Si-H stretching vibrations and b) longitudinal and transversal optical mode of the Si-O vibration resulted from ozone (grey line) and O_2 DBD (black line) modification.

tral region between 800 cm^{-1} and 1300 cm^{-1} is shown in figure 6.3b. Strong positive absorptions bands arise in this part of the spectrum, which can be assigned to the transversal (TO) and longitudinal (LO) optical modes of the asymmetric Si-O stretching vibration in a SiO_x layer formed due to the ozone exposure and after O_2-DBD treatment respectively. The maximum of the LO mode after a 300 s ozone exposure at room temperature appears at 1180 cm^{-1} and of the TO mode at 1050 cm^{-1} respectively. The position of the TO mode after a DBD treatment does not change, while the LO mode shifts to higher values (1225 cm^{-1} after 20 s O_2-DBD). For thin oxide films on silicon the intensity of the FTIR absorption bands correlates straight proportional with the oxide thickness, this was proven by Cui et al. until a thickness of about 5 nm [4]. The lowering of the number of scans combined with a decreasing of the spectral resolution makes the in-situ ME-FTIRAS setup suitable for kinetic measurements of the ozone induced oxidation of the hydrogen terminated Si surfaces with a time resolution in the range of 5 s. The so caused decrease of the signal to noise ratio is acceptable and still allows the acquisition of spectra in appropriate quality as is shown in figure 6.4a. The spectrum shown in figure 6.4a is a snapshot of an online measurement of the oxidation process, which has been selected at an arbitrary point of time during the ozone formation inside of the chamber. The dominant feature of this spectrum is the vibration band of ozone at 1050 cm^{-1} [7, 16]. Unfortunately, this absorption peak of the O_3 molecule interferes with the TO band of the simultaneously formed SiO_x layer. For this reason the heights of the peaks were considered for the analyses of oxidation kinetics, not the areas of the absorption bands as usual. In case of DBD oxidation a linear dependence of the measured peak area to the peak height was observed, so that this interpretation of the measured data does not influence the conclusions discussed

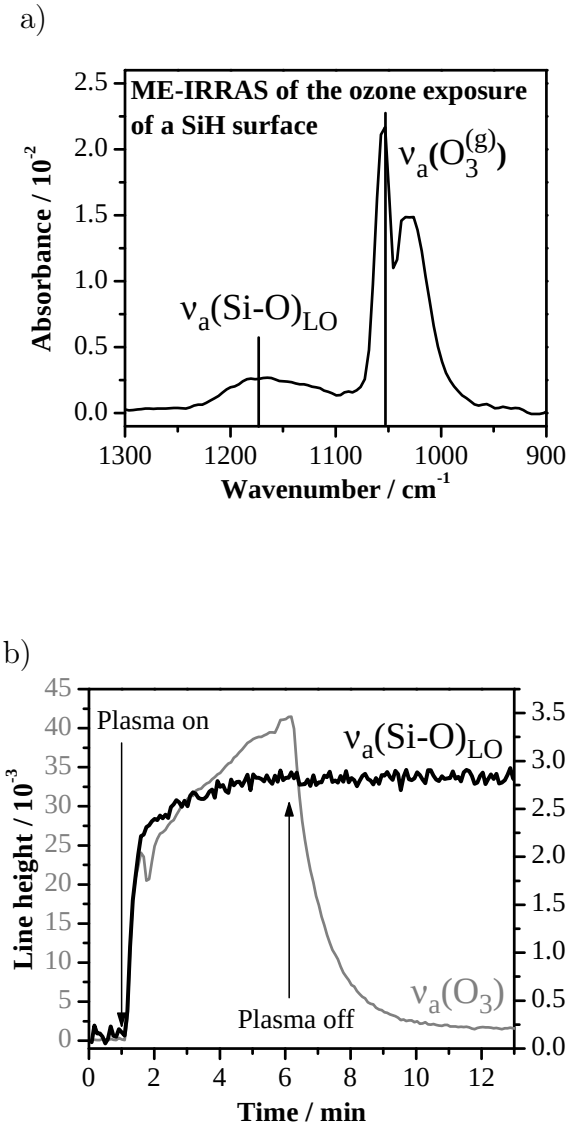

Figure 6.4: In-situ ME-IRRAS measurements of (a) the ozone induced modification of a hydrogen terminated silicon wafer surface and (b) of the kinetics of ozone induced oxide growth on hydrogen terminated Si (black line, right y-axis), with the kinetic of ozone generation (grey line, left y-axis).

here. Figure 6.4b shows the measured peak height of the LO mode over the time of ozone exposure (black line, right y-scale). The ozone was generated as described in the experimental section by a barrier discharge in the vicinity of the silicon wafer. The plasma was switched on after 60 s of the experiment and switched off after 360 s (indicated by arrows in figure 6.4b). The trend of ozone concentration is represented by means of the height of the feature at 1050 cm^{-1} in the FTIR spectrum (grey line, left y-scale). A fast initial growth of the Si-O signal was measured immediately after the switching-on the plasma, followed by a slower increase which ends in a plateau region. The ozone concentration does not achieve the maximum value before the plasma was switched off and decrease to the zero value within of further 300 s. There appears a reproducible slight drop in the trend of the ozone concentration at that time of the change over of the Si-O signal from the fast initial growth to the slow further increase. This behavior can be explained with adsorption of ozone on the freshly formed oxide film due to the dipole moment of ozone of 0.53 D [17, 11]. The ozone exposure leads to an oxidation of both sides of the silicon wafer in a uniform manner, as was proved by XPS measurements (see below). The kinetic is characterized by a fast initial oxide growth of 80 % of the maximum value within the first 30 s of oxidation followed by a slow increase of the signal until the DBD was switched off after 300 s. Trends in figure 6.5 compares the dependence of oxide thickness on the treatment time of the ozone exposed wafer to the O_2-DBD treated sample. It has to be considered, that the x-axis represents the plasma on time. Since the ozone fills the volume of the chamber, the plasma on time is equivalent to the time of O_3-exposure. However, the DBD treatment takes place in a small volume beneath each electrode only; the wafer (20 mm x 20 mm) was moved under both electrodes during the plasma on time (see figure 6.1). In this case the

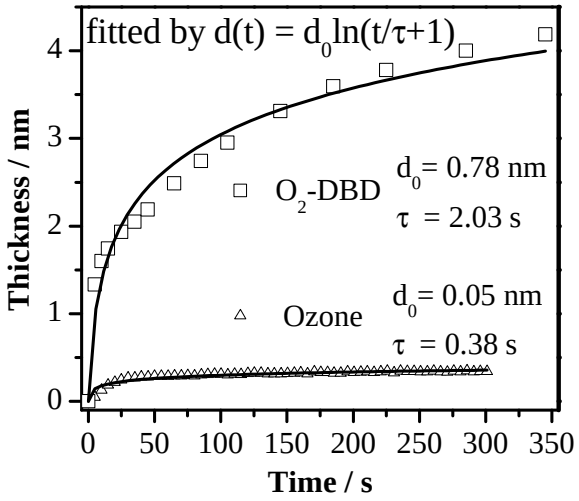

Figure 6.5: Kinetics of oxide growth on a hydrogen terminated silicon surface induced by O_2-DBD treatment and ozone exposure respectively, measured by in-situ ME-IRRAS, IR intensity was converted to oxide thickness by complementary XPS analysis.

plasma on time is not equivalent to the time of DBD treatment on each position on the wafer. This fact implies a linear mismatch of plotted time to the effective treatment time. Since only the shape of the kinetics was analyzed here this inaccuracy does not affect the drawn conclusions. It is quite evident in figure 6.5, that the DBD effect considerably dominates over the time. The FTIR intensity and oxide thickness respectively are an order of magnitude higher for the DBD modification compared to the ozone exposure within a treatment time of 300 s. Best fits were obtained for both measured trends by using the same empirical direct logarithmic law as in case of DBD oxidation of the native oxide on silicon (see contribution from Michel and

Giza [12]). The low temperature oxidation model, witch results in a direct logarithmic law is based upon the consideration of a thickness-independent surface charge, leading to a thickness-independent electrical field across the oxide as the driving force for anion movement to the Si/SiO_2 interface. Oxygen anions can be formed at the silicon surface by dissociation of ozone to molecular and atomic oxygen followed by an electron capture from the discharge. It can be assumed that the surface concentration of adsorbed oxygen ions is higher in the direct contact to the barrier discharge, which results in the higher oxidation rate observed for the O_2-DBD treatment. This direct logarithmic law was discussed in more detail in section 1.4.1. Compared to the LO mode position on DBD treated native oxide on silicon a similar value was found after the DBD treatment of hydrogen terminated wafer. A shift of the measured frequency of about 10 cm^{-1} over the DBD treatment time and oxide thickness respectively could be observed. A corresponding shift of the TO mode could not be detected. A significant shift of the maximum of the LO mode was observed during the oxidation in the ozone atmosphere. The trend of the peak position over the oxide thickness is shown in figure 6.6. For a better determination of the peak position a FFT flattening over five measured points was performed. The first evaluable appearance of the $\nu_a(Si\text{-}O)_{LO}$ vibration was after 15 s of exposure at 1130 cm^{-1}, as mentioned above the corresponding TO mode was hidden by the ozone signal. As is shown in the extended view of the ozone data in figure 6.6 the LO peak position increased almost linearly with the oxide thickness by 47 cm^{-1} to the maximum value of 1177 cm^{-1}, within the range of investigated thickness velues. Oxidation of silicon in ozone containing atmospheres at elevated temperatures (200 – 500 °C) has been studied by Cui et al. [3]. Special attention was paid to the position of the LO mode depending on treatment condi-

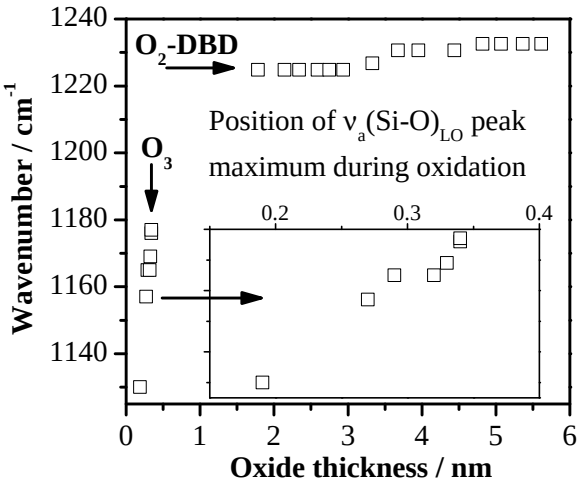

Figure 6.6: Position of the LO mode maximum of the asymmetric Si-O vibration peak maximum over the oxide thickness.

tions. The highest shifts were observed during the oxidation in pure oxygen atmosphere and were explained by the formation of a considerable suboxide layer at the SiO_2/Si interface. Oxides with a higher SiO_2 content were observed during oxidation in ozone containing atmospheres by a shift of the LO mode to higher frequencies. However, the corresponding shift of the TO mode was not considered. However, the latter was discussed in other publications [13, 5]. A change of the density of the formed oxides accompanied by a change of the angle of the O-Si-O bond results also in a simultaneously shift of both TO and LO mode. However, no evidence was found for a shift of the TO mode during the ozone exposure from the here presented studies due to the interference with the ozone vibration. Moreover, no shift could be observed compared to the DBD formed layer. For comparison, the LO

shift measured between the ozone and the DBD caused peak positions was found to be 45 cm^{-1}. This behavior cannot be explained by suboxides and density effects only, in particular due to the lack of a TO mode shift comparing the ozone induced with the DBD caused TO position (see figure 6.3b). In agreement with the conclusions of the results of the DBD treatment of the native oxide layer a porosity of the formed oxide has to be considered as an explanation. Figure 6.7 shows the Si2p region of the XPS measurements on silicon wafers modified by 300 s of ozone exposure and O_2-DBD respectively. In contradiction to the hydrogen terminated Si(111) surface the modified surfaces show significant contribution of Si in higher oxidation states. Similar spectra were measured at the front side and at the backside of the ozone exposed sample and at the backside of the DBD treated wafer. The shift of the binding energy of the oxidized species compared to the Si0 signal at 99.2 eV is in case of ozone exposure (grey line) +3.8 eV and in case of the DBD treatment (black line) +4.8 eV. Both signals shifts originate from the oxidation state +IV of the Si atom. Analogue to the results on the DBD treatment of native oxides the shift difference can be explained by the enhanced build-up of charge density in the oxide film under X-ray bombardment during the measurement [9]. The oxide layer thickness was determined from the XPS data by

$$d_{SiO_2} = \lambda_{SiO_2} \cos\Theta \ln\left(1 + \frac{I_{SiO_2}}{\beta I_{Si}}\right) \tag{6.1}$$

where λ_{SiO_2} = 3.5 nm [15], $\beta = \frac{I_{SiO_2}}{I_{Si}}$ = 0.75 and Θ = 45°. An oxide layer thickness of 4.3 nm on the DBD treated sample and of 0.34 nm on the ozone exposed sample was obtained from the Si_{4+}/Si_0 intensity ratio using eq. 6.1. By means of the determined thickness values of the ozone and DBD

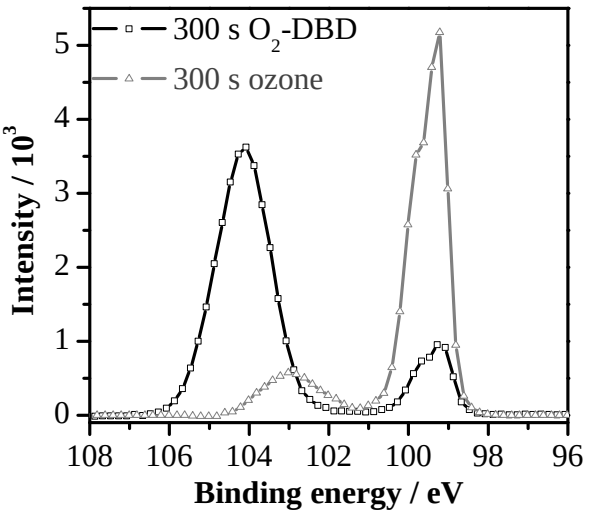

Figure 6.7: Ex-situ XPS on a SiH surfaces modified by ozone exposure and O_2-DBD treatment respectively.

treated samples the corresponding ME-IRRAS absorption bands intensities were calibrated.

6.4 Conclusions

The impact of dielectric barrier discharge (DBD) in oxygen and of pure ozone at room temperature on a hydrogen terminated silicon surfaces was investigated. Both treatments were able to significantly reduce the amount of hydrocarbon contaminations on the surfaces. An oxide layer of 4.3 nm thickness was found to be formed by means of the DBD treatment, however a significant oxide formation by exposure to pure ozone was detected as well. It was found, that the formation of oxides in both treatment cases follows

a direct logarithmic law for the dependence of oxide thickness on treatment time. This leads to the assumption of an oxidation process determined by highly reactive species, primary negative oxygen ions from the discharge and ozone dissociation. A significant porosity of the formed oxide layers was indicated by the shift of the peak position of the LO part of the asymmetric Si-O vibration measured by means of in-situ ME-FT-IRRA spectroscopy.

6.5 References

[1] P. Amirfeiz, S. Bengtsson, M. Bergh, E. Zanghellini, and L. Borjesson. Formation of silicon structures by plasma-activated wafer bonding. *Journal of the Electrochemical Society*, 147(7):2693–2698, 2000.

[2] Y. J. Chabal and K. Raghavachari. Applications of infrared absorption spectroscopy to the microelectronics industry. *Surface Science*, 502:41–50, 2002.

[3] Z. J. Cui, J. M. Madsen, and C. G. Takoudis. Rapid thermal oxidation of silicon in ozone. *Journal of Applied Physics*, 87(11):8181–8186, 2000.

[4] Z. J. Cui and C. G. Takoudis. Characterization of ultrathin silicon oxide films with mirror-enhanced polarized reflectance Fourier transform infrared spectroscopy. *Journal of Applied Physics*, 89(9):5170–5176, 2001.

[5] R. A. B. Devine. Structural nature of the Si/SiO_2 interface through infrared spectroscopy. *Applied Physics Letters*, 68(22):3108–3110, 1996.

[6] B. Eliasson, M. Hirth, and U. Kogelschatz. Ozone synthesis from oxygen in dielectric barrier discharges. *Journal of Physics D-Applied Physics*, 20(11):1421–1437, 1987.

[7] J. M. Flaud and R. Bacis. The ozone molecule: infrared and microwave spectroscopy. *Spectrochimica Acta Part a-Molecular and Biomolecular Spectroscopy*, 54(1):3–16, 1998.

[8] M. Gabriel, B. Johnson, R. Suss, M. Reiche, and M. Eichler. Wafer direct bonding with ambient pressure plasma activation. *Microsystem Technologies-Micro-and Nanosystems-Information Storage and Processing Systems*, 12(5):397–400, 2006.

[9] S. Iwata and A. Ishizaka. Electron spectroscopic analysis of the SiO_2/Si system and correlation with metal-oxide-semiconductor device characteristics. *Journal of Applied Physics*, 79(9):6653–6713, 1996.

[10] G. Kissinger and W. Kissinger. Void-free silicon-wafer-bond strengthening in the 200-400 degrees-C range. *Sensors and Actuators a-Physical*, 36(2):149–156, 1993.

[11] K. Koike, T. Fukuda, S. Ichimura, and A. Kurokawa. High-concentration ozone generator for oxidation of silicon operating at atmospheric pressure. *Review of Scientific Instruments*, 71(11):4182–4187, 2000.

[12] B. Michel, M. Giza, M. Krumrey, M. Eichler, G. Grundmeier, and C.-P. Klages. Investigations on the effect of dielectric barrier discharge (DBD) on silicon surfaces. Part I: Surface roughness, cleaning, and oxidation. *Submitted to Journal of Applied Physics*, in 2008.

[13] K. T. Queeney, M. K. Weldon, J. P. Chang, Y. J. Chabal, A. B. Gurevich, J. Sapjeta, and R. L. Opila. Infrared spectroscopic analysis of the Si/SiO_2 interface structure of thermally oxidized silicon. *Journal of Applied Physics*, 87(3):1322–1330, 2000.

[14] J. Raacke, M. Giza, and G. Grundmeier. Combination of FTIR reflection absorption spectroscopy and work function measurement for in-situ studies of plasma modification of polymer and metal surfaces. *Surface and Coatings Technology*, 200(1-4):280–283, 2005.

[15] M. P. Seah and W. A. Dench. Quantitative electron spectroscopy of surfaces: A standard data base for electron inelastic mean free paths in solids. *Surface and Interface Analysis*, 1(1):2–11, 1979.

[16] B. C. Stratton, R. Knight, D. R. Mikkelsen, A. Blutke, and J. Vavruska. Synthesis of ozone at atmospheric pressure by a quenched induction-coupled plasma torch. *Plasma Chemistry and Plasma Processing*, 19(2):191–216, 1999.

[17] A. G. Streng. Tables of ozone properties. *Journal of chemical and engineering data*, 6(3):431–436, 1961.

[18] T. Suni, K. Henttinen, I. Suni, and J. Makinen. Effects of plasma activation on hydrophilic bonding of Si and SiO_2. *Journal of the Electrochemical Society*, 149(6):G348–G351, 2002.

Chapter 7

Overall Conlusions – Outlook

A permanent adhesion of a coating to the substrate material depends strongly on the interface chemistry. Appropriate docking sites for the functional groups of the coating material as well as an electronic structure of the interface, which reduces the driving force for migration of electrolyte along the interface are essential to avoid an easy de-adhesion of coatings.

In the here presented work low temperature plasmas at low and atmospheric pressure were applied to solid surfaces for tailoring of the surface chemistry as well as for band gap and Fermi level engineering. For an in-situ analysis of the plasma induced changes on the studied surfaces a special experimental setup was developed. Fourier transform infrared reflection absorption spectroscopy with a sensitivity in the sub-nanometer range as well as Kelvin probe measurements could be applied in-situ to study the changes of surface chemistry and electronic structure of the surfaces.

For a better understanding of the involved processes and mechanisms model systems were identified and used instead of the often undefined technical samples.

A self-assembly monolayer of octadecyl mercaptan was used as model for a polymeric surface with terminating methyl groups. By means of in-situ IR-

RAS it could be shown, that short remote oxygen plasma treatments lead to a step by step etching of the organic chains with an introduction of terminating carbonyl functions. The involved electric dipole moment of the carbonyl functions could be proved by means of in-situ Kelvin probe measurements on the modified self-assembly film.

The influence of discharges in different gas atmospheres at low pressure on polished oxide covered iron surfaces was studied by means of in-situ IRRAS and Kelvin probe measurements as well. A correlation of the different reducing and oxidizing plasmas with the oxide composition in terms of the ratio of the concentrations of the two oxidation states of iron +II and +III within the oxide layer was found. Except of the different vibration frequencies in the FTIR spectrum of both oxidation states, a significant change of the electronic structure could be shown by means of the work function measurements by the Kelvin probe technique.

New concepts of corrosion protection of metal surfaces by means of inorganic coatings require the application of alloys as coating material. The composition of the outermost surface layer of such coatings, especially of the covering oxide films differs in the most cases from the bulk composition. Depending on the diffusivity of each species during the cooling period after the deposition at elevated temperatures or alloying of the several components after the deposition, the concentration of one or two components can dominate within the covering oxide. Aluminum is an example for a material with an extreme high diffusivity.

The influence of a plasma pretreatment of the native oxide layer on aluminum on the adsorption of an adhesion promoting layer in terms of a self-assembly film of octadecylphosphonic acid was investigated here. By means of subsequent water vapor and argon plasma modifications of the passive film on alu-

minum, different densities of hydroxides could be adjusted within the formed oxide layer. The modifications were proved by means of in-situ IRRAS and complementary ex-situ XPS measurements. Afterwards, a monolayer of the octadecylphosphonic acid was adsorbed from a solution. The adsorption process was monitored by means of a quartz crystal micro balance and the formed layer was proved by ex-situ IRRAS and XPS. It could be shown, that the water plasma induced increase of hydroxide density within the oxide layer strongly accelerates the adsorption process of the ODPA. This acceleration can be explained by the adsorption of phosphonic acid via hydrogen bonds prior to a condensation reaction, leading to the finally adsorbed phosphonate.

Another example for corrosion protecting films are coatings based on the MgZn alloy. One of the thermodynamical stable phases of these alloys is the $MgZn_2$ phase. Plasma modification of the passive films on the $MgZn_2$ alloy was performed in this work and the influence on the corrosion protection was analyzed. By means of in-situ IRRAS, in-situ Kelvin probe and ex-situ XPS measurements as well as scanning Kelvin probe measurements on polymer coated material, different surface states could be identified and the effects on the corrosion determined de-adhesion of the polymer coating was studied. The donor site density and the magnesium content within the semiconducting oxide layer on $MgZn_2$ could be increased by means of a Ar/H_2 plasma cleaning of the surface, this led to a increase of the band gap and to a shift of the Fermi level resulting in a lower Volta potential difference to a electrolyte filled defect at the free corrosion potential of the Zn/Zn^{2+} system. A cathodic de-adhesion of the polymer coating, caused by the potential difference driven migration of electrolyte along the interface was inhibited. Contrary to this a subsequent oxygen plasma treatment heals the defects within the oxide and

increases the oxide thickness significantly. The resulting increase of the Volta potential difference to more anodic values compared to the defect potential led to an accelerated de-adhesion process. The latter modification emerged as irreversible.

Finally, the influence of a plasma treatment by atmospheric pressure in terms of a dielectric barrier discharge in an oxygen atmosphere on a hydrogen terminated silicon wafer was investigated. Plasma activated silicon is suitable for wafer bonding at low temperature. In the here presented studies, as well the direct DBD treatment as the influence of ozone, as a reactive species formed in the discharge in oxygen, on the SiH surfaces were analyzed. So called mirror enhanced IRRAS was applied for in-situ FTIR measurements of oxide film formation. The results were complementary verified by means of ex-situ XPS. A significant reduction of the amount of of hydrocarbon contaminations and an oxide layer formation was found after both kinds of modification. The oxidation kinetic was found to follow a direct logarithmic law, which indicates an oxidation process determined by highly reactive oxygen anions formed by the discharge or ozone dissociation. A shift of the frequency of the Si-O vibration, measured by means of the ME-FT-IRRA spectroscopy led to the conclusion, that a porous oxide layer was formed on the silicon substrates.

The results and conclusions presented in this work show first signs for further investigations on the discussed fields. The plasma technology is suitable for the introduction of further functional groups on polymeric surfaces, which can be appropriate analyzed in-situ with a sensitivity down to the sub-nanometer range by means of the developed experimental setup.

The influence of another gas compositions for the applied plasmas on the

surface chemistry and electronic structure of the metallic coatings could be a focus of further studies. What is the role of hydrogen for the increase of donor states in the native oxide layer on $MgZn_2$? A hint could be obtained by the comparison of the results presented here with a modification in a pure argon atmosphere. The OH^- ions in a water vapor plasma are known to be a very oxidizing species, the influence of a water plasma instead of pure oxygen plasma on the chemical composition and the electronic structure of the $MgZn_2$ surfaces could be analyzed. Moreover, a detailed comparison of plasma induced effects on $MgZn_2$ to the effects on Mg and Zn samples modified in the same way, could deliver new aspects to confirm the conclusions drawn here.

The effort for the realization of a vacuum setup to modify technical substrates is for the industry in many cases much higher than for a plasma technology at atmospheric pressure. The experimental setup presented here allows the comparison of the modifications by vacuum plasmas with the modifications by a dielectric barrier discharge at atmospheric pressure. The modifications of the surface chemistry on iron, aluminum and $MgZn_2$ as discussed in this work could be tried to be obtained by means of a DBD treatment in an appropriate gas atmosphere.

The plasma oxidized and activated silicon wafer are known to be bondable with an appropriate strength at low temperature. The origin for this bonding behavior is discussed in the literature very intensively. A more nanoscopic approach to this topic potentially provides the application of force distance spectroscopy by means of an atomic force microscope on modified silicon surfaces with AFM tips terminated by appropriate functional groups.

However, the developed experimental setup provides the possibility for low temperature plasma modifications at low and atmospheric pressure of any

kind of materials as well as for the in-situ characterization of the effects on the surface chemistry and electronic structure for materials with an surface reflectivity suitable for the application of IRRAS or ME-IRRAS and a surface conductivity suitable for the Kelvin probe measurements.

Chapter 8

Attachment – List of symbols

8.1 Latin symbols

A	frontal area of a KP tip
$A_{p,s}$	absorption of light, polarized parallel (p) or perpendicular (s) to the plane of incidence
a_{Me^+}	activity of metal ions
C_f	sensitivity factor of the QCM
c	atomic concentration obtained by XPS
d	distance between plates of a capacitor or electrodes
d_0	thickness constant
Δd	vibration amplitude of the KP
E	field of stationary ions in a plasma
e	elementary charge

E_F	Fermi energy
$E_{v,c}$	energy levels of the valence and conducting bands respectively
E_{pot}	potential energy between charged particles
E_{th}	thermal energy of plasma species
F	electric field
F	Faraday constant
$I_{0,l,s,p}$	intensity of light after reflection on a metal surface with (l) or without (0) adsorbate, polarized parallel (p) or perpendicular (s) to the plane of incidence
k_B	Boltzmann's constant
L	dimension of the plasma
N_D	number of charge carriers inside of a sphere with the radius λ_D
n_e	electron number density
M	mass of the ions
p	gas pressure
R	universal gas constant
T	absolute temperature
T_e	temperature of electrons
ΔV	potential difference

V_b	breakdown voltage
v_B	Bohm velocity
W(x)	energy barrier for migrating ions in an oxide

8.2 Greek symbols

α	electron affinity
Γ	Coulomb coupling constant
γ	second Townsend coefficient
δ	collectively shift of electrons in the field E
ϵ	dielectric constant
ϵ_0	permittivity of vacuum
Θ	degeneracy parameter
λ_D	Debay length
λ_i	mean free path of the ions in a plasma
ν	phonon frequency
τ	average time between electron-neutral collisions
τ	time constant
Φ	work function
Φ_P	plasma potential
Φ_W	floating potential of a wall in a plasma

$\Delta\Psi$	Volta potential difference
Ω	volume of oxide created per oxidizing species
ω	frequency of KP tip
ω_p	plasma frequency

8.3 Abbreviations

AC	alternating current
AFM	atomic force microscopy
DBD	dielectric barrier discharge
DC	direct current
FT-IRRAS	Fourier transform infrared reflection absorption spectroscopy
FWHM	full width at half maximum
HOPG	highly ordered pyrolythic graphite
KP	Kelvin probe
LN_2	liquid nitrogen
LO	longitudinal optical mode of a vibration
MCT detector	mercury cadmium telluride detector
ME-FT-IRRAS	mirror enhanced FT-IRRRAS
ODM	octadecyl mercaptan

ODPA	octadecylphosphonic acid
PE-CVD	plasma enhanced chemical vapor deposition
PVD	physical vapor deposition
QCM	quartz crystal microbalance
RF	radio frequency
RMS	root-mean-squared roughness
SAM	self-assembly monolayer
SD	standard deviation
SKP	scanning Kelvin probe
TO	transversal optical mode of a vibration
ToF-SIMS	time of flight secondary ion mass spectrometry
XPS	X-ray photoelectron spectroscopy